Current plate motions

C. DeMets,[1],* R. G. Gordon,[2] D. F. Argus[2] and S. Stein[2]

[1] Acoustics Division, Naval Research Laboratory, Washington, DC 20375, USA
[2] Department of Geological Sciences, Northwestern University, Evanston, IL 60208, USA

SUMMARY

We determine best-fitting Euler vectors, closure-fitting Euler vectors, and a new global model (NUVEL-1) describing the geologically current motion between 12 assumed-rigid plates by inverting plate motion data we have compiled, critically analysed, and tested for self-consistency. We treat Arabia, India and Australia, and North America and South America as distinct plates, but combine Nubia and Somalia into a single African plate because motion between them could not be reliably resolved. The 1122 data from 22 plate boundaries inverted to obtain NUVEL-1 consist of 277 spreading rates, 121 transform fault azimuths, and 724 earthquake slip vectors. We determined all rates over a uniform time interval of 3.0 m.y., corresponding to the centre of the anomaly 2A sequence, by comparing synthetic magnetic anomalies with observed profiles. The model fits the data well. Unlike prior global plate motion models, which systematically misfit some spreading rates in the Indian Ocean by 8–$12 \, \text{mm yr}^{-1}$, the systematic misfits by NUVEL-1 nowhere exceed $\sim 3 \, \text{mm yr}^{-1}$. The model differs significantly from prior global plate motion models. For the 30 pairs of plates sharing a common boundary, 29 of 30 P071, and 25 of 30 RM2 Euler vectors lie outside the 99 per cent confidence limits of NUVEL-1. Differences are large in the Indian Ocean where NUVEL-1 plate motion data and plate geometry differ from those used in prior studies and in the Pacific Ocean where NUVEL-1 rates are systematically 5–$20 \, \text{mm yr}^{-1}$ slower than those of prior models. The strikes of transform faults mapped with GLORIA and Seabeam along the Mid-Atlantic Ridge greatly improve the accuracy of estimates of the direction of plate motion. These data give Euler vectors differing significantly from those of prior studies, show that motion about the Azores triple junction is consistent with plate circuit closure, and better resolve motion between North America and South America. Motion of the Caribbean plate relative to North or South America is about $7 \, \text{mm yr}^{-1}$ slower than in prior global models. Trench slip vectors tend to be systematically misfit wherever convergence is oblique, and best-fitting poles determined only from trench slip vectors differ significantly from their corresponding closure-fitting Euler vectors. The direction of slip in trench earthquakes tends to be between the direction of plate motion and the normal to the trench strike. Part of this bias may be due to the neglect of lateral heterogeneities of seismic velocities caused by cold subducting slabs, but the larger part is likely caused by independent motion of fore-arc crust and lithosphere relative to the overriding plate.

Key words: earthquake slip vectors, plate tectonics, seafloor spreading, transform faults.

INTRODUCTION

In this paper we review available data describing current plate motions and present a new global plate motion

* Now at MS 238–332, Jet Propulsion Laboratory, 4800 Oak Grove Drive, Pasadena, CA 91109, USA.

model, NUVEL-1. Many new high-quality plate motion data have become available since the publication of global plate motion models P071 (Chase 1978) and RM2 (Minster & Jordan 1978). These new data give a significantly improved global plate motion model for two reasons. Some regions of the world, especially in high latitutdes, that were

sparsely surveyed before are well surveyed now. Moreover, many new data, including dense aeromagnetic surveys, GLORIA and Seabeam surveys of transform faults, and centroid-moment tensor (CMT) focal mechanisms, place accurate limits on plate motion.

The improved distribution of data gives stronger tests for plate-circuit closure and the accuracy of the rigid-plate hypothesis (Gordon *et al.* 1987). Prior studies defined problems that include the following: what caused the systematic misfits to Indian Ocean plate motion data noted by Minster & Jordan (1978), and what is the relation, if any, of these misfits to the large earthquakes that occur along and near Ninetyeast Ridge and the Chagos Bank (Stein & Okal 1978; Stein 1978)? What is the velocity of North America relative to South America and where is the boundary between them? What is the velocity of the Caribbean plate relative to neighbouring plates? Does it move as fast as 40 mm yr^{-1} as suggested by Sykes, McCann & Kafka (1982), or does it move more slowly ($\sim$20 mm yr^{-1}) as suggested by Jordan (1975)? What caused the misfit to North Atlantic transform fault trends in RM2? How accurately do trench slip vectors reflect motion between major plates? Are they significantly biased by arc-parallel strike–slip faulting, as suggested by Fitch (1972) and Jarrard (1986a)?

Other important problems are potentially answerable by systematic analysis of the new plate motion data. How consistent are slip vectors from earthquake focal mechanisms, which reflect plate motion over years or decades, with spreading rates and the strikes of transform faults, which average plate motion over hundreds of thousands to several millions of years? What is the best estimate of Pacific–North America motion, a widely used reference for comparison with geologically and geodetically determined slip rates on faults in the western United States? More generally, do the data now available require any changes to the traditional plate tectonic model of rigid plates divided by three types of discrete plate boundaries? Our attempts to answer most of these questions are presented here, but some detailed analysis and discussion are given elsewhere (DeMets *et al.* 1987; DeMets, Gordon & Argus 1988; Stein *et al.* 1986b, 1988; Argus & Gordon 1989; Argus *et al.* 1989; Gordon & DeMets 1989; Gordon, DeMets & Argus 1989).

Initially we compiled a data set of published spreading rates, transform faults, and earthquake slip vectors, and followed prior studies in comparing published synthetic magnetic anomalies with the observed magnetic profiles to assess the fit and accuracy of spreading rates. Unfortunately, the spreading rates reported by different workers were often inconsistent. Moreover in several regions, for example along the Central Indian Ridge and the Galapagos spreading centre, Minster & Jordan's (1978) data are inconsistent with Chase's (1978) data. We were usually unable to resolve these inconsistencies from published information. We thus obtained as many original magnetic profiles across mid-ocean ridges as we could, and compared these, and published profiles we were otherwise unable to obtain, with synthetic magnetic anomalies we computed. The effort not only eliminated the inconsistencies that corrupted prior data and our initial data, but gave important changes in spreading rates along the Pacific–Antarctic Rise, the East Pacific Rise, the Chile Rise, the Gulf (of California) Rise, the Central Indian Ridge, and the Southeast Indian Ridge.

Although we use many more data than were used in prior global plate motion models P071 and RM2, we fit the data with the same number of adjustable parameters as the former model and three more than the latter. Three parameters are needed to specify an *Euler vector,* the term that Chase (1978) gives to the angular velocity vector describing the motion between two plates. An Euler vector is commonly described either by its three Cartesian components or by its latitude, longitude, and rotation rate. An Euler vector derived only from data along a single plate boundary is termed a *best-fitting* vector, whereas an Euler vector (for the same plate pair) derived only from data from all other plate boundaries is termed a *closure-fitting* vector (Minster *et al.* 1974; Minster & Jordan 1984).

NUVEL-1 was determined from 1122 data along 22 plate boundaries and is described by the relative positions of 12 points in 3-D angular velocity space. The origin is arbitrary and could be chosen to coincide with any of the 12 points. Hence, the 11 Euler vectors of Table 1 fully describe NUVEL-1 relative to an arbitrarily fixed Pacific plate. The Euler vector describing the motion between any unlisted plate pair can be derived by vector subtraction of the two entries for each plate. Table 2(a) gives the 30 Euler vectors for all pairs of plates sharing a boundary and Table 2(b) gives the 36 Euler vectors for all other possible pairs of

Table 1. NUVEL-1 Euler vectors (Pacific plate fixed).

Plate	Latitude °N	Longitude °E	ω (deg–m.y.$^{-1}$)	ω_x	ω_y (radians–m.y.$^{-1}$)	ω_z
Africa	59.160	−73.174	0.9695	0.002511	−0.008303	0.014529
Antarctica	64.315	−83.984	0.9093	0.000721	−0.006841	0.014302
Arabia	59.658	−33.193	1.1616	0.008570	−0.005607	0.017496
Australia	60.080	1.742	1.1236	0.009777	0.000297	0.016997
Caribbean	54.195	−80.802	0.8534	0.001393	−0.008602	0.012080
Cocos	36.823	−108.629	2.0890	−0.009323	−0.027657	0.021853
Eurasia	61.066	−85.819	0.8985	0.000553	−0.007567	0.013724
India	60.494	−30.403	1.1539	0.008555	−0.005020	0.017528
Nazca	55.578	−90.096	1.4222	−0.000023	−0.014032	0.020476
North America	48.709	−78.167	0.7829	0.001849	−0.008826	0.010267
South America	54.999	−85.752	0.6657	0.000494	−0.006646	0.009517

Additional Euler Vectors (Pacific Plate Fixed)

Plate	Latitude °N	Longitude °E	ω (deg–m.y.$^{-1}$)	ω_x	ω_y	ω_z
Juan de Fuca	35.0	26.0	0.53	0.00681	0.00332	0.00531
Philippine	0.	−47.	1.0	0.0119	0.0128	0.000

Each named plate moves counterclockwise relative to the Pacific plate. The Juan de Fuca-Pacific 3.0 Ma Euler vector is taken from Wilson (1988) and the Philippine-Pacific Euler vector is taken from Seno *et al.* (1987).

Table 2(a). NUVEL-1 Euler vectors: pairs of plates sharing a boundary.

Plate Pair	Latitude °N	Longitude °E	ω (deg–m.y.$^{-1}$)	σ_{max}	σ_{min}	ζ_{max}	σ_ω (deg–m.y.$^{-1}$)
			Pacific Ocean				
na-pa	48.7	−78.2	0.78	1.3	1.2	−61	0.01
co-pa	36.8	−108.6	2.09	1.0	0.6	−33	0.05
co-na	27.9	−120.7	1.42	1.8	0.7	−67	0.05
co-nz	4.8	−124.3	0.95	2.9	1.5	−88	0.05
nz-pa	55.6	−90.1	1.42	1.8	0.9	−1	0.02
nz-an	40.5	−95.9	0.54	4.5	1.9	−9	0.02
nz-sa	56.0	−94.0	0.76	3.6	1.5	−10	0.02
an-pa	64.3	−84.0	0.91	1.2	1.0	81	0.01
pa-au	−60.1	−178.3	1.12	1.0	0.9	−58	0.02
eu-pa	61.1	−85.8	0.90	1.3	1.1	90	0.02
co-ca	24.1	−119.4	1.37	2.5	1.2	−60	0.06
nz-ca	56.2	−104.6	0.58	6.5	2.2	−31	0.04
			Atlantic Ocean				
eu-na	62.4	135.8	0.22	4.1	1.3	−11	0.01
af-na	78.8	38.3	0.25	3.7	1.0	77	0.01
af-eu	21.0	−20.6	0.13	6.0	0.7	−4	0.02
na-sa	16.3	−58.1	0.15	5.9	3.7	−9	0.01
af-sa	62.5	−39.4	0.32	2.6	0.8	−11	0.01
an-sa	86.4	−40.7	0.27	3.0	1.2	−24	0.01
na-ca	−74.3	−26.1	0.11	25.5	2.6	−52	0.03
ca-sa	50.0	−65.3	0.19	15.1	4.3	−2	0.03
			Indian Ocean				
au-an	13.2	38.2	0.68	1.3	1.0	−63	0.00
af-an	5.6	−39.2	0.13	4.4	1.3	−42	0.01
au-af	12.4	49.8	0.66	1.2	0.9	−39	0.01
au-in	−5.6	77.1	0.31	7.4	3.1	−43	0.07
in-af	23.6	28.5	0.43	8.8	1.5	−74	0.06
ar-af	24.1	24.0	0.42	4.9	1.3	−65	0.05
in-eu	24.4	17.7	0.53	8.8	1.8	−79	0.06
ar-eu	24.6	13.7	0.52	5.2	1.7	−72	0.05
au-eu	15.1	40.5	0.72	2.1	1.1	−45	0.01
in-ar	3.0	91.5	0.03	26.1	2.4	−58	0.04

The first plate moves counterclockwise relative to the second plate. Plate abbreviations: pa, Pacific; na, North America; sa, South America; af, Africa; co, Cocos; nz, Nazca; eu, Eurasia; an, Antarctica; ar, Arabia; in, India; au, Australia; ca, Caribbean. See Figure 3 for plate geometries. One sigma-error ellipses are specified by the angular lengths of the principal axes and by the azimuths (ζ_{max}, given in degrees clockwise from north) of the major axis. The rotation rate uncertainty is determined from a one-dimensional marginal distribution, whereas the lengths of the principal axes are determined from a two-dimensional marginal distribution.

Table 2(b). NUVEL-1 Euler vectors: pairs of plates not sharing a boundary.

Plate Pair	Latitude °N	Longitude °E	ω (deg–m.y.$^{-1}$)	σ_{max}	σ_{min}	ζ_{max}	σ_ω (deg–m.y.$^{-1}$)
ca-af	−64.7	−165.0	0.16	19.5	9.8	−86	0.03
co-af	17.9	−121.4	1.37	1.7	0.8	−83	0.05
nz-af	43.5	−113.9	0.49	5.2	2.2	−26	0.02
ar-an	21.9	8.9	0.49	5.9	1.6	−80	0.04
ca-an	−49.7	−69.1	0.17	17.3	5.1	−06	0.03
co-an	18.1	−115.8	1.39	1.4	0.8	−78	0.05
eu-an	−37.8	−103.0	0.05	25.1	14.5	49	0.01
in-an	21.9	13.1	0.50	9.9	1.7	−84	0.05
ar-au	4.7	−101.6	0.35	7.5	2.4	61	0.05
ar-ca	34.9	22.7	0.54	7.0	4.6	−63	0.05
au-ca	21.9	46.7	0.76	3.9	3.2	−56	0.02
in-ca	34.2	26.6	0.55	9.4	4.4	−66	0.06
ar-co	−8.7	50.9	1.65	1.8	1.2	−72	0.07
au-co	−8.2	55.7	1.96	1.3	0.6	−79	0.05
in-co	−8.5	51.7	1.67	1.9	1.3	73	0.09
ca-eu	−51.0	−50.9	0.12	22.7	6.5	−25	0.03
co-eu	20.0	−116.2	1.36	1.6	1.0	−81	0.05
nz-eu	46.1	−95.1	0.54	4.8	2.5	−09	0.02
an-na	60.5	119.6	0.27	4.2	2.0	−22	0.01
ar-na	44.1	25.6	0.59	4.8	1.4	−39	0.04
au-na	29.1	49.0	0.79	1.6	1.0	−53	0.01
in-na	43.3	29.6	0.61	7.5	1.5	−52	0.06
nz-na	61.5	−109.8	0.67	4.0	1.8	−24	0.02
ar-nz	−13.9	44.4	0.71	4.2	2.2	31	0.05
au-nz	−11.3	55.6	1.01	2.2	1.3	43	0.02
in-nz	−13.3	46.4	0.73	5.3	1.9	42	0.07
af-pa	59.2	−73.2	0.97	1.1	1.0	86	0.01
ar-pa	59.7	−33.2	1.16	3.8	0.9	−88	0.02
ca-pa	54.2	−80.8	0.85	3.4	1.2	−11	0.03
in-pa	60.5	−30.4	1.15	5.5	1.1	82	0.02
sa-pa	55.0	−85.8	0.67	1.8	1.6	−64	0.01
ar-sa	44.4	7.3	0.65	5.2	1.5	−59	0.04
au-sa	32.8	36.8	0.79	1.3	1.2	18	0.01
co-sa	28.0	−115.0	1.51	1.5	0.8	−56	0.05
eu-sa	77.6	−86.3	0.25	4.8	1.4	−66	0.02
in-sa	44.2	11.4	0.66	8.1	1.7	−69	0.04

The conventions are the same as in Table 2a.

plates. The Euler vectors given here differ slightly from all Euler vectors we have previously published from interim data sets.

Below we first discuss our methods, data, and assumptions. We next describe the model, first in general and then in more detail, and discuss the tectonic implications of some patterns that emerged from the results. We then analyse plate-circuit closure about three-plate and global plate circuits, and discuss the implications of our results.

METHODS

To construct the global model, we analyse data on four levels. First, from magnetic and bathymetric data and, when needed, the along-track derivatives of Seasat altimetric data, we estimate spreading rates, transform fault azimuths, and their associated errors. We compute slip vectors from published focal mechanisms, and estimate their errors. We tried to estimate errors that were consistent with those of Chase (1978) and Minster & Jordan (1978) for comparable data. Second, we examine plate motion data along a single plate boundary, find best-fitting angular velocity vectors, test the internal consistency of data, and compare the results with those of prior studies. Third, we analyse closure about local plate circuits by inverting data from circuits of three or more plates (Gordon *et al.* 1987). Fourth, we simultaneously invert all the data to find the set of Euler vectors that fit the data best in a least-squares sense, while being constrained to consistency with global plate circuit closure. We also examine plate-circuit closure through comparison of the best-fitting and closure-fitting vectors for each plate pair with data along a common boundary.

The rates are determined from analysis of magnetic profiles across spreading centres. All but a few rates were determined by comparison of synthetic anomalies we computed with observed profiles, half of which were obtained in digital form from the National Geophysical Data Center (NGDC). After projecting a magnetic profile onto the direction orthogonal to the spreading ridge, we compared the observed profile with many synthetic profiles, usually computed at spreading-rate increments of 1 mm yr^{-1}. We sought the synthetic profile that best fit the distance between the centre of anomaly 2A on both sides of a spreading centre. For ridges with separation rates faster than ~55 mm yr^{-1}, we fit the narrow positive peak in the middle of the 2A sequence corresponding to the portion of chron 2A between reversed subchrons chron 2A-1 and 2A-2 in the Harland *et al.* (1982) time-scale. Here, 'positive' refers to the polarity of the anomaly when deskewed or

reduced to the pole (Blakely & Cox 1972; Schouten & McCamy 1972). For ridges with separation rates between $\sim$20 and $\sim$55 mm yr^{-1}, this narrow positive peak is typically not observed and we fit the negative anomaly between the two main positive peaks of anomaly 2A. Across ridges with separation rates less than $\sim$20 mm yr^{-1} (e.g., the Southwest Indian, Arctic, and northern Mid-Atlantic ridges), where anomaly 2A is a single positive anomaly lacking features distinguishing its centre, we fit the entire anomaly. By estimating rates over an interval that is as uniform as possible, we try to avoid difficulties that might be caused by accelerations of plate motions over the past few m.y. Moreover, NUVEL-1 can be easily corrected for any future changes in the geomagnetic reversal time-scale by dividing the rates of rotation by the ratio between any revised age for anomaly 2A and the age used here.

A small part of the differences between our spreading rates and those used in P071 and RM2 is due to differences in magnetic reversal time-scales. We use the Harland et al. (1982) time-scale, whereas Chase (1978) and Minster & Jordan (1978) used the Talwani, Windisch & Langseth (1971) time-scale (Fig. 1). However, the differences are miniscule, less than 3 per cent for the age of anomaly 2A, and can account for only a small fraction of the revisions we make to spreading rates.

The global plate motion model was derived using an iterative, linearized, weighted, least-squares procedure (Chase 1972; Minster et al. 1974). We minimized the total, weighted, least-squares error

$$\chi^2 = \sum_{i=1}^{N} \left[\frac{d_i^{\text{obs}} - d_i^{\text{pred}}(\mathbf{m})}{\sigma_i} \right]^2 \tag{1}$$

where d_i^{obs} is the ith plate motion datum, d_i^{pred} is the prediction of the ith plate motion datum, and σ_i is the standard error assigned to the ith datum. The prediction is a function of the plate motion model, $\mathbf{m}$, which consists of the Euler vectors describing the motion of each plate relative to an arbitrarily fixed plate. The plate motion data are of two types: directions (including both transform fault azimuths and earthquake slip vectors) and rates. Each type requires a different fitting function; we adopted fitting functions proposed by Chase (1972).

The predicted rate of plate motion is given by

$$d_i^{\text{pred}} = \mathbf{v}_i \cdot \hat{\mathbf{n}}_i \tag{2}$$

where $\mathbf{v}_i$ ($= \boldsymbol{\omega} \times \mathbf{r}_i$) is the linear velocity predicted at $\mathbf{r}_i$, which is the position vector for the ith datum, $\boldsymbol{\omega}$ is the trial Euler vector describing the motion between the two relevant

plates, and $\hat{\mathbf{n}}_i$ is a unit vector tangent to the surface of Earth at $\mathbf{r}_i$ and orthogonal to the strike of the magnetic lineations (Fig. 2).

Chase (1972) defined the misfit of a direction to be the magnitude of a vector difference, $\mathbf{e}_i = (\hat{\mathbf{s}}_i - \hat{\mathbf{x}}_i)$, where $\hat{\mathbf{s}}_i$ is the unit vector parallel to the observed transform azimuth or slip vector, and $\hat{\mathbf{x}}_i$ is the unit vector in the predicted direction of motion

$$d_i^{\text{pred}} = \hat{\mathbf{x}}_i = \frac{\boldsymbol{\omega} \times \mathbf{r}_i}{|\boldsymbol{\omega} \times \mathbf{r}_i|}. \tag{3}$$

Both $\hat{\mathbf{x}}_i$ and $\hat{\mathbf{s}}_i$ are tangent to the surface of Earth and perpendicular to $\mathbf{r}_i$, the vector giving the data location. Because e_i, the magnitude of $\mathbf{e}_i$, is given by $2\sin(\alpha_i/2)$, where α_i is the angle between $\hat{\mathbf{s}}_i$ and $\hat{\mathbf{x}}_i$ (Fig. 2), Chase's (1972) vector equation can be replaced with a scalar equation. We therefore minimized

$$\left[\frac{\hat{\mathbf{s}}_i - \hat{\mathbf{x}}_i(\mathbf{m})}{\sigma_i} \right]^2 = \left[\frac{2\sin(\alpha_i/2)}{\sigma_i} \right]^2. \tag{4}$$

Minster et al. (1974) proposed fitting functions different from Chase's (1972). After experimenting with both, we adopted Chase's fitting functions for several reasons. Our program using Chase's formulation ran six to eight times faster than that based on Minster et al.'s, probably because Chase's formulation in Cartesian coordinates requires fewer function and subroutine calls than Minster et al.'s formulation in spherical coordinates. While both formulations have non-linear fitting functions for the azimuthal data, Chase's rate fitting function (equation 2) is linear, whereas Minster et al.'s is not. This linearity may reduce the chance of finding solutions that are local, not global,
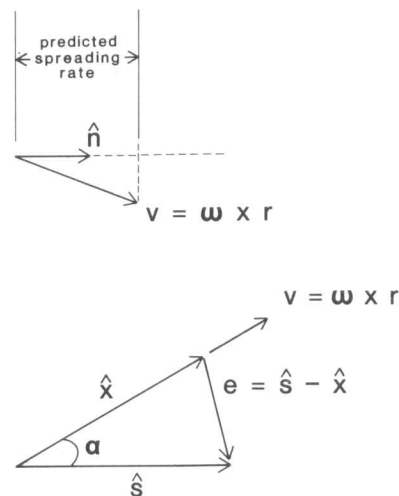
Figure 2. Functions used here to fit plate motion models to observed rates and directions of plate motion. Top: the predicted spreading rate is the projection of $\mathbf{v}$ (the predicted linear plate velocity) onto $\hat{\mathbf{n}}$ (a unit vector normal to the strike of the spreading centre). The misfit is the difference between the spreading rate observed perpendicular to the strike of the spreading centre and the projection of $\mathbf{v}$ on to $\hat{\mathbf{n}}$. Bottom: the predicted direction of plate motion is represented by the unit vector, $\hat{\mathbf{x}}$, which is parallel to $\mathbf{v}$. The observed direction of plate motion is represented by the unit vector, $\hat{\mathbf{s}}$. The misfit is the magnitude of $\mathbf{e}$, the vector difference between observed and predicted unit vectors.
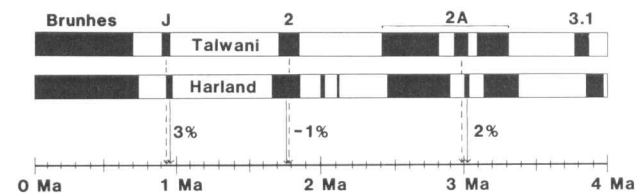

Figure 1. Comparison since 4.0 Ma of the geomagnetic reversal time-scale used here (Harland et al. 1982) with the time-scale used by Chase (1978) and Minster & Jordan (1978) (Talwani et al. 1971). We determined rates by seeking the best fit to the centre of anomaly 2A, which is 2 per cent older in the Harland et al. time-scale than in the Talwani et al. time-scale.

Table 3. NUVEL-1 data.

Lat. °N	Lon. °E	Datum	σ	Model	ι	Ridge Strike	Source or Reference

Pacific-North America: Spreading Rates

Lat. °N	Lon. °E	Datum	σ	Model	ι	Ridge Strike	Source or Reference
23.67	-108.42	48	3	49.1	0.172	s30w	Golfo-81
23.60	-108.45	48	3	49.2	0.172	s30w	NGDC Gam-2
23.55	-108.45	50	5	49.3	0.062	s30w	NGDC Hypo
23.40	-108.45	50	5	49.4	0.062	s30w	Marsur-78
23.35	-108.50	46	4	49.5	0.097	s30w	Golfo-81

Pacific-North America: Transform Azimuths

Lat. °N	Lon. °E	Datum	σ	Model	ι	Source or Reference
23.10	-108.40	-60.0	5	-54.6	0.094	Macdonald et al. (1979)
24.10	-109.00	-47.0	10	-53.4	0.024	Dauphin & Ness (1989)
25.00	-109.60	-49.0	5	-52.2	0.098	Dauphin & Ness (1989)
25.70	-110.00	-53.0	10	-51.3	0.025	Dauphin & Ness (1989)
26.80	-111.20	-53.0	10	-49.5	0.025	Dauphin & Ness (1989)
29.20	-113.50	-49.0	10	-45.9	0.025	Dauphin & Ness (1989)

Pacific-North America: Slip Vectors

Lat. °N	Lon. °E	Datum	σ	Model	ι	Source or Reference
22.90	-108.07	-52.0	15	-55.0	0.010	CMT 9.25.86
23.19	-107.99	-57.0	10	-54.8	0.024	Goff et al. (1987)
23.80	-108.73	-53.0	10	-53.8	0.024	Goff et al. (1987)
23.89	-108.37	-55.0	20	-54.0	0.006	CMT 7.12.83
24.25	-108.80	-47.0	25	-53.4	0.004	CMT 11.25.83
24.85	-109.04	-43.0	20	-52.7	0.006	CMT 10.09.84
25.12	-109.55	-54.0	10	-52.1	0.025	Goff et al. (1987)
25.20	-109.26	-48.0	10	-52.2	0.025	Goff et al. (1987)
25.25	-109.24	-49.0	10	-52.2	0.025	Goff et al. (1987)
26.09	-109.89	-48.0	20	-51.0	0.006	CMT 6.13.80
26.21	-110.29	-46.0	25	-50.6	0.004	CMT 10.25.84
26.32	-110.28	-50.0	10	-50.5	0.025	Goff et al. (1987)
26.34	-110.21	-49.0	10	-50.5	0.025	Goff et al. (1987)
26.74	-110.81	-48.0	20	-49.8	0.006	CMT 3.23.79
26.88	-110.80	-52.0	10	-49.6	0.025	Goff et al. (1987)
27.36	-111.13	-52.0	10	-49.0	0.025	Goff et al. (1987)
27.99	-111.51	-47.0	20	-48.1	0.006	CMT 11.26.78
28.29	-112.14	-53.0	10	-47.5	0.025	Goff et al. (1987)
29.03	-113.03	-39.0	20	-46.3	0.006	CMT 2.07.82
29.27	-112.97	-40.0	15	-46.0	0.011	CMT 11.21.77
29.49	-113.40	-48.0	10	-45.6	0.025	Goff et al. (1987)
29.60	-113.48	-40.0	20	-45.4	0.006	CMT 8.30.80
29.68	-113.74	-55.0	10	-45.2	0.025	Goff et al. (1987)
29.69	-113.58	-38.0	20	-45.3	0.006	CMT 9.21.80
30.04	-113.96	-41.0	25	-44.7	0.004	CMT 6.27.84
30.65	-113.93	-46.0	20	-44.1	0.007	CMT 9.06.84
50.80	-130.00	-15.0	20	-17.0	0.006	Tobin & Sykes (1968)
51.13	-131.09	-21.0	20	-17.1	0.006	CMT 6.24.84
53.92	-133.63	-28.0	20	-14.5	0.005	CMT 8.30.84
54.10	-132.60	-26.0	20	-13.6	0.006	Hodgson & Milne (1951)
56.31	-135.57	-16.0	20	-12.3	0.005	Perez & Jacob (1980)
56.77	-135.91	-18.0	20	-11.9	0.005	Perez & Jacob (1980)
57.69	-136.07	-26.0	20	-10.7	0.005	Perez & Jacob (1980)
55.70	-155.80	-24.0	20	-25.4	0.003	Stauder & Bollinger (1966)
55.31	-156.39	-27.0	15	-26.1	0.006	House & Jacob (1983)
55.44	-157.53	-28.0	15	-26.7	0.006	CMT 2.13.79
55.05	-157.61	-42.0	15	-27.1	0.006	CMT 1.02.85
55.91	-158.28	-22.0	15	-26.7	0.006	House & Jacob (1983)
54.51	-158.98	-37.0	15	-28.3	0.006	CMT 2.14.83
54.60	-159.00	-27.0	15	-28.2	0.006	CMT 2.14.83
54.87	-159.27	-39.0	15	-28.2	0.006	CMT 10.26.85
54.40	-159.34	-23.0	15	-28.6	0.006	CMT 11.14.85
54.84	-159.57	-33.0	15	-28.4	0.006	CMT 10.09.85
55.05	-160.51	-15.0	15	-28.7	0.005	House & Jacob (1983)
54.53	-161.24	-30.0	15	-29.5	0.005	CMT 1.27.79
54.36	-161.26	-31.0	20	-29.7	0.003	CMT 2.22.85
54.25	-162.51	-63.0	20	-30.5	0.003	House & Jacob (1983)
53.75	-163.32	-25.0	15	-31.3	0.005	House & Jacob (1983)
54.10	-163.34	-15.0	15	-31.0	0.005	House & Jacob (1983)
54.16	-164.08	-27.0	15	-31.4	0.005	CMT 12.27.83
53.75	-164.70	-21.0	15	-32.0	0.005	House & Jacob (1983)
55.29	163.38	-51.0	15	-49.8	0.004	CMT 5.31.82
55.05	162.45	-51.0	20	-50.4	0.002	CMT 3.06.85
54.73	164.26	-52.0	15	-49.4	0.004	CMT 1.09.83
54.46	161.94	-55.0	20	-50.9	0.002	CMT 4.01.86
53.56	161.15	-55.0	20	-51.6	0.002	CMT 6.17.86
53.37	160.79	-59.0	20	-51.9	0.002	CMT 5.19.85
52.85	159.22	-54.0	15	-53.0	0.004	Kurita & Ando (1974)
52.60	160.52	-56.0	20	-52.3	0.002	CMT 12.21.77
52.57	160.93	-47.0	15	-52.0	0.004	CMT 8.05.83
52.45	160.35	-50.0	15	-52.4	0.004	CMT 4.04.83
52.41	160.85	-51.0	20	-52.1	0.002	CMT 6.03.85
52.32	160.48	-60.0	20	-52.4	0.002	CMT 12.02.77
52.07	159.85	-58.0	20	-52.8	0.002	CMT 4.18.85
52.06	159.86	-60.0	15	-52.8	0.004	CMT 6.17.83
51.58	159.21	-46.0	20	-53.3	0.002	CMT 4.03.85

Cocos-Pacific: Spreading Rates

Lat. °N	Lon. °E	Datum	σ	Model	ι	Ridge Strike	Source or Reference
17.66	-105.37	72	6	77.1	0.035	n08w	NGDC Scan 11
17.27	-105.50	75	5	78.5	0.048	n08w	NGDC Scan 11
17.20	-105.40	74	5	78.8	0.048	n08w	NGDC Marsur 1978
16.88	-105.36	77	7	80.0	0.024	n08w	NGDC Yaquina 71-10
16.80	-105.36	80	4	80.3	0.072	n08w	NGDC Umitaka Maru 3
16.63	-105.39	77	4	80.9	0.071	n08w	NGDC Scan 11
16.25	-105.19	80	4	82.5	0.068	n08w	NGDC Scan 11
15.78	-105.44	83	6	84.0	0.030	n08w	NGDC Kana Keoki 71-04
14.70	-104.45	87	6	88.6	0.027	n10w	NGDC Tripod 3
14.18	-103.33	91	4	91.2	0.058	n10w	NGDC Scan 10
12.88	-104.00	95	4	95.6	0.055	n10w	NGDC Swansong
12.79	-104.30	96	4	95.7	0.055	n10w	NGDC Yaquina 69
11.92	-103.80	101	4	99.2	0.054	n10w	NGDC DSDP 16
11.20	-103.75	104	4	101.8	0.054	n10w	NGDC Kana Keoki 80 21
11.08	-103.75	107	4	102.2	0.054	n10w	NGDC Kana Keoki 80 21
9.40	-104.10	112	10	108.0	0.009	n10w	NGDC DSDP 54
9.20	-104.10	111	4	108.7	0.057	n10w	NGDC Papagayo 1
9.20	-104.10	112	5	108.7	0.036	n10w	NGDC Conrad 20 02
7.80	-102.80	114	10	114.4	0.010	n10w	NGDC DSDP 54
7.30	-102.70	117	4	116.2	0.066	n10w	NGDC Vema 20 03
6.30	-102.60	120	8	119.7	0.018	n10w	NGDC Conrad 20 11
5.40	-102.50	125	6	122.8	0.036	n10w	NGDC Oceanographer 7101
3.30	-102.10	132	6	130.1	0.045	n10w	NGDC Vema 32 10
3.10	-102.20	131	8	130.7	0.026	n10w	NGDC Scan 9
3.10	-102.20	134	6	130.7	0.046	n10w	NGDC Conrad 10 04

Cocos-Pacific: Transform Azimuths

Lat. °N	Lon. °E	Datum	σ	Model	ι	Source or Reference
15.38	-105.30	80.0	3	82.8	0.175	Madsen et al. (1986)
10.20	-104.00	82.0	2	81.8	0.253	Gallo et al. (1986)
8.34	-103.50	80.0	5	81.5	0.035	Gallo et al. (1987)

Cocos-Pacific: Slip Vectors

Lat. °N	Lon. °E	Datum	σ	Model	ι	Source or Reference
15.18	-104.45	80.0	20	81.0	0.004	CMT 10.22.78
10.37	-103.87	80.0	15	81.5	0.005	CMT 12.25.78
10.21	-103.69	78.0	20	81.3	0.002	CMT 6.03.86
8.62	-102.97	78.0	20	80.5	0.002	CMT 5.10.86
8.55	-103.22	83.0	20	81.0	0.002	CMT 7.28.79
8.50	-103.00	76.0	15	80.6	0.004	Molnar & Sykes (1969)
8.39	-103.37	88.0	20	81.2	0.002	CMT 4.01.85

Cocos-North America: Slip Vectors

Lat. °N	Lon. °E	Datum	σ	Model	ι	Source or Reference
18.83	-103.91	26.0	20	33.6	0.007	CMT 3.9.81
18.80	-103.80	35.0	15	33.5	0.012	Eissler & McNally (1984)
18.72	-103.30	30.0	15	33.1	0.011	Eissler & McNally (1984)
18.48	-103.00	32.0	15	33.3	0.011	Dean & Drake (1978)
18.41	-102.98	23.0	15	33.5	0.011	CMT 4.30.86
18.35	-102.30	38.0	20	32.8	0.006	Chael & Stewart (1982)
18.30	-102.50	36.0	15	33.2	0.010	Molnar & Sykes (1969)
18.27	-102.79	27.0	25	33.6	0.004	CMT 1.6.79
18.25	-102.69	22.0	20	33.5	0.006	CMT 9.25.85
18.24	-102.53	25.0	20	33.4	0.006	CMT 5.5.86
18.22	-101.89	19.0	20	32.7	0.005	CMT 7.26.81
18.18	-102.57	17.0	15	33.6	0.010	CMT 9.19.85
18.17	-102.55	13.0	20	33.6	0.006	CMT 10.29.85
18.01	-102.11	24.0	15	33.4	0.010	CMT 10.25.81
17.82	-101.67	31.0	15	33.4	0.010	CMT 9.21.85
17.81	-101.28	17.0	15	32.9	0.009	CMT 3.14.79
17.46	-101.46	26.0	15	33.9	0.009	Chael & Stewart (1982)
17.45	-100.65	40.0	20	33.1	0.005	Chael & Stewart (1982)
17.41	-100.88	23.0	15	33.4	0.009	CMT 1.26.79
17.30	-100.10	44.0	15	32.8	0.008	Molnar & Sykes (1969)
17.25	-99.58	33.0	20	32.4	0.004	Molnar & Sykes (1969)

Table 3. (*continued*)

17.03	-99.74	-3.0	15	33.0	0.007		CMT 3.19.78
17.12	-99.57	37.0	20	32.7	0.004		*Molnar & Sykes* (1969)
17.02	-98.76	14.0	25	32.1	0.003		CMT 5.29.86
16.80	-98.74	25.0	20	32.5	0.004		CMT 6.7.87
16.76	-98.51	34.0	15	32.4	0.007		CMT 7.2.84
16.51	-98.41	35.0	20	32.8	0.004		CMT 7.21.81
16.59	-98.32	31.0	15	32.6	0.007		CMT 6.7.82
16.62	-98.15	40.0	15	32.4	0.007		CMT 6.7.82
16.25	-98.25	20.0	20	33.2	0.004		CMT 11.30.84
16.90	-97.70	14.0	25	31.4	0.002		*Dean & Drake* (1978)
16.60	-97.80	36.0	15	32.1	0.007		*Dean & Drake* (1978)
16.59	-97.70	35.0	15	32.0	0.007		*Chael & Stewart* (1982)
16.41	-97.11	45.0	20	31.9	0.004		CMT 7.31.80
16.23	-96.48	32.0	20	31.7	0.003		CMT 12.13.84
16.31	-95.83	36.0	15	31.0	0.006		*Molnar & Sykes* (1969)
16.30	-95.80	31.0	15	31.0	0.006		*Chael & Stewart* (1982)
16.26	-95.71	06.0	20	31.0	0.003		CMT 8.4.80
16.00	-97.90	40.0	15	33.3	0.007		*Molnar & Sykes* (1969)
15.77	-96.80	37.0	15	32.8	0.006		*Chael & Stewart* (1982)
16.01	-96.59	37.0	15	32.2	0.006		CMT 11.29.78
16.05	-96.48	26.0	15	32.0	0.006		CMT 12.28.78
16.06	-96.30	18.0	20	31.8	0.003		CMT 2.14.81
15.90	-96.20	39.0	15	32.1	0.006		*Molnar & Sykes* (1969)

Cocos-Nazca: Spreading Rates

2.30	-99.60	44	4	43.9	0.110	n90w	*Hey et al.* (1977)
2.40	-99.00	45	4	44.9	0.101	n90w	*Hey et al.* (1977)
2.40	-98.70	46	4	45.4	0.096	n90w	*Hey et al.* (1977)
2.30	-98.00	51	4	46.6	0.087	n90w	NGDC *Oceanographer* 7101
2.40	-96.00	48	4	49.9	0.064	n90w	*Hey et al.* (1977)
2.40	-94.00	54	4	53.1	0.048	n90w	*Hey et al.* (1977)
2.50	-93.20	54	3	54.3	0.078	n90w	NGDC Indomed 15
2.40	-93.00	55	4	54.6	0.043	n90w	*Hey et al.* (1977)
2.40	-92.50	55	4	55.4	0.041	n90w	*Hey et al.* (1977)
2.00	-91.60	60	7	56.8	0.012	n90w	NGDC *Kana Keoki* 7812 7
0.90	-89.70	58	6	59.7	0.016	n90w	NGDC *Kana Keoki* 7812 6
0.80	-89.20	58	6	60.5	0.017	n90w	NGDC Cocos Tow 4
0.90	-88.40	61	5	61.7	0.025	n90w	NGDC *Vema* 21 04
0.80	-88.30	62	4	61.8	0.040	n90w	NGDC *Kana Keoki* 78 12 6
0.90	-88.00	60	4	62.2	0.041	n90w	*Raff* (1968)
0.90	-87.40	63	4	63.1	0.044	n90w	*Raff* (1968)
0.90	-87.40	62	4	63.1	0.044	n90w	NGDC *Kana Keoki* 78 12 6
0.90	-87.00	65	4	63.7	0.046	n90w	*Raff* (1968)
0.80	-86.70	64	4	64.1	0.048	n90w	NGDC *Kana Keoki* 78 12 6
0.80	-86.40	64	6	64.6	0.022	n90w	NGDC *Kana Keoki* 78 12 6
0.80	-86.20	64	6	64.9	0.023	n90w	NGDC South Tow 2
0.80	-86.20	59	4	64.9	0.051	n90w	NGDC Tripod 2
0.80	-86.10	65	4	65.0	0.052	n90w	*Raff* (1968)
0.80	-85.70	58	7	65.6	0.018	n90w	NGDC DSDP 16
3.20	-83.90	67	5	68.1	0.046	n90w	NGDC DSDP 68
3.30	-83.50	69	3	68.7	0.135	n90w	*Kana Keoki* 71 04
3.30	-83.20	69	4	69.1	0.079	n90w	*Hey et al.* (1977)
3.30	-83.20	68	5	69.1	0.051	n90w	NGDC *Iguana* 3
3.30	-83.20	71	4	69.1	0.079	n90w	NGDC *Conrad* 13 08

Cocos-Nazca: Transform Azimuths

1.40	-85.30	5.0	5	5.8	0.117	*Sclater & Klitgord* (1973)
2.50	-84.50	6.0	3	4.4	0.314	*Lonsdale & Klitgord* (1978)
5.00	-82.60	-1.0	5	1.6	0.106	*Lonsdale & Klitgord* (1978)

Cocos-Nazca: Slip Vectors

1.93	-101.13	35.0	20	7.6	0.018	CMT 5.11.85
2.48	-98.49	26.0	25	5.8	0.009	CMT 2.27.87
2.00	-90.50	-1.0	10	5.6	0.037	*Forsyth* (1972)
1.50	-85.30	0.0	20	5.7	0.007	*Molnar & Sykes* (1969)
1.49	-85.27	6.0	15	5.8	0.013	CMT 5.14.77
4.01	-82.50	-5.0	20	2.7	0.007	CMT 11.26.83
4.04	-82.50	0.0	20	2.6	0.007	CMT 2.28.77
5.07	-82.61	3.0	10	1.5	0.027	*Pennington* (1981)
5.28	-82.65	0.0	20	1.2	0.007	CMT 7.06.77
5.28	-82.67	2.0	15	1.2	0.012	CMT 7.30.80
5.39	-82.63	0.0	15	1.1	0.012	*Molnar & Sykes* (1969)
5.43	-82.60	4.0	20	1.1	0.007	CMT 5.05.83
5.44	-82.65	3.0	20	1.1	0.007	CMT 2.4.80
5.59	-82.63	3.0	10	0.9	0.027	*Pennington* (1981)
5.61	-82.63	4.0	15	0.9	0.012	*Molnar & Sykes* (1969)
5.71	-82.64	3.0	10	0.8	0.027	*Pennington* (1981)

Nazca-Pacific: Spreading Rates

-7.00	-107.00	130	20	134.2	0.006	n30e	NGDC Many profiles 6-8°S
-10.50	-110.20	150	15	145.4	0.010	n20e	NGDC Many profiles 8-13°S
-12.00	-111.20	140	14	147.8	0.012	n18e	NGDC *Chain* 100 11
-12.60	-111.00	150	6	148.3	0.063	n18e	NGDC Rispo 2
-16.60	-113.10	141	10	152.6	0.023	n13e	NGDC DSDP 92
-17.00	-113.70	151	6	152.9	0.063	n13e	NGDC *Vema* 19 05
-19.50	-113.50	157	5	154.4	0.091	n12e	NGDC *Oceanog.* 7302 *Conrad* 13
-21.50	-114.00	153	10	155.6	0.023	n12e	NGDC *Oceanog.* 7302 *Conrad* 13
-28.30	-112.00	156	10	157.6	0.025	n10e	NGDC *Eltanin* 29
-30.50	-112.10	157	5	158.0	0.108	n13e	NGDC *Oceanographer* 73 3
-31.00	-111.90	159	5	158.1	0.110	n13e	NGDC *Yaquina* 7304
-31.30	-112.00	159	7	158.1	0.056	n13e	NGDC *Yaquina* 7304

Nazca-Pacific: Transform Azimuths

-3.70	-103.30	102.0	5	98.6	0.025	*Searle* (1983)
-4.00	-104.20	102.0	8	99.1	0.010	*Searle* (1983)
-4.50	-105.50	102.0	5	99.8	0.026	*Searle* (1983)
-6.00	-107.00	107.0	10	100.6	0.007	*Mammerickx et al.* (1975)
-9.00	-108.50	97.0	10	101.2	0.006	*Kureth & Rea* (1982)
-13.50	-112.00	110.0	10	102.8	0.006	*Mammerickx et al.* (1975)

Nazca-Pacific: Slip Vectors

-2.37	-102.48	115.0	20	98.2	0.002	CMT 1.11.84
-3.71	-102.51	93.0	20	98.1	0.002	CMT 9.21.85
-3.91	-103.97	95.0	20	99.0	0.002	CMT 3.01.81
-3.97	-104.07	96.0	20	99.0	0.002	CMT 2.06.80
-4.06	-104.37	91.0	20	99.2	0.002	CMT 1.16.86
-4.45	-104.82	94.0	15	99.4	0.003	CMT 3.22.86
-4.36	-104.88	98.0	20	99.5	0.002	CMT 5.15.84
-4.59	-105.51	97.0	20	99.8	0.002	CMT 10.10.84
-4.60	-105.80	103.0	15	100.0	0.003	*Anderson & Sclater* (1972)
-4.53	-105.87	97.0	20	100.1	0.002	CMT 8.28.84
-4.40	-105.90	105.0	20	100.1	0.002	*Anderson et al.* (1974)
-4.50	-106.00	104.0	15	100.2	0.003	*Anderson & Sclater* (1972)
-4.86	-105.92	95.0	20	100.1	0.002	CMT 10.08.80
-4.65	-106.05	99.0	15	100.2	0.003	CMT 3.01.84
-4.56	-106.17	95.0	15	100.2	0.003	CMT 9.12.78
-8.97	-108.34	92.0	20	101.1	0.002	CMT 7.30.80
-8.98	-108.54	120.0	20	101.3	0.002	CMT 5.08.79
-9.07	-109.07	80.0	20	101.6	0.002	CMT 5.13.86
-8.90	-109.47	79.0	20	101.8	0.002	CMT 8.21.86
-13.37	-111.34	100.0	20	102.5	0.002	CMT 6.13.78
-13.30	-111.50	105.0	10	102.6	0.006	*Anderson & Sclater* (1972)
-13.22	-112.15	104.0	20	103.0	0.002	CMT 7.08.79
-13.34	-111.59	100.0	20	102.6	0.002	CMT 1.07.86
-28.70	-112.70	118.0	10	102.6	0.005	*Anderson et al.* (1974)
-28.78	-112.65	107.0	20	102.6	0.001	CMT 8.21.83
-29.01	-112.60	98.0	15	102.5	0.002	CMT 9.12.82
-29.39	-112.30	108.0	20	102.4	0.001	CMT 7.15.77

Nazca-Antarctica: Spreading Rates

-37.80	-94.10	58	6	59.3	0.094	n02w	NGDC *Oceanographer* 7008
-43.40	-82.80	62	6	60.3	0.109	n10w	NGDC *Eltanin* 19
-44.50	-82.50	61	5	60.4	0.162	n10w	*Herron et al.* (1981)
-44.60	-78.30	63	5	60.4	0.164	n10w	*Herron et al.* (1981)

Nazca-Antarctica: Transform Azimuths

-34.90	-108.00	105.0	10	99.4	0.029	*Anderson-Fontana et al.* (1987)
-35.25	-106.00	102.0	10	97.9	0.027	*Anderson-Fontana et al.* (1987)
-35.90	-103.00	96.0	10	95.5	0.025	*Anderson-Fontana et al.* (1987)
-36.18	-101.00	91.0	10	94.0	0.024	*Anderson-Fontana et al.* (1987)
-41.30	-88.50	80.0	10	84.3	0.019	*Klitgord et al.* (1973)
-44.68	-80.00	71.0	10	77.9	0.018	*Herron et al.* (1981)
-45.72	-77.50	71.0	10	76.1	0.018	*Herron et al.* (1981)
-45.90	-76.30	69.0	10	75.2	0.018	*Herron et al.* (1981)

Nazca-Antarctica: Slip Vectors

-35.14	-106.85	98.0	20	98.5	0.007	CMT 4.14.79
-35.24	-106.68	95.0	20	98.4	0.007	CMT 6.09.87
-35.39	-106.62	100.0	20	98.4	0.007	CMT 12.19.78
-35.38	-105.87	97.0	15	97.8	0.012	CMT 1.27.80
-35.47	-104.77	96.0	20	96.9	0.007	CMT 6.28.78

Table 3. (*continued*)

-35.58	-104.63	100.0	20	96.8	0.007	CMT 8.03.80
-35.52	-104.61	101.0	20	96.8	0.007	CMT 8.27.82
-35.89	-103.75	96.0	20	96.1	0.006	CMT 8.01.86
-35.83	-103.30	96.0	20	95.8	0.006	CMT 8.22.81
-35.90	-102.94	97.0	20	95.5	0.006	CMT 9.26.80
-36.01	-102.60	97.0	15	95.2	0.011	CMT 1.14.79
-36.00	-102.60	91.0	15	95.2	0.011	P. Lundgren
						(personal communication, 1985)
-35.52	-102.59	95.0	15	95.2	0.011	CMT 3.06.78
-35.97	-102.20	93.0	20	94.9	0.006	CMT 1.12.86
-35.80	-102.17	93.0	25	94.9	0.004	CMT 6.10.81
-36.20	-100.90	82.0	15	93.9	0.010	*Anderson et al.* (1974)
-35.78	-100.81	94.0	15	93.8	0.011	CMT 4.03.78
-36.17	-100.70	98.0	20	93.7	0.006	CMT 8.22.81
-36.12	-100.69	94.0	20	93.7	0.006	CMT 6.19.86
-36.10	-100.47	98.0	25	93.6	0.004	CMT 6.24.86
-36.13	-100.04	92.0	20	93.2	0.006	CMT 11.09.83
-36.37	-98.86	92.0	20	92.3	0.006	CMT 5.06.85
-36.40	-98.80	82.0	15	92.2	0.010	P. Lundgren
						(personal communication, 1985)
-36.25	-98.75	94.0	20	92.2	0.006	CMT 5.10.84
-36.50	-98.61	94.0	15	92.1	0.010	CMT 10.22.80
-36.60	-98.20	66.0	15	91.8	0.009	P. Lundgren
						(personal communication, 1985)
-36.30	-98.10	86.0	15	91.7	0.010	P. Lundgren
						(personal communication, 1985)
-36.31	-98.03	94.0	20	91.6	0.006	CMT 7.12.79
-36.25	-98.02	92.0	15	91.6	0.010	CMT 11.12.85
-36.28	-97.95	93.0	20	91.6	0.006	CMT 6.10.79
-36.27	-97.53	91.0	20	91.3	0.005	CMT 12.05.86
-36.60	-97.50	80.0	15	91.2	0.010	P. Lundgren
						(personal communication, 1985)
-36.30	-97.37	91.0	20	91.1	0.005	CMT 6.05.86
-36.50	-97.20	81.0	15	91.0	0.010	P. Lundgren
						(personal communication, 1985)
-36.30	-97.20	79.0	20	91.0	0.005	*Anderson et al.* (1974)
-37.20	-95.30	60.0	15	89.5	0.009	P. Lundgren
						(personal communication, 1985)
-38.89	-92.19	89.0	20	87.1	0.005	CMT 3.14.87
-38.63	-91.65	87.0	15	86.7	0.009	CMT 7.10.85
-39.02	-91.61	90.0	20	86.7	0.005	CMT 9.01.85
-41.55	-90.65	92.0	20	86.0	0.005	CMT 11.27.77
-41.32	-89.27	89.0	20	84.9	0.005	CMT 4.26.77
-41.25	-85.78	83.0	20	82.2	0.005	CMT 8.06.85
-41.38	-85.85	86.0	20	82.3	0.005	CMT 5.16.81
-41.70	-84.00	86.0	10	80.9	0.018	*Anderson et al.* (1974)
-41.89	-83.77	96.0	25	80.7	0.003	CMT 10.08.79
-44.61	-80.10	79.0	20	78.0	0.005	CMT 4.09.80
-44.86	-79.41	80.0	15	77.5	0.008	CMT 5.29.78
-44.46	-78.84	83.0	15	77.1	0.008	CMT 12.25.86
-45.12	-76.67	80.0	25	75.5	0.003	CMT 11.28.86
-45.61	-75.29	78.0	20	74.5	0.005	CMT 2.22.77
-45.71	-75.99	77.0	20	75.0	0.005	CMT 2.14.87

Nazca-South America: Slip Vectors

0.85	-79.63	84.0	10	80.4	0.017	*Suarez et al.* (1983)
0.67	-80.07	85.0	20	80.7	0.004	CMT 3.01.79
0.42	-79.94	77.0	15	80.7	0.007	CMT 11.22.83
-1.25	-81.07	94.0	20	81.6	0.004	CMT 5.08.77
-1.89	-80.88	78.0	15	81.5	0.007	CMT 5.06.81
-5.62	-81.39	80.0	20	82.1	0.003	CMT 5.14.87
-6.41	-81.42	91.0	15	82.2	0.006	CMT 12.27.81
-6.90	-80.40	73.0	15	81.6	0.006	*Stauder* (1975)
-8.33	-79.97	91.0	20	81.4	0.003	CMT 12.27.81
-10.70	-78.60	60.0	10	80.8	0.013	*Abe* (1972)
-12.46	-76.73	100.0	20	79.8	0.003	CMT 6.15.87
-14.90	-75.80	89.0	15	79.4	0.006	*Stauder* (1975)
-14.98	-75.47	90.0	20	79.2	0.003	CMT 8.13.85
-15.04	-75.60	79.0	20	79.3	0.003	CMT 7.19.85
-15.10	-75.56	79.0	20	79.3	0.003	CMT 8.14.85
-15.52	-75.24	91.0	20	79.2	0.003	CMT 6.15.80
-16.47	-73.51	93.0	20	78.3	0.003	CMT 4.15.78
-16.69	-72.95	76.0	15	78.0	0.006	CMT 3.07.80
-20.26	-70.45	82.0	20	76.8	0.003	CMT 6.21.81
-20.72	-70.37	73.0	20	76.8	0.003	CMT 2.21.85

-21.80	-70.00	86.0	10	76.6	0.013	*Stauder* (1973)
-23.10	-70.10	74.0	15	76.7	0.006	*Stauder* (1973)
-23.11	-70.93	78.0	20	77.2	0.003	CMT 5.30.80
-23.75	-70.62	91.0	20	77.0	0.003	CMT 1.07.81
-24.08	-70.08	71.0	15	76.8	0.006	CMT 3.22.87
-24.10	-70.30	81.0	15	76.9	0.006	*Stauder* (1973)
-24.20	-70.07	78.0	15	76.8	0.006	CMT 3.06.87
-24.30	-70.55	70.0	20	77.0	0.003	CMT 3.15.87
-24.49	-70.17	85.0	15	76.8	0.006	CMT 3.05.87
-24.57	-70.58	76.0	15	77.0	0.006	CMT 3.05.87
-25.50	-70.70	89.0	15	77.1	0.006	*Stauder* (1973)
-25.79	-70.52	67.0	20	77.0	0.003	CMT 7.24.84
-25.87	-70.79	84.0	20	77.2	0.003	CMT 7.02.77
-26.25	-70.59	77.0	15	77.1	0.006	CMT 10.09.83
-26.55	-70.70	95.0	20	77.2	0.003	CMT 3.04.84
-26.62	-70.77	78.0	15	77.2	0.006	CMT 10.04.83
-27.15	-71.05	73.0	20	77.4	0.003	CMT 5.20.79
-27.87	-71.20	79.0	20	77.4	0.003	CMT 8.02.79
-27.90	-70.90	73.0	10	77.3	0.012	*Stauder* (1973)
-28.25	-70.74	78.0	20	77.2	0.003	CMT 10.05.77
-29.46	-71.13	92.0	20	77.4	0.003	CMT 2.03.84
-29.95	-71.54	110.0	20	77.6	0.003	CMT 3.23.80
-30.00	-71.50	100.0	20	77.6	0.003	*Stauder* (1973)
-30.24	-71.28	82.0	15	77.5	0.005	CMT 5.19.85
-30.33	-71.59	87.0	15	77.7	0.005	CMT 5.19.87
-30.60	-71.40	87.0	20	77.6	0.003	*Stauder* (1973)
-30.60	-71.50	79.0	20	77.6	0.003	*Stauder* (1973)
-30.67	-71.36	92.0	20	77.6	0.003	CMT 11.08.84
-30.70	-71.20	73.0	15	77.5	0.005	*Stauder* (1973)
-30.72	-71.21	81.0	15	77.5	0.005	CMT 6.11.84
-31.50	-71.00	82.0	15	77.4	0.005	*Stauder* (1973)
-31.80	-71.90	78.0	20	77.8	0.003	CMT 4.19.84
-32.13	-72.04	66.0	20	77.9	0.003	CMT 1.27.87
-32.48	-71.68	90.0	20	77.7	0.003	CMT 6.11.85
-32.50	-71.20	90.0	15	77.5	0.005	*Malgrange et al.* (1981)
-32.57	-71.70	85.0	10	77.7	0.012	*Choy & Dewey* (1988)
-32.65	-71.62	80.0	10	77.7	0.012	*Choy & Dewey* (1988)
-32.65	-71.42	78.0	15	77.6	0.005	CMT 7.17.85
-32.72	-71.65	94.0	20	77.7	0.003	CMT 6.11.80
-32.74	-71.64	60.0	10	77.7	0.012	*Choy & Dewey* (1988)
-32.88	-72.00	84.0	15	77.9	0.005	CMT 7.07.85
-32.90	-72.00	92.0	20	77.9	0.003	CMT 7.11.85
-33.01	-72.14	78.0	20	78.0	0.003	CMT 3.07.85
-33.07	-71.49	86.0	20	77.6	0.003	CMT 4.28.85
-33.10	-72.16	90.0	20	78.0	0.003	CMT 3.12.85
-33.12	-71.62	72.0	10	77.7	0.012	*Choy & Dewey* (1988)
-33.13	-71.72	75.0	10	77.7	0.012	*Choy & Dewey* (1988)
-33.28	-71.72	77.0	20	77.7	0.003	CMT 2.21.85
-33.30	-72.22	69.0	20	78.0	0.003	CMT 3.23.85
-33.36	-72.12	99.0	20	78.0	0.003	CMT 7.06.85
-33.38	-72.13	84.0	20	78.0	0.003	CMT 7.28.86
-33.38	-72.17	100.0	20	78.0	0.003	CMT 7.05.85
-33.42	-71.74	97.0	20	77.8	0.003	CMT 10.11.79
-33.50	-71.90	88.0	20	77.8	0.003	*Stauder* (1973)
-33.53	-72.02	79.0	20	77.9	0.003	CMT 4.15.85
-33.60	-71.89	83.0	15	77.8	0.005	CMT 3.23.81
-33.80	-71.90	80.0	20	77.8	0.003	CMT 4.26.79
-33.84	-71.43	88.0	10	77.6	0.012	*Choy & Dewey* (1988)
-33.88	-72.30	95.0	20	78.0	0.003	CMT 5.19.85
-33.95	-71.96	75.0	20	77.9	0.003	CMT 3.04.85
-34.00	-72.20	74.0	20	78.0	0.003	*Stauder* (1973)
-34.06	-71.59	80.0	10	77.7	0.012	*Choy & Dewey* (1988)
-34.10	-72.10	87.0	20	77.9	0.003	CMT 3.26.86
-34.20	-72.23	70.0	10	78.0	0.012	*Choy & Dewey* (1988)
-34.20	-71.72	90.0	20	77.7	0.003	CMT 3.05.85
-34.28	-72.11	99.0	20	77.9	0.003	CMT 3.23.85
-34.28	-72.46	78.0	20	78.1	0.003	CMT 5.17.85
-34.35	-72.13	85.0	20	78.0	0.003	CMT 3.24.85
-36.42	-73.08	71.0	20	78.4	0.003	CMT 9.14.83
-37.78	-72.87	82.0	20	78.3	0.003	CMT 2.3.87
-37.78	-73.59	122.0	20	78.7	0.002	CMT 6.02.85
-37.80	-73.40	81.0	15	78.6	0.005	*Stauder* (1973)
-37.93	-73.50	86.0	20	78.6	0.003	CMT 3.29.80
-38.10	-73.40	101.0	20	78.6	0.003	*Stauder* (1973)
-38.10	-73.00	80.0	10	78.4	0.012	*Stauder* (1973)
-38.20	-73.20	81.0	15	78.5	0.005	*Stauder* (1973)

Table 3. (*continued*)

-38.42	-73.49	84.0	15	78.6	0.005		CMT 8.12.85
-38.50	-73.50	70.0	20	78.6	0.003		*Stauder* (1973)
-46.30	-74.80	87.0	20	79.1	0.003		*Stauder* (1973)

Antarctic-Pacific: Spreading Rates

-35.60	-110.70	100	3	98.9	0.111	n12e	NGDC *Eltanin* 24
-35.90	-110.70	100	3	98.7	0.111	n12e	NGDC *Oceanographer* 7008
-41.90	-111.30	95	4	96.0	0.059	n12e	NGDC *Oceanographer* 7008
-43.00	-111.00	97	5	95.4	0.037	n12e	*Molnar et al.* (1975)
-44.50	-112.20	94	4	94.4	0.057	n12e	NGDC *Eltanin* 20
-51.00	-117.50	88	3	89.1	0.100	n16e	NGDC South Tow 2
-51.60	-118.10	95	4	88.5	0.056	n16e	NGDC *Eltanin* 19
-53.10	-118.00	89	5	87.3	0.036	n16e	NGDC *Eltanin* 43
-54.40	-118.40	84	4	86.1	0.056	n17e	NGDC *Conrad* 1212
-54.40	-138.40	83	4	81.9	0.057	n26e	NGDC *Eltanin* 23
-58.60	-148.50	77	10	74.9	0.010	n32e	NGDC *Eltanin* 19
-58.50	-149.00	75	7	74.7	0.020	n35e	*Pitman et al.* (1968)
-60.50	-151.00	76	6	72.1	0.028	n35e	*Pitman et al.* (1968)
-61.20	-153.00	78	8	70.7	0.016	n36e	NGDC *Umitaka Maru* 66-b
-62.50	-159.20	62	5	67.1	0.042	n40e	NGDC *Umitaka Maru* 6402-b
-63.20	-163.30	62	4	64.7	0.068	n42e	NGDC *Eltanin* 42
-63.80	-168.30	62	5	62.0	0.045	n45e	NGDC *Eltanin* 33
-63.30	-167.40	62	4	62.9	0.070	n45e	NGDC *Monsoon* 6
-65.00	-174.00	57	10	58.3	0.012	n50e	*Pitman et al.* (1968)
-65.30	-174.10	52	4	58.0	0.074	n50e	NGDC Gecs-gmv
-63.20	170.00	54	5	51.9	0.053	n55e	NGDC *Eltanin* 50

Antarctic-Pacific: Transform Azimuths

-49.90	-115.00	108.0	8	104.5	0.013		Seasat & *Molnar et al.* (1975)
-55.60	-124.50	113.0	5	109.8	0.037		Seasat & *Molnar et al.* (1975)
-54.70	-131.00	115.0	5	112.6	0.037		Seasat & *Molnar et al.* (1975)
-56.70	-142.00	120.0	5	118.2	0.040		Seasat & *Molnar et al.* (1975)
-63.00	-161.00	123.0	15	130.4	0.006		Seasat
-63.50	173.80	149.0	5	142.9	0.080		Seasat & *Molnar et al.* (1975)
-63.00	169.00	132.0	15	144.5	0.009		Seasat
-62.30	165.50	137.0	15	145.0	0.010		Seasat

Antarctic-Pacific: Slip Vectors

-49.69	-115.40	105.0	15	104.6	0.004		CMT 1.26.83
-49.75	-114.54	101.0	20	104.3	0.002		CMT 11.29.83
-49.91	-114.14	99.0	15	104.1	0.004		CMT 1.07.81
-49.92	-113.59	99.0	20	103.8	0.002		CMT 1.14.87
-49.92	-115.58	100.0	20	104.8	0.002		CMT 11.02.77
-52.85	-118.89	111.0	20	106.7	0.002		CMT 4.23.83
-52.91	-118.55	122.0	20	106.5	0.002		CMT 5.23.78
-53.87	-117.91	108.0	20	106.4	0.002		CMT 7.04.77
-54.53	-119.04	102.0	25	107.0	0.001		CMT 8.05.81
-56.01	-121.51	99.0	20	108.5	0.002		CMT 8.14.80
-56.25	-122.39	106.0	15	109.0	0.004		CMT 4.07.85
-56.08	-122.44	104.0	15	109.0	0.004		CMT 3.12.79
-55.86	-123.34	107.0	15	109.3	0.004		CMT 7.05.83
-56.00	-123.40	113.0	10	109.4	0.009		*Molnar et al.* (1975)
-55.97	-123.65	110.0	20	109.5	0.002		CMT 8.18.85
-54.96	-126.88	106.0	20	110.8	0.002		CMT 12.6.86
-55.20	-127.24	114.0	20	111.0	0.002		CMT 4.27.77
-55.42	-127.62	112.0	20	111.2	0.002		CMT 1.9.81
-55.76	-127.76	113.0	20	111.4	0.002		CMT 3.30.85
-55.35	-128.93	111.0	20	111.8	0.002		CMT 8.06.86
-55.59	-128.94	107.0	15	111.9	0.004		CMT 7.16.84
-55.46	-129.14	107.0	20	112.0	0.002		CMT 10.27.77
-55.03	-132.11	111.0	20	113.2	0.002		CMT 11.27.78
-54.24	-132.50	107.0	20	113.1	0.002		CMT 9.11.85
-54.33	-132.82	113.0	20	113.3	0.002		CMT 6.10.79
-54.03	-135.52	112.0	20	114.4	0.002		CMT 4.19.81
-54.76	-135.93	113.0	15	114.8	0.004		CMT 5.26.84
-54.80	-136.00	119.0	10	114.9	0.009		*Molnar et al.* (1975)
-54.56	-136.54	114.0	15	115.0	0.004		CMT 5.25.84
-56.80	-140.09	117.0	20	117.4	0.003		CMT 8.18.84
-57.08	-140.59	120.0	20	117.7	0.003		CMT 6.06.86
-56.97	-141.79	116.0	20	118.2	0.003		CMT 2.25.86
-56.58	-142.42	121.0	15	118.3	0.004		CMT 1.02.84
-56.47	-142.45	116.0	20	118.3	0.003		CMT 12.1.79
-56.60	-142.50	119.0	10	118.4	0.010		*Molnar et al.* (1975)
-56.54	-142.57	113.0	20	118.4	0.003		CMT 12.27.78
-56.15	-142.93	118.0	20	118.4	0.002		CMT 1.01.77
-56.19	-144.22	125.0	20	119.0	0.003		CMT 1.26.82
-55.92	-144.57	127.0	20	119.0	0.002		CMT 2.8.78
-57.80	-147.66	120.0	20	121.2	0.003		CMT 7.6.79
-59.46	-150.89	122.0	20	123.4	0.003		CMT 11.10.79
-63.02	-157.73	120.0	20	128.8	0.003		CMT 9.18.78
-62.86	-161.43	132.0	20	130.5	0.003		CMT 8.4.79
-63.58	-168.21	145.0	20	134.4	0.004		CMT 8.23.81
-64.87	-170.54	144.0	20	136.8	0.004		CMT 10.22.79
-65.72	-175.71	133.0	20	140.4	0.005		CMT 12.9.80
-65.70	-179.30	129.0	15	142.2	0.009		*Molnar et al.* (1975)
-65.83	179.84	138.0	15	142.8	0.009		CMT 11.15.81
-65.34	176.97	124.0	20	143.7	0.005		CMT 9.5.85
-63.49	172.19	145.0	15	143.7	0.009		CMT 10.24.77
-63.20	169.67	146.0	20	144.4	0.005		CMT 7.3.78
-63.34	169.47	152.0	15	144.7	0.010		CMT 8.14.83
-62.88	166.32	138.0	20	145.5	0.006		CMT 5.25.80
-62.45	165.76	145.0	20	145.1	0.006		CMT 1.24.78

Eurasia-North America: Spreading Rates

86.50	43.00	12	3	11.4	0.074	n69e	*Vogt et al.* (1979)
84.90	7.50	13	3	12.8	0.065	n42e	*Feden et al.* (1979)
84.10	0.00	13	2	13.2	0.249	n34e	*Feden et al.* (1979)
83.40	-4.50	15	3	13.5	0.059	n32e	*Feden et al.* (1979)
73.70	8.50	17	4	15.7	0.023	n29e	*Kovacs et al.* (1982)
72.50	3.00	15	4	14.5	0.022	n59e	*Vogt et al.* (1982)
71.80	-2.50	14	3	13.1	0.033	n66e	*Kovacs et al.* (1982)
69.60	-16.00	17	2	18.0	0.130	n16e	*Vogt et al.* (1980)
69.30	-16.00	17.5	2.0	18.1	0.073	n14e	*Vogt et al.* (1980)
68.50	-18.00	18	2	18.4	0.070	n16e	*Vogt et al.* (1980)
67.90	-18.50	18	2	18.6	0.122	n13e	*Vogt et al.* (1980)
61.60	-27.00	19	2	18.3	0.088	n36e	*Talwani et al.* (1971)
60.20	-29.10	19	2	18.4	0.087	n36e	*Talwani et al.* (1971)
44.50	-28.20	25	4	22.9	0.023	n22e	*Argus et al.* (1989) (NGDC)
43.80	-28.50	24	3	23.4	0.043	n18e	*Argus et al.* (1989) (NGDC)
43.30	-29.00	23	3	23.4	0.045	n18e	*Argus et al.* (1989) (NGDC)
42.90	-29.30	25.5	2.0	23.5	0.102	n18e	*Argus et al.* (1989) (NGDC)
42.70	-29.30	23	2	23.7	0.110	n00e	*Argus et al.* (1989) (NGDC)
42.30	-29.30	23.5	2.0	23.4	0.112	n05w	*Argus et al.* (1989) (NGDC)
41.70	-29.20	24.5	3.0	23.8	0.051	n00e	*Argus et al.* (1989) (NGDC)

Eurasia-North America: Transform Azimuths

80.00	1.00	125.5	5	124.6	0.099		*Perry et al.* (1978)
78.80	5.00	127.0	10	126.8	0.025		*Perry et al.* (1978)
71.30	-9.00	114.0	3	112.5	0.198		*Perry et al.* (1978)
52.60	-33.20	95.9	3	95.6	0.118		*Searle* (1981)
52.10	-30.90	95.5	2	96.7	0.256		*Searle* (1981)

Eurasia-North America: Slip Vectors

80.30	-1.93	125.0	20	122.6	0.006		CMT 10.08.86
80.20	-0.70	130.0	20	123.5	0.006		*Chapman & Solomon* (1976)
79.81	2.90	134.0	20	126.0	0.006		*Chapman & Solomon* (1976)
79.80	2.90	139.0	20	126.0	0.006		*Chapman & Solomon* (1976)
70.97	-6.86	116.0	20	113.8	0.005		*Chapman & Solomon* (1976)
71.19	-8.03	113.0	15	113.1	0.008		CMT 11.20.79
71.23	-8.21	110.0	20	113.0	0.005		*Savostin & Karasik* (1981)
71.49	-10.36	106.0	20	111.7	0.004		*Savostin & Karasik* (1981)
71.62	-11.51	111.0	15	111.0	0.008		CMT 7.30.84
52.82	-34.25	98.0	10	95.1	0.011		*Bergman & Solomon* (1988)
52.80	-34.20	101.0	20	95.1	0.003		*Engeln et al.* (1986)
52.70	-33.30	100.0	20	95.6	0.003		*Engeln et al.* (1986)
52.71	-32.00	98.0	10	96.2	0.011		*Bergman & Solomon* (1988)
52.50	-31.85	103.0	20	96.3	0.003		*Engeln et al.* (1986)

Africa-North America: Spreading Rates

36.80	-33.20	21.5	2.0	20.7	0.068	n28e	*Macdonald* (1977)
36.80	-33.20	20.5	2.0	20.7	0.068	n28e	*Rabinowitz & Schouten* (1985)
36.50	-33.70	22	3	20.4	0.028	n32e	*Rabinowitz & Schouten* (1985)
36.00	-34.10	20	3	20.5	0.028	n32e	*Rabinowitz & Schouten* (1985)
35.00	-36.50	21	4	21.9	0.020	n07e	*LeDouaran et al.* (1982)
34.30	-37.00	21	3	21.5	0.029	n29e	*LeDouaran et al.* (1982)
31.90	-40.50	23	4	22.3	0.017	n28e	*Rabinowitz & Schouten* (1985)
30.90	-41.70	23	4	22.7	0.018	n27e	*Rabinowitz & Schouten* (1985)
30.50	-41.90	22	3	23.2	0.033	n22e	*Rabinowitz & Schouten* (1985)
29.60	-43.00	23	3	23.8	0.036	n15e	*LeDouaran et al.* (1982)
27.50	-44.20	24	3	24.0	0.037	n22e	*Rabinowitz & Schouten* (1985)

Table 3. (*continued*)

26.90	-44.50	26	4	24.5	0.022	n16e	*Rabinowitz & Schouten* (1985)
26.20	-44.80	22	3	23.5	0.037	n30e	*McGregor et al.* (1977)
25.70	-45.00	24	4	24.2	0.022	n24e	*Rabinowitz & Schouten* (1985)
25.30	-45.40	22.5	2	24.4	0.089	n24e	*Rabinowitz & Schouten* (1985)
25.10	-45.40	24.5	2	24.4	0.090	n24e	*Rona & Gray* (1980)
24.50	-46.10	23	4	24.6	0.023	n23e	*Rabinowitz & Schouten* (1985)
24.20	-46.30	24.5	2	25.1	0.097	n15e	*Rona & Gray* (1980)
23.00	-45.00	25	4	25.2	0.025	n08e	*Rabinowitz & Schouten* (1985)
22.80	-45.00	25	2	25.1	0.100	n04e	*Rabinowitz & Schouten* (1985)

Africa-North America: Transform Azimuths

35.20	-35.60	104.5	2	103.6	0.203	*Roest et al.* (1984)
33.70	-38.70	104.5	2	103.4	0.216	*Roest et al.* (1984)
30.00	-42.40	101.5	3	102.9	0.100	*Roest et al.* (1984)
23.70	-45.70	98.0	2	102.2	0.220	*Roest et al.* (1984) & *Pockalny et al.* (1988)

Africa-North America: Slip Vectors

35.43	-36.03	102.0	20	103.6	0.002	CMT 4.29.85
35.41	-36.01	101.0	10	103.7	0.008	CMT 6.06.82
35.35	-36.08	100.0	10	103.7	0.008	*Bergman & Solomon* (1988)
35.14	-35.45	101.0	15	103.6	0.004	CMT 7.14.80
33.79	-38.64	101.0	10	103.4	0.009	*Bergman & Solomon* (1988)
33.78	-38.46	102.0	15	103.4	0.004	CMT 5.07.84
33.69	-38.60	103.0	15	103.4	0.004	CMT 5.03.84
28.74	-43.58	91.0	20	102.8	0.002	*Engeln et al.* (1986)
23.83	-45.94	100.0	10	102.2	0.009	*Bergman & Solomon* (1988)
23.86	-45.57	100.0	10	102.2	0.009	*Bergman & Solomon* (1988)
23.81	-45.44	106.0	15	102.2	0.004	CMT 11.28.81
23.74	-45.17	102.0	15	102.2	0.004	CMT 3.12.77

Africa-Eurasia: Transform Azimuths

36.90	-23.50	257.0	5	260.2	0.187	*Laughton et al.* (1972)
37.00	-22.60	265.0	3	263.3	0.399	*Laughton et al.* (1972)
37.10	-21.70	265.0	3	266.3	0.384	*Laughton et al.* (1972)
37.10	-20.50	-90.0	7	270.4	0.098	*Laughton et al.* (1972)

Africa-Eurasia: Slip Vectors

37.75	-17.25	-89.0	25	-79.2	0.022	CMT 10.17.83
37.22	-14.93	-50.0	25	-71.5	0.042	*Grimison & Chen* (1986) ·
36.96	-11.84	267.0	25	-62.0	0.066	*Grimison & Chen* (1986)
36.01	-10.57	-35.0	25	-57.0	0.092	*Fukao* (1973)
35.99	-10.34	-60.0	25	-56.3	0.098	*Grimison & Chen* (1986)
36.23	-7.61	-35.0	25	-49.8	0.104	*Grimison & Chen* (1986)

Africa-South America: Spreading Rates

-6.00	-11.70	33	6	34.1	0.018	n10w	*van Andel et al.* (1973)
-7.60	-13.40	35	6	34.4	0.018	n10w	*van Andel et al.* (1973)
-8.00	-13.50	34	2	34.4	0.160	n08w	*Brozena* (1986)
-8.40	-13.30	33	6	34.5	0.018	n08w	*van Andel et al.* (1973)
-9.20	-13.20	39	6	34.6	0.017	n08w	*van Andel et al.* (1973)
-10.50	-13.00	34	3	34.8	0.068	n09w	*Brozena* (1986)
-13.50	-14.50	36	4	35.0	0.034	n19w	*Brozena* (1986)
-15.00	-13.50	34	2	35.4	0.136	n16w	*Brozena* (1986)
-17.00	-14.00	36	3	35.6	0.061	n10w	*Brozena* (1986)
-24.90	-13.50	37	6	34.5	0.013	n05e	*Dickson et al.* (1968)
-28.00	-13.00	36	3	35.7	0.053	n05w	*Dickson et al.* (1968)
-30.50	-13.50	35	3	35.1	0.051	n00e	*Dickson et al.* (1968)
-31.10	-13.40	35	5	35.7	0.019	n17w	*Welch et al.* (1986)
-31.70	-13.40	34	3	35.7	0.052	n14w	*Welch et al.* (1986)
-33.00	-14.50	35	3	35.6	0.051	n14w	*Welch et al.* (1986)
-33.90	-14.60	34	4	35.6	0.029	n10w	*Welch et al.* (1986)
-38.50	-17.00	36	6	35.1	0.013	n10w	*Dickson et al.* (1968)
-40.00	-16.00	36	3	34.7	0.051	n05w	*Loomis & Morgan* (1973)
-42.00	-16.00	32	4	34.4	0.029	n05w	*Dickson et al.* (1968)
-43.00	-16.00	35	3	34.2	0.052	n05w	*Loomis & Morgan* (1973)
-54.20	-1.30	28	5	30.9	0.023	n25w	NGDC *Chain* 115-4
-54.50	-1.10	30	3	30.8	0.064	n25w	NGDC *Chain* 115-4
-54.60	-1.00	30	5	30.8	0.023	n25w	NGDC *Chain* 115-4

Africa-South America: Transform Azimuths

15.30	-45.80	95.5	3	94.0	0.128	*Roest et al.* (1984)
12.60	-44.60	90.0	3	93.1	0.108	*Collette et al.* (1979)
12.20	-43.80	90.0	3	92.6	0.101	*Collette et al.* (1979)
10.80	-42.30	91.5	2	91.7	0.197	*Macdonald et al.* (1986)
7.80	-37.00	92.0	8	88.6	0.008	*Emery & Uchupi* (1984)
4.00	-32.00	90.0	5	86.0	0.016	*Emery & Uchupi* (1984)
1.00	-28.00	84.0	5	84.1	0.015	*Emery & Uchupi* (1984)
-0.80	-21.50	82.0	2	81.0	0.110	*Belderson et al.* (1984)
-1.20	-14.50	76.0	3	77.8	0.069	*Emery & Uchupi* (1985)
-7.00	-12.50	77.7	2	77.3	0.150	*Brozena* (1986)
-11.50	-14.00	77.5	3	78.2	0.056	*Brozena* (1986)
-32.30	-14.00	80.0	2	78.5	0.098	D. Forsyth (personal communication, 1985)
-34.20	-14.80	80.0	3	78.8	0.042	D. Forsyth (personal communication, 1985)
-54.20	-2.00	65.0	10	71.0	0.006	*Sclater et al.* (1976a)

Africa-South America: Slip Vectors

15.34	-45.92	97.0	10	94.1	0.012	*Bergman & Solomon* (1988)
15.30	-45.78	98.0	10	94.0	0.011	*Bergman & Solomon* (1988)
15.25	-45.15	97.0	10	93.6	0.011	*Bergman & Solomon* (1988)
14.14	-45.18	100.0	20	93.6	0.003	*Engeln et al.* (1986)
12.84	-44.57	95.0	15	93.1	0.004	CMT 6.09.87
12.05	-43.79	101.0	20	92.6	0.002	*Engeln et al.* (1986)
10.79	-43.51	92.0	10	92.4	0.009	*Bergman & Solomon* (1988)
10.83	-43.43	90.0	10	92.4	0.008	CMT 1.10.85
10.83	-43.23	96.0	20	92.2	0.002	*Engeln et al.* (1986)
10.77	-43.11	92.0	10	92.2	0.008	*Bergman & Solomon* (1988)
10.79	-42.23	96.0	15	91.7	0.003	CMT 3.20.84
10.72	-42.02	97.0	20	91.5	0.002	*Engeln et al.* (1986)
10.72	-41.68	87.0	10	91.3	0.008	*Bergman & Solomon* (1988)
8.80	-39.87	92.0	15	90.3	0.003	CMT 8.13.80
8.05	-38.79	102.0	20	89.6	0.001	*Engeln et al.* (1986)
8.15	-38.76	93.0	10	89.6	0.006	CMT 11.01.84
8.10	-38.55	89.0	15	89.5	0.003	CMT 11.05.78
8.04	-38.39	95.0	15	89.4	0.003	CMT 12.06.81
8.11	-38.09	90.0	10	89.3	0.006	*Engeln et al.* (1986)
7.39	-36.10	88.0	15	88.1	0.002	CMT 4.22.81
7.30	-34.86	85.0	10	87.4	0.005	*Engeln et al.* (1986)
7.08	-34.87	80.0	15	87.5	0.002	CMT 12.24.85
7.10	-34.04	89.0	15	87.0	0.002	CMT 7.26.80
7.07	-33.85	94.0	20	86.9	0.001	CMT 8.30.84
0.67	-30.39	84.0	15	85.3	0.002	CMT 6.22.84
0.86	-29.88	83.0	10	85.0	0.004	CMT 10.12.85
0.83	-29.82	88.0	10	85.0	0.004	CMT 3.20.78
0.77	-29.69	87.0	10	84.9	0.004	CMT 3.20.78
0.11	-29.60	80.0	15	84.9	0.001	CMT 7.24.80
0.82	-28.98	90.0	20	84.6	0.001	*Engeln et al.* (1986)
0.95	-28.43	88.0	10	84.3	0.004	CMT 6.06.85
0.97	-28.29	89.0	20	84.2	0.001	*Engeln et al.* (1986)
0.93	-28.09	82.0	15	84.1	0.002	CMT 9.19.84
1.14	-27.71	85.0	15	83.9	0.002	CMT 6.22.78
0.89	-27.11	85.0	15	83.6	0.002	CMT 11.14.79
0.95	-27.08	82.0	15	83.6	0.002	CMT 11.02.81
0.93	-26.83	85.0	15	83.5	0.002	CMT 7.01.85
0.80	-26.77	81.0	15	83.5	0.002	CMT 6.15.86
0.90	-26.77	88.0	20	83.4	0.001	*Engeln et al.* (1986)
0.87	-26.50	88.0	20	83.3	0.001	*Engeln et al.* (1986)
0.75	-26.14	88.0	20	83.1	0.001	CMT 3.23.86
0.81	-25.45	89.0	20	82.8	0.001	*Engeln et al.* (1986)
0.11	-25.35	84.0	10	82.8	0.004	CMT 11.01.80
-1.19	-24.68	87.0	10	82.5	0.004	CMT 8.12.82
-1.30	-24.30	99.0	20	82.4	0.001	*Engeln et al.* (1986)
-0.99	-23.48	87.0	15	81.9	0.002	CMT 12.08.84
-0.85	-22.13	85.0	20	81.3	0.001	*Engeln et al.* (1986)
-0.97	-21.86	81.0	10	81.2	0.004	CMT 1.03.82
-0.84	-21.81	77.0	10	81.1	0.004	CMT 10.13.83
-0.51	-19.92	80.0	15	80.2	0.002	CMT 12.29.86
-0.50	-19.90	80.0	20	80.2	0.001	*Engeln et al.* (1986)
-0.52	-19.86	77.0	10	80.2	0.005	CMT 4.22.84
-0.58	-19.77	83.0	15	80.1	0.002	CMT 10.09.84
-0.38	-19.55	80.0	15	80.0	0.002	CMT 6.04.85
-0.22	-19.19	79.0	15	79.8	0.002	CMT 6.07.87
-0.32	-19.17	83.0	20	79.8	0.001	*Engeln et al.* (1986)
-0.04	-19.14	77.0	10	79.8	0.005	CMT 5.05.87
-0.13	-18.83	79.0	10	79.6	0.005	CMT 7.07.81
-0.30	-18.60	88.0	20	79.6	0.001	*Engeln et al.* (1986)
-0.14	-18.24	74.0	15	79.4	0.002	CMT 3.12.87
-0.19	-18.03	89.0	20	79.3	0.001	*Engeln et al.* (1986)
-0.02	-17.88	83.0	10	79.2	0.005	CMT 6.24.86

Table 3. (continued)

-0.14	-17.80	81.0	15	79.2	0.002		CMT 8.11.86
-0.16	-17.72	76.0	15	79.1	0.002		CMT 2.22.79
-0.13	-17.76	81.0	10	79.1	0.005		CMT 1.02.87
0.27	-16.98	87.0	20	78.7	0.001		*Engeln et al.* (1986)
-1.48	-15.61	76.0	15	78.3	0.003		CMT 3.19.78
-1.40	-15.06	76.0	10	78.0	0.006		CMT 12.07.84
-1.18	-14.51	79.0	15	77.8	0.003		CMT 2.27.85
-1.43	-14.07	85.0	20	77.6	0.002		*Engeln et al.* (1986)
-1.15	-14.04	77.0	15	77.5	0.003		CMT 7.28.77
-1.28	-13.98	75.0	15	77.5	0.003		CMT 12.05.84
-1.11	-13.87	79.0	20	77.5	0.002		*Engeln et al.* (1986)
-1.30	-13.59	93.0	20	77.4	0.002		*Engeln et al.* (1986)
-0.98	-13.48	76.0	15	77.3	0.003		CMT 3.26.77
-1.55	-12.69	75.0	15	77.0	0.003		CMT 6.30.87
-6.83	-11.59	75.0	15	76.9	0.003		CMT 10.16.80
-6.94	-12.57	68.0	15	77.4	0.003		CMT 8.10.81
-7.06	-12.59	71.0	15	77.4	0.003		CMT 10.21.84
-7.02	-12.81	73.0	15	77.5	0.003		CMT 7.19.84
-11.69	-13.62	70.0	15	78.1	0.002		CMT 2.24.77
-11.88	-13.74	73.0	15	78.2	0.002		CMT 11.05.84
-32.25	-13.43	73.0	15	78.2	0.002		CMT 11.18.85
-35.82	-15.98	76.0	10	79.2	0.004		CMT 7.26.81
-35.50	-16.08	81.0	15	79.3	0.002		CMT 4.05.85
-35.67	-16.24	79.0	10	79.4	0.004		CMT 5.16.79
-35.20	-16.63	77.0	10	79.6	0.004		CMT 1.13.79
-35.56	-17.04	78.0	10	79.7	0.003		CMT 6.03.81
-35.59	-17.55	75.0	15	80.0	0.002		CMT 12.23.84
-35.86	-17.65	78.0	10	80.0	0.003		CMT 8.10.78
-47.65	-12.93	76.0	10	77.2	0.004		CMT 3.14.86
-46.91	-10.79	85.0	15	76.2	0.002		CMT 7.05.85
-54.30	-2.40	66.0	20	71.2	0.001		*Forsyth* (1975)
-54.07	-1.78	77.0	15	71.0	0.003		CMT 11.12.78

Antarctic-South America: Spreading Rates

-55.30	-1.60	20	5	18.6	0.022	n05w	NGDC *Chain* 115 3
-56.00	-4.70	19	4	18.4	0.036	n05w	NGDC *Chain* 115 3
-56.10	-4.70	19	4	18.3	0.036	n05w	NGDC *Chain* 115 3
-56.20	-4.70	19	4	18.3	0.036	n05w	*Barker & Lawver* (1988)
-58.90	-16.50	19	3	16.7	0.064	n12w	*Barker & Lawver* (1988)
-59.80	-18.50	19	5	16.3	0.024	n13w	*Lawver & Dick* (1983)
-60.50	-19.50	19	3	16.2	0.069	n10w	*Barker & Lawver* (1988)

Antarctic-South America: Transform Azimuths

-55.70	-3.00	85.0	3	86.4	0.243	*Sclater et al.* (1976a)
-56.60	-5.50	86.0	10	86.5	0.021	*Barker & Lawver* (1988)
-57.20	-6.50	86.0	10	86.6	0.021	*Barker & Lawver* (1988)
-58.00	-9.10	85.0	5	86.7	0.084	*Lawver & Dick* (1983)
-58.00	-14.20	85.0	5	87.2	0.080	*Lawver & Dick* (1983)
-59.10	-17.20	89.0	7	87.5	0.044	*Barker & Lawver* (1988)
-60.90	-20.20	89.5	5	87.7	0.098	*Barker & Lawver* (1988)
-60.90	-23.80	89.5	5	88.1	0.105	*Barker & Lawver* (1988)

Antarctic-South America: Slip Vectors

-55.50	-2.60	88.0	10	86.4	0.022	*Forsyth* (1975)
-58.30	-15.30	90.0	10	87.3	0.020	*Forsyth* (1975)
-57.91	-7.19	83.0	15	86.6	0.010	CMT 2.04.80
-57.97	-10.66	84.0	15	86.9	0.009	CMT 6.21.80
-58.32	-15.21	91.0	20	87.3	0.005	CMT 8.02.86
-58.31	-15.65	85.0	15	87.4	0.009	CMT 6.22.84
-59.03	-16.44	79.0	20	87.4	0.005	CMT 4.27.84
-59.29	-16.83	87.0	20	87.4	0.005	CMT 8.24.84
-60.80	-19.70	98.0	10	87.6	0.024	*Forsyth* (1975)
-60.90	-19.77	83.0	15	87.6	0.011	CMT 9.13.81
-48.21	-75.88	67.0	20	92.9	0.016	CMT 8.01.83
-52.84	-75.10	83.0	20	93.1	0.019	CMT 6.06.79

Caribbean-North America: Spreading Rates

18.00	-81.50	15	5	11.8	0.466	n10w	*Rosencrantz et al.* (1988)

Caribbean-North America: Transform Azimuths

19.70	-75.00	86.0	5	78.1	0.274	*Holcombe et al.* (1973)
19.70	-77.00	83.0	5	77.7	0.202	*Holcombe et al.* (1973)
19.20	-80.00	79.0	5	77.2	0.144	*Holcombe et al.* (1973)
17.50	-83.00	79.0	5	76.8	0.157	*Holcombe et al.* (1973)
16.90	-85.00	75.0	5	76.5	0.208	*Holcombe et al.* (1973)
16.40	-87.00	72.0	5	76.2	0.290	*Holcombe et al.* (1973)

Caribbean-North America: Slip Vectors

15.27	-89.25	66.0	15	75.9	0.047	*Kanamori & Stewart* (1978)
16.61	-86.85	67.0	15	76.2	0.031	CMT 8.20.77
16.70	-86.61	66.0	15	76.3	0.030	CMT 8.20.77
16.82	-85.90	70.0	15	76.4	0.027	*Molnar & Sykes* (1969)
16.96	-85.60	75.0	15	76.4	0.025	*Molnar & Sykes* (1969)
16.72	-86.11	71.0	20	76.3	0.016	CMT 6.11.81
16.84	-85.71	72.0	20	76.4	0.015	CMT 3.20.80
17.53	-83.37	85.0	15	76.7	0.018	CMT 4.10.82
18.90	-81.19	81.0	15	77.0	0.015	*Molnar & Sykes* (1969)

Caribbean-South America: Slip Vectors

17.56	-62.11	58.0	20	86.1	0.079	CMT 11.23.82
17.69	-61.57	83.0	20	85.5	0.086	CMT 5.29.78
16.75	-61.39	77.0	15	85.4	0.146	*Stein et al.* (1982)
16.71	-61.47	69.0	15	85.5	0.143	CMT 1.30.82
16.64	-61.25	58.0	20	85.3	0.078	CMT 10.09.79
12.10	-60.95	74.0	15	85.4	0.116	CMT 11.28.85

Cocos-Caribbean: Slip Vectors

15.70	-95.80	14.0	20	24.5	0.014	*Dean & Drake* (1978)
15.60	-95.10	27.0	15	24.3	0.024	*Dean & Drake* (1978)
15.40	-95.50	23.0	25	25.0	0.009	*Dean & Drake* (1978)
15.30	-94.70	29.0	20	24.6	0.013	*Dean & Drake* (1978)
15.72	-94.50	2.0	15	23.7	0.022	CMT 3.12.87
15.67	-94.52	44.0	20	23.8	0.013	CMT 3.15.87
15.33	-94.55	51.0	25	24.5	0.008	CMT 5.10.84
15.00	-94.30	25.0	25	25.0	0.008	*Dean & Drake* (1978)
15.06	-94.24	40.0	20	24.8	0.012	CMT 10.13.84
15.00	-93.80	25.0	20	24.7	0.012	*Dean & Drake* (1978)
14.70	-93.70	15.0	20	25.2	0.012	*Dean & Drake* (1978)
14.60	-93.20	11.0	20	25.1	0.011	*Dean & Drake* (1978)
14.60	-92.80	40.0	20	24.9	0.011	*Dean & Drake* (1978)
14.52	-92.60	26.0	15	24.9	0.020	*Chael & Stewart* (1982)
14.50	-93.40	30.0	20	25.4	0.012	*Dean & Drake* (1978)
14.31	-92.98	34.0	20	25.5	0.011	CMT 12.13.83
14.51	-92.90	15.0	20	25.1	0.011	*Dean & Drake* (1978)
14.43	-92.78	32.0	20	25.2	0.011	CMT 4.5.81
14.50	-92.40	30.0	20	24.8	0.011	*Dean & Drake* (1978)
14.38	-92.24	30.0	20	25.0	0.011	CMT 8.3.84
13.92	-92.20	13.0	20	25.7	0.010	CMT 5.11.78
14.30	-92.00	53.0	15	25.0	0.018	*Molnar & Sykes* (1969)
14.53	-91.68	35.0	15	24.4	0.019	*Molnar & Sykes* (1969)
13.30	-92.30	16.0	20	26.8	0.010	*Dean & Drake* (1978)
13.62	-91.41	29.0	20	25.8	0.010	CMT 9.2.80
13.83	-90.88	26.0	15	25.2	0.017	CMT 10.27.79
13.33	-90.06	50.0	20	25.6	0.009	CMT 10.21.86
13.15	-89.64	31.0	15	25.6	0.016	CMT 12.6.78
12.62	-88.39	43.0	20	25.8	0.008	CMT 12.19.86
13.10	-88.60	38.0	25	25.2	0.005	*Dean & Drake* (1978)
12.10	-87.50	30.0	25	26.1	0.005	*Dean & Drake* (1978)
12.50	-87.40	34.0	15	25.5	0.014	*Molnar & Sykes* (1969)
12.28	-87.43	46.0	20	25.9	0.008	CMT 3.13.87
11.75	-87.36	41.0	20	26.6	0.008	CMT 12.19.78
11.91	-86.77	33.0	20	26.1	0.008	CMT 5.3.85
12.00	-86.60	47.0	15	25.9	0.013	*Dean & Drake* (1978)
11.66	-86.36	28.0	15	26.2	0.013	CMT 4.8.87
11.46	-87.48	29.0	20	27.0	0.008	CMT 4.2.87
11.50	-86.40	31.0	20	26.5	0.007	*Dean & Drake* (1978)
11.20	-86.60	20.0	15	27.0	0.013	*Dean & Drake* (1978)
11.40	-86.20	32.0	15	26.5	0.013	*Molnar & Sykes* (1969)
11.44	-86.16	32.0	15	26.4	0.013	CMT 12.20.84
10.21	-85.25	30.0	20	27.6	0.007	*Burbach et al.* (1984)
10.20	-85.22	30.0	15	27.6	0.012	CMT 8.23.78
9.61	-84.11	32.0	20	27.8	0.006	CMT 8.17.82
9.60	-84.10	6.0	20	27.8	0.006	*Molnar & Sykes* (1969)
9.28	-84.05	32.0	20	28.2	0.006	CMT 9.25.85
8.95	-83.48	24.0	15	28.3	0.011	CMT 8.24.79
8.90	-83.40	30.0	15	28.3	0.011	*Molnar & Sykes* (1969)
8.73	-83.12	30.0	15	28.4	0.010	CMT 4.3.83
8.55	-82.75	30.0	15	28.4	0.010	CMT 8.7.77
8.50	-82.94	16.0	25	28.6	0.004	CMT 4.9.84
8.43	-83.39	12.0	20	28.8	0.006	CMT 9.23.83
8.28	-82.93	10.0	15	28.8	0.010	CMT 5.9.83

Table 3. (*continued*)

8.06	-82.72	24.0	15	29.0	0.010		CMT 10.12.83
8.00	-82.69	18.0	15	29.0	0.010		CMT 4.7.83

Africa-Antarctica: Spreading Rates

-54.70	0.00	14	3	13.8	0.052	n45w	NGDC *Chain* 115 3
-53.90	3.50	14	3	13.8	0.052	n45w	NGDC *Chain* 115 3
-54.00	4.00	14	4	13.9	0.029	n45w	NGDC *Chain* 115 3
-52.20	14.50	16	3	14.2	0.053	n55w	*Norton* (1976)
-44.70	36.20	15	4	14.7	0.032	n75w	*Bergh & Norton* (1976)
-44.50	37.00	16	4	14.7	0.033	n75w	*Bergh & Norton* (1976)
-44.20	38.50	16	3	14.7	0.058	n75w	*Bergh & Norton* (1976)
-44.20	38.80	16	3	14.7	0.058	n75w	*Bergh & Norton* (1976)
-43.30	39.50	16	3	14.7	0.059	n75w	*Schlich & Patriat* (1971)
-40.00	45.60	18	4	14.7	0.034	n90w	*Fisher & Sclater* (1983)
-38.80	47.30	16	4	14.8	0.034	n80w	*Schlich & Patriat* (1971
-26.20	68.50	16	4	14.0	0.039	n90w	*Tapscott et al.* (1980)

Africa-Antarctica: Transform Azimuths

-54.30	1.80	44.0	5	45.6	0.076	*Sclater et al.* (1976a)
-54.30	6.00	40.0	5	41.5	0.067	*Sclater et al.* (1978)
-53.50	9.00	39.0	5	38.5	0.060	*Sclater et al.* (1978)
-52.20	14.00	36.0	5	33.6	0.051	*Norton* (1976)
-53.00	25.50	27.0	15	23.8	0.005	*DeMets et al.* (1988)
-51.00	29.00	25.0	8	20.6	0.015	*DeMets et al.* (1988)
-48.00	32.00	19.0	15	17.8	0.004	*DeMets et al.* (1988)
-45.50	35.20	15.0	3	15.1	0.097	*Fisher & Sclater* (1983)
-44.30	38.20	16.0	10	12.8	0.009	*Bergh & Norton* (1976)
-43.80	39.30	13.0	5	12.0	0.036	*Fisher & Sclater* (1983)
-42.00	42.60	8.0	4	9.6	0.059	*Fisher & Sclater* (1983)
-39.40	46.20	8.0	3	7.2	0.118	*Fisher & Sclater* (1983)
-36.70	52.30	4.0	4	3.6	0.077	*Fisher & Sclater* (1983)
-35.70	53.30	6.0	5	3.1	0.052	*Fisher & Sclater* (1983)
-35.10	54.10	7.0	7	2.7	0.028	*Fisher & Sclater* (1983)
-33.00	57.00	2.0	3	1.3	0.171	*Sclater et al.* (1981)
-31.70	58.40	2.0	5	0.8	0.067	*Sclater et al.* (1981)
-30.00	60.80	-4.0	5	-0.1	0.074	*Sclater et al.* (1981)

Africa-Antarctica: Slip Vectors

-54.85	0.89	51.0	15	46.6	0.009	CMT 2.19.77
-54.76	1.42	50.0	20	46.1	0.005	CMT 3.29.85
-54.60	1.70	47.0	10	45.8	0.019	*Forsyth* (1975)
-54.48	2.07	44.0	15	45.4	0.008	CMT 12.17.78
-54.37	5.82	34.0	15	41.7	0.008	CMT 11.17.79
-54.40	5.90	40.0	10	41.7	0.017	*Forsyth* (1975)
-53.90	8.70	47.0	10	38.9	0.015	*Norton* (1976)
-53.20	9.94	37.0	20	37.6	0.004	CMT 1.5.86
-52.98	10.08	36.0	15	37.4	0.006	CMT 1.10.86
-53.35	26.10	23.0	10	23.4	0.011	*Wald & Wallace* (1986)
-52.92	26.26	20.0	10	23.2	0.011	*Wald & Wallace* (1986)
-52.48	27.99	24.0	10	21.7	0.010	*Wald & Wallace* (1986)
-52.08	28.02	20.0	10	21.6	0.010	CMT 8.3.83
-51.87	28.07	18.0	10	21.5	0.010	CMT 12.8.77
-51.84	28.23	20.0	10	21.4	0.010	*Wald & Wallace* (1986)
-51.89	28.93	20.0	15	20.8	0.004	PDE 8.83
-50.90	29.10	26.0	15	20.6	0.004	*Norton* (1976)
-48.43	31.38	24.0	15	18.4	0.004	CMT 11.11.86
-48.20	31.76	12.0	25	18.0	0.001	CMT 6.6.84
-47.67	32.54	17.0	15	17.4	0.004	CMT 8.21.78
-47.13	32.49	15.0	20	17.3	0.002	CMT 8.26.78
-45.60	34.10	17.0	15	15.9	0.004	*Norton* (1976)
-45.54	35.13	18.0	15	15.2	0.004	*Wald & Wallace* (1986)
-45.44	34.98	10.0	10	15.3	0.009	*Wald & Wallace* (1986)
-44.90	35.70	25.0	15	14.7	0.004	*Norton* (1976)
-43.70	39.50	8.0	10	11.8	0.009	*Wald & Wallace* (1986)
-43.43	40.78	3.0	10	10.9	0.009	*Wald & Wallace* (1986)
-42.96	41.96	9.0	15	10.1	0.004	CMT 10.14.86
-38.90	46.20	14.0	15	7.2	0.005	*Norton* (1976)
-39.09	46.24	5.0	20	7.2	0.003	CMT 3.12.79
-36.20	52.50	5.0	20	3.5	0.003	*Norton* (1976)
-36.44	52.85	2.0	15	3.3	0.006	PDE 5.84
-35.69	53.41	4.0	15	3.0	0.006	CMT 12.17.85
-35.63	53.50	5.0	15	3.0	0.006	CMT 12.17.85
-34.77	54.13	3.0	15	2.7	0.006	CMT 12.24.85
-32.00	57.11	-5.0	25	1.4	0.003	CMT 5.25.86
-32.64	57.48	6.0	25	1.1	0.003	CMT 3.1.87
-29.85	60.73	5.0	15	0.0	0.008	CMT 1.23.81
-29.94	60.82	5.0	15	-0.1	0.008	CMT 11.29.82

Australia-Africa: Spreading Rates

-12.00	66.00	37	4	35.8	0.044	n35w	*Fisher et al.* (1971)
-12.37	66.51	39	5	36.5	0.028	n35w	NGDC *Chain* 99 5
-12.78	66.40	36	6	36.8	0.019	n35w	NGDC *Circe* 6
-15.52	67.00	37	10	39.6	0.006	n35w	NGDC *Conrad* 14 12
-16.00	66.00	38	4	39.4	0.040	n30w	*Fisher et al.* (1971)
-18.93	65.87	42	3	42.2	0.066	n30w	NGDC *Antipodes* 5
-19.50	66.00	41	3	42.8	0.065	n30w	*Fisher et al.* (1971)
-19.58	68.76	46	8	44.2	0.009	n30w	NGDC *Vema* 29 3
-20.30	66.50	44	4	43.7	0.036	n30w	*McKenzie & Sclater* (1971)
-21.39	68.65	45	3	45.7	0.061	n30w	NGDC *Vema* 18 11
-21.57	69.00	45	4	46.0	0.034	n30w	NGDC *Dodo* 8
-21.95	67.96	47	3	45.9	0.061	n30w	NGDC *Vema* 20 9
-23.82	69.66	51	4	48.2	0.032	n30w	NGDC *Indomed* 6
-24.43	69.63	51	5	48.7	0.020	n30w	NGDC *Indomed* 6
-24.50	69.84	50	3	48.9	0.057	n30w	NGDC *Indomed* 6
-24.77	69.80	50	4	49.1	0.032	n30w	NGDC *Indomed* 6
-24.94	69.88	50	3	49.3	0.056	n30w	NGDC *Monsoon* 4a

Australia-Africa: Transform Azimuths

-5.50	68.50	45.0	5	44.0	0.089	*Fisher et al.* (1971)
-9.00	67.30	52.0	3	50.6	0.214	*Engel & Fisher* (1975)
-13.50	66.50	57.0	3	56.7	0.177	*Engel & Fisher* (1975)
-16.00	66.50	60.0	5	58.8	0.057	*Fisher et al.* (1971)
-17.40	66.20	62.0	3	60.4	0.151	*Engel & Fisher* (1975)
-20.00	67.00	60.0	10	61.0	0.012	*Fisher et al.* (1971)
-22.50	69.00	65.0	15	59.8	0.005	*Fisher et al.* (1971)

Australia-Africa: Slip Vectors

-8.94	67.67	40.0	20	49.9	0.005	CMT 10.12.78
-9.32	67.18	48.0	15	51.2	0.008	CMT 8.19.81
-12.11	65.40	52.0	15	57.2	0.008	CMT 10.27.84
-13.61	65.90	55.0	20	57.7	0.004	CMT 8.14.78
-13.68	66.29	65.0	15	57.2	0.007	D. Woods (personal communication, 1985)
-14.04	65.93	54.0	15	58.1	0.007	CMT 6.11.84
-16.58	66.77	57.0	15	58.9	0.006	CMT 12.1.85
-17.20	66.79	56.0	15	59.3	0.006	CMT 4.14.80
-17.21	66.67	58.0	15	59.5	0.006	CMT 11.7.81
-17.55	66.04	57.0	20	60.7	0.003	CMT 8.22.79
-17.97	65.36	58.0	20	62.1	0.003	CMT 11.29.80
-18.07	65.62	57.0	15	61.7	0.006	CMT 9.17.84
-19.86	66.43	66.0	15	61.7	0.005	CMT 6.21.86
-20.43	67.92	65.0	20	59.9	0.003	CMT 9.23.83
-23.01	69.26	54.0	25	59.7	0.002	CMT 9.24.78
-23.01	69.17	48.0	25	59.8	0.002	CMT 8.21.85
-23.04	69.07	61.0	25	60.0	0.002	CMT 8.21.85

Australia-Antarctica: Spreading Rates

-25.81	70.23	56	3	57.6	0.062	n45w	NGDC *Indomed* 6
-26.17	71.57	57	3	58.6	0.060	n45w	NGDC *Indomed* 6
-26.37	71.96	58	3	58.9	0.059	n45w	NGDC *Indomed* 6
-26.67	72.07	59	3	59.1	0.059	n45w	NGDC *Indomed* 6
-27.00	72.70	63	4	60.0	0.032	n45w	NGDC *Dodo* 8
-28.00	74.00	60	10	60.9	0.005	n45w	*Sclater et al.* (1976b)
-28.00	74.20	61	4	61.0	0.031	n45w	NGDC *Vema* 29 03
-29.50	75.20	60	6	62.2	0.013	n45w	NGDC *DSDP* 26
-31.30	75.90	63	5	63.5	0.018	n45w	*Schlich* (1982)
-32.20	77.10	63	5	64.4	0.017	n45w	*Schlich* (1982)
-34.80	78.60	65	5	66.2	0.016	n45w	*Schlich* (1982)
-36.00	78.80	67	5	66.8	0.016	n45w	*Schlich* (1982)
-40.90	78.80	69	5	68.8	0.015	n45w	*Schlich* (1982)
-41.30	81.30	70	7	69.5	0.007	n50w	NGDC *Conrad* 11-05
-42.40	90.00	73	5	72.1	0.013	n55w	*McKenzie & Sclater* (1971)
-42.40	90.10	72	7	72.1	0.007	n55w	NGDC *Eltanin* 49
-43.50	92.60	74	10	73.0	0.003	n55w	NGDC *Eltanin* 47
-44.00	93.80	73	10	73.3	0.003	n55w	NGDC *Conrad* 8-02
-46.90	96.40	71	5	74.1	0.013	n60w	NGDC *Eltanin* 54
-49.75	110.20	73	5	75.4	0.014	n70w	NGDC *Eltanin* 49
-50.10	111.80	74	5	75.4	0.015	n70w	NGDC *DSDP* 28
-50.00	114.00	75	6	75.4	0.010	n70w	*Weissel & Hayes* (1972)
-49.80	118.70	76	2	75.1	0.101	n71w	*Vogt et al.* (1983)
-49.80	121.90	75	3	75.0	0.068	n75w	*Vogt et al.* (1983)

Table 3. (*continued*)

-50.00	125.00	76	3	74.5	0.049	n83w	*Vogt et al.* (1983)
-50.10	128.50	75	2	74.2	0.117	n83w	*Vogt et al.* (1983)
-50.40	131.00	73	2	73.8	0.123	n83w	*Vogt et al.* (1983)
-50.20	131.80	73	3	73.7	0.055	n85w	NGDC *Eltanin* 41A
-50.20	131.90	75	5	73.7	0.020	n85w	NGDC *Eltanin* 35
-50.20	132.10	73	4	73.6	0.031	n85w	NGDC *Eltanin* 41
-50.30	132.50	73	4	73.6	0.031	n85w	NGDC *Eltanin* 41
-50.30	133.90	73	3	73.3	0.057	n85w	NGDC *Eltanin* 39
-50.40	135.00	73	3	73.1	0.059	n85w	NGDC *Eltanin* 34
-52.00	140.00	72	5	71.8	0.022	s85w	NGDC *Eltanin* 36
-54.70	145.00	70	3	70.6	0.067	s80w	NGDC *Eltanin* 34
-62.50	157.80	68	4	67.5	0.039	s60w	NGDC *Eltanin* 27
-62.40	158.10	69	3	67.4	0.070	s60w	NGDC *Eltanin* 37
-62.30	158.60	68	4	67.3	0.039	s60w	NGDC *Aries* 2

Australia-Antarctica: Transform Azimuths

-26.20	71.00	47.0	5	47.0	0.037	*Tapscott et al.* (1980)
-36.50	79.00	48.0	15	44.4	0.003	*McKenzie & Sclater* (1971)
-39.50	78.50	42.0	15	45.9	0.003	*McKenzie & Sclater* (1971)
-41.00	80.50	39.0	15	44.6	0.003	*McKenzie & Sclater* (1971)
-43.00	84.50	34.0	15	41.6	0.003	*McKenzie & Sclater* (1971)
-46.00	96.00	29.0	15	32.8	0.003	*McKenzie & Sclater* (1971)
-49.60	120.50	16.0	4	14.4	0.034	*Vogt et al.* (1983)
-49.30	121.50	17.0	6	13.7	0.015	*Vogt et al.* (1983)
-49.00	126.10	12.0	5	10.3	0.022	*Vogt et al.* (1983)
-49.30	127.30	11.0	3	9.4	0.061	*Vogt et al.* (1983)
-52.00	140.00	-6.0	10	-1.0	0.006	*DeMets et al.* (1988)
-56.50	147.50	-13.0	8	-8.8	0.010	*DeMets et al.* (1988)
-61.50	154.50	-26.0	10	-17.2	0.007	*DeMets et al.* (1988)

Australia-Antarctica: Slip Vectors

-36.84	78.17	51.0	15	45.2	0.003	CMT 7.18.85
-36.65	78.68	46.0	15	44.7	0.003	CMT 3.20.79
-36.20	78.81	51.0	15	44.4	0.003	CMT 7.14.81
-38.35	78.05	43.0	15	45.9	0.003	CMT 11.16.85
-38.91	78.08	38.0	15	46.0	0.003	D. Woods (personal communication, 1985)
-37.44	78.19	54.0	20	45.4	0.002	CMT 4.13.87
-38.85	78.31	45.0	15	45.8	0.003	CMT 12.28.86
-38.50	78.70	37.0	15	45.3	0.003	D. Woods (personal communication, 1985)
-40.44	78.50	39.0	10	46.2	0.007	D. Woods (personal communication, 1985)
-41.63	79.66	52.0	10	45.5	0.007	CMT 6.25.81
-41.76	80.07	61.0	10	45.2	0.007	D. Woods (personal communication, 1985)
-41.17	80.49	30.0	10	44.6	0.007	D. Woods (personal communication, 1985)
-41.31	80.52	49.0	10	44.6	0.007	D. Woods (personal communication, 1985)
-41.32	80.51	49.0	15	44.6	0.003	CMT 8.21.80
-42.37	83.97	25.0	25	41.9	0.001	CMT 7.4.79
-41.20	85.47	43.0	20	40.3	0.002	CMT 7.29.79
-43.39	91.66	50.0	20	35.8	0.001	CMT 9.7.84
-46.09	95.41	21.0	15	33.3	0.003	CMT 6.9.82
-45.15	95.80	59.0	25	32.9	0.000	CMT 6.13.85
-45.76	96.05	36.0	15	32.8	0.003	CMT 3.2.87
-45.80	96.10	17.0	10	32.7	0.006	*Banghar & Sykes* (1969)
-45.56	96.18	36.0	15	32.6	0.003	CMT 1.16.79
-45.47	96.29	28.0	10	32.5	0.006	D. Woods (personal communication, 1985)
-47.80	99.27	31.0	15	30.5	0.003	CMT 3.21.81
-47.87	99.42	27.0	15	30.4	0.003	CMT 5.23.77
-47.35	100.03	33.0	15	29.9	0.003	CMT 2.14.82
-47.21	100.04	35.0	20	29.8	0.001	CMT 4.30.86
-48.96	121.27	15.0	20	13.9	0.001	CMT 6.16.86
-49.54	125.96	16.0	10	10.3	0.001	CMT 3.11.80
-49.65	125.98	9.0	15	10.3	0.002	CMT 12.9.83
-49.13	127.27	9.0	25	9.4	0.000	CMT 6.5.87
-50.95	138.99	-3.0	15	0.1	0.003	CMT 12.5.86
-51.02	139.36	0.0	20	-0.2	0.001	CMT 7.6.80
-51.76	139.60	-6.0	20	-0.6	0.001	CMT 6.23.83
-53.80	140.80	-5.0	20	-2.2	0.002	CMT 2.27.78
-54.17	143.80	-6.0	15	-4.8	0.003	CMT 1.11.85
-54.29	143.73	-5.0	20	-4.8	0.002	CMT 12.26.86
-54.52	144.72	-6.0	15	-5.7	0.003	CMT 10.13.77

-55.20	146.10	-13.0	15	-7.1	0.003	*Banghar & Sykes* (1969)
-55.11	146.15	-12.0	15	-7.1	0.003	CMT 11.26.85
-55.30	146.20	-22.0	25	-7.2	0.001	*Banghar & Sykes* (1969)
-54.98	146.30	-8.0	15	-7.2	0.003	CMT 7.3.85
-55.29	146.03	-14.0	20	-7.1	0.002	CMT 9.27.81
-55.53	146.41	-10.0	15	-7.5	0.003	CMT 5.4.84
-55.64	146.93	-5.0	20	-8.0	0.002	CMT 6.28.81
-56.32	146.62	-14.0	20	-8.0	0.002	CMT 6.27.78
-55.49	147.06	-9.0	15	-8.0	0.003	CMT 4.6.84
-55.49	147.42	-38.0	25	-8.3	0.001	CMT 12.23.80
-55.80	147.32	-12.0	20	-8.4	0.002	CMT 8.19.80
-55.84	147.25	-12.0	20	-8.3	0.002	CMT 5.9.80
-56.30	146.93	-12.0	20	-8.2	0.002	CMT 6.16.85
-56.57	147.33	-7.0	20	-8.7	0.002	CMT 6.20.79
-56.63	147.44	-13.0	15	-8.8	0.003	CMT 2.24.87
-56.74	147.53	-18.0	15	-8.9	0.003	CMT 1.27.84
-56.75	147.19	-15.0	15	-8.6	0.003	CMT 5.31.86
-56.83	147.32	-12.0	20	-8.8	0.002	CMT 12.1.86
-57.42	147.62	-14.0	20	-9.2	0.002	CMT 8.5.79
-57.59	148.08	-11.0	15	-9.7	0.003	CMT *Scott & Kanamori* (1985)
-58.94	149.11	-14.0	20	-11.2	0.002	CMT 12.12.80
-59.76	149.47	-19.0	15	-11.8	0.003	CMT 7.8.85
-59.78	150.24	-10.0	15	-12.5	0.003	CMT 4.9.81
-59.63	150.29	-17.0	15	-12.5	0.003	CMT 9.11.77
-60.04	150.59	-17.0	15	-13.0	0.003	CMT 9.26.77
-60.05	152.98	-21.0	15	-15.2	0.003	CMT 7.5.86
-60.16	153.18	-23.0	15	-15.4	0.003	CMT 12.31.84
-60.17	154.71	-28.0	15	-16.8	0.003	CMT 4.25.85
-60.65	154.37	-22.0	15	-16.7	0.003	CMT 6.13.81
-61.16	153.87	-21.0	20	-16.4	0.002	CMT 1.28.87
-61.27	154.37	-25.0	20	-17.0	0.002	CMT 10.17.79
-61.30	154.78	-24.0	20	-17.4	0.002	CMT 4.2.78
-61.31	154.05	-22.0	20	-16.7	0.002	CMT 10.12.80
-61.50	154.34	-22.0	20	-17.0	0.002	CMT 5.14.78
-61.67	154.95	-23.0	20	-17.7	0.002	CMT 2.21.81
-61.81	154.31	-25.0	15	-17.1	0.003	CMT 7.23.86
-61.86	154.81	-30.0	15	-17.6	0.003	CMT 4.27.83
-62.51	155.02	-26.0	15	-18.1	0.003	CMT 3.1.86
-62.95	155.77	-24.0	20	-19.0	0.002	CMT 4.6.87
-63.09	155.72	-23.0	15	-19.0	0.003	CMT 5.8.85

Arabia-India: Fault Trends

21.00	61.80	30.0	5	27.8	0.459	*Matthews* (1966)
18.00	60.20	23.0	5	22.3	0.534	*Matthews* (1966)

Arabia-India: Slip Vectors

24.58	66.23	41.0	15	37.5	0.270	*Quittmeyer & Kafka* (1984)
23.79	64.73	28.0	15	34.6	0.176	*Quittmeyer & Kafka* (1984)
21.87	62.32	12.0	15	29.5	0.067	*Quittmeyer & Kafka* (1984)
20.91	62.44	26.0	15	28.3	0.055	CMT 4.7.85
14.94	57.96	23.0	15	16.4	0.171	CMT 12.14.85
14.57	58.09	10.0	15	16.0	0.188	CMT 12.5.81

Africa-India: Spreading Rates

9.95	57.51	25	3	24.5	0.175	s60e	NGDC *USS Wilkes*
9.50	58.50	27	4	25.3	0.083	s60e	*McKenzie & Sclater* (1971)
7.90	59.10	26	4	25.9	0.057	s50e	*McKenzie & Sclater* (1971)
7.25	59.60	27	3	26.5	0.093	s50e	NGDC *USS Wilkes*
7.06	59.87	28	3	26.7	0.091	s50e	NGDC *Vema* 19 10
6.80	60.00	29	3	26.9	0.089	s50e	*McKenzie & Sclater* (1971)
6.84	60.16	25	4	27.0	0.050	s50e	NGDC *Vema* 19 10
6.72	60.18	25	3	27.0	0.088	s50e	NGDC *Vema* 19 10
5.54	61.66	29	3	28.3	0.088	s50e	NGDC *Indomed* 4
5.43	61.70	29	3	28.4	0.089	s50e	NGDC *Vema* 34 08
5.30	61.80	27	4	28.5	0.050	s50e	*McKenzie & Sclater* (1971)
4.20	62.20	28	4	29.2	0.055	s50e	*McKenzie & Sclater* (1971)
4.20	62.20	27	5	29.2	0.035	s50e	*McKenzie & Sclater* (1971)
3.70	63.30	29	5	29.9	0.041	s50e	*McKenzie & Sclater* (1971)
1.48	67.01	33	10	32.2	0.021	s45e	NGDC *Chain* 100 5
-0.05	67.35	33	10	33.0	0.026	s45e	NGDC *Antipodes* 10
-0.10	67.17	32	10	32.9	0.026	s45e	NGDC *Vema* 34 6
-2.83	67.10	32	5	30.4	0.162	s25e	NGDC *Conrad* 12 15

Africa-India: Transform Azimuths

11.00	57.50	210.0	5	208.3	0.204	*Laughton et al.* (1970)
0.50	67.00	223.0	10	214.6	0.047	*Fisher et al.* (1971)

Table 3. (*continued*)

Africa-India: Slip Vectors

10.76	57.00	216.0	15	209.0	0.024		CMT 9.17.86
11.28	57.49	209.0	15	207.9	0.022		CMT 4.8.83
11.28	57.25	209.0	15	208.0	0.023		CMT 5.30.78
11.74	57.71	208.0	15	207.1	0.021		CMT 4.20.80
-1.00	67.45	214.0	15	215.6	0.023		CMT 5.9.85
-1.40	67.77	215.0	15	215.7	0.023		CMT 9.9.85
-1.41	67.75	217.0	15	215.7	0.023		CMT 7.16.81

Africa-Arabia: Spreading Rates

13.50	57.50	24	4	25.2	0.053	s58e	*Cochran* (1981)
13.70	57.30	25	4	25.0	0.050	s58e	*Cochran* (1981)
13.90	57.00	25	4	24.7	0.047	s58e	*Cochran* (1981)
14.50	56.80	24	3	24.4	0.077	s58e	*Cochran* (1981)
14.60	56.40	24	3	24.1	0.072	s58e	*Cochran* (1981)
14.70	55.90	24	3	23.6	0.091	s80e	*Cochran* (1981)
14.90	55.60	23.5	3	23.8	0.078	s73e	*Laughton et al.* (1970)
14.80	54.80	23	3	23.3	0.068	s73e	*Laughton et al.* (1970)
14.41	53.60	24	3	22.6	0.056	s73e	*Laughton et al.* (1970)
13.20	51.00	19	4	21.5	0.023	s68e	*Cochran* (1981)
13.40	50.90	21	4	21.3	0.023	s68e	*Laughton et al.* (1970)
13.50	50.70	21	3	21.2	0.039	s68e	*Laughton et al.* (1970)
13.40	50.40	21.5	3	20.9	0.038	s70e	*Tamsett & Girdler* (1982)
12.15	45.85	15	3	17.3	0.063	s80e	*Girdler et al.* (1980)
12.15	45.65	18.5	2.5	17.1	0.065	s80e	*Girdler et al.* (1980)
12.10	45.55	16	3	17.1	0.066	s80e	*Tamsett & Girdler* (1982)
12.08	45.47	18.5	2.5	17.0	0.067	s80e	*Girdler et al.* (1980)
12.05	45.25	17.5	2.5	16.9	0.069	s80e	*Girdler et al.* (1980)
12.05	45.17	16.5	2.5	16.8	0.070	s80e	*Girdler et al.* (1980)
12.10	45.10	16.5	2.5	16.8	0.071	s80e	*Girdler et al.* (1980)
12.10	44.92	16.5	2.5	16.6	0.073	s80e	*Girdler et al.* (1980)
12.15	44.81	16	3	16.6	0.074	s80e	*Girdler et al.* (1980)
12.05	44.59	15.5	2.5	15.7	0.077	s85e	*Girdler et al.* (1980)
12.08	44.50	15.5	2.5	15.6	0.078	s85e	*Girdler et al.* (1980)
12.05	44.29	16.5	2.5	15.5	0.081	s85e	*Girdler et al.* (1980)

Africa-Arabia: Transform Azimuths

13.90	51.70	206.0	5	205.5	0.208	R. Searle (personal communication, 1987)
13.30	49.60	209.0	7	207.8	0.102	*Tamsett & Searle* (1988)
13.20	49.40	208.0	5	208.1	0.198	*Tamsett & Searle* (1988)
12.60	48.00	205.0	5	210.3	0.195	*Tamsett & Searle* (1988)

Africa-Arabia: Slip Vectors

14.64	53.77	203.0	20	203.3	0.014	CMT 7.8.79
14.29	51.82	208.0	15	204.8	0.024	CMT 1.28.84
14.00	51.70	210.0	15	205.3	0.023	*Sykes* (1970)
13.78	51.62	203.0	20	205.7	0.013	CMT 12.22.79

''ι'' is the data importance, a measure of the information content of a datum (*Minster et al.*, 1974). ''σ'' is the standard error assigned to a datum. Rates and their standard errors are listed in millimeters per year. Azimuths and their standard errors are listed in degrees clockwise from north. All rates were determined by comparison of observed profiles to synthetic magnetic anomaly profiles that we computed. Rates determined from data we obtained from the National Geophysical Data Center data are referenced NGDC. Slip vectors referenced as CMT are determined from Harvard centroid-moment tensor solutions (Dziewonski *et al.*, 1981, 1983abc, 1984abc, 1985abcd, 1986abc, 1987abcdefg, 1988abcd). Slip vectors referenced as PDE are from the U.S. Geological Survey *Preliminary Determination of Epicenters* bulletins.

minima. Chase's rate fitting function, which fits the spreading rate measured perpendicular to the ridge (Fig. 2), has a further advantage over Minster *et al.*'s (1974), which fits the total plate separation rate, because the latter formulation presumes the direction of plate motion is known before it is solved for. On the other hand, Minster *et al.*'s (1974) formulation simplifies implementation of constraint equations fixing the latitude and longitude of an Euler vector.

Importances (Table 3) measure the information contribu-

tion of each datum to the model (Minster *et al.* 1974). The importance of a datum depends on its assigned uncertainty and on how much it duplicates information contributed by other data. The total data importance equals the number of independent model parameters, which is 33 for the 12-plate NUVEL-1 model. The procedures used to evaluate the consistency of the data with plate circuit closure are similar to those previously described (Gordon *et al.* 1987; DeMets *et al.* 1988; Argus *et al.* 1989).

DATA

The 1122 data from 22 plate boundaries (Table 3) describe current plate motions more accurately than do the 260 and 330 data used to derive models P071 and RM2, respectively (Fig. 3). Only 107 data, mainly slip vectors, are carried over from prior global data sets. The data comprise 277 spreading rates, 121 transform azimuths, and 724 slip vectors (504 from CMT solutions and 90 from other studies using waveform analysis) (Fig. 4). The data include new marine geophysical data (mainly magnetic profiles) covering several previously poorly surveyed regions: the Arctic Ridge, the Mid-Atlantic Ridge north of Iceland, the Chile Rise, portions of the Southwest and Southeast Indian ridges, the southern Mid-Atlantic ridge, and the American–Antarctic Ridge. Rates were determined only from analysis of magnetic anomalies across mid-ocean ridges. Earthquake slip vectors were rotated to the horizontal. No data from continent–continent or other diffuse plate boundaries were used, but we used many slip vectors from subduction zones where oceanic lithosphere underthrusts continental lithosphere. We avoided using slip vectors from regions where the seismicity in the overriding plate is widely dispersed.

All but 10 of the transform faults with azimuths that we used offset two mid-ocean ridge segments. Except for transforms in the Gulf of California, all transforms offsetting mid-ocean ridges are within oceanic lithosphere. The five transforms north of the Gulf Rise are in a more complex
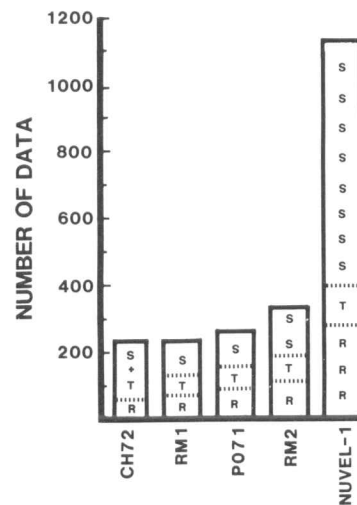
Figure 3. Number of data used to derive various global plate motion models: CH72 (Chase 1972), RM1 (Minster *et al.* 1974), P071 (Chase 1978), RM2 (Minster & Jordan 1978), and NUVEL-1. Data are of three types: slip vector azimuths (S), transform fault azimuths (T), and spreading rates (R).
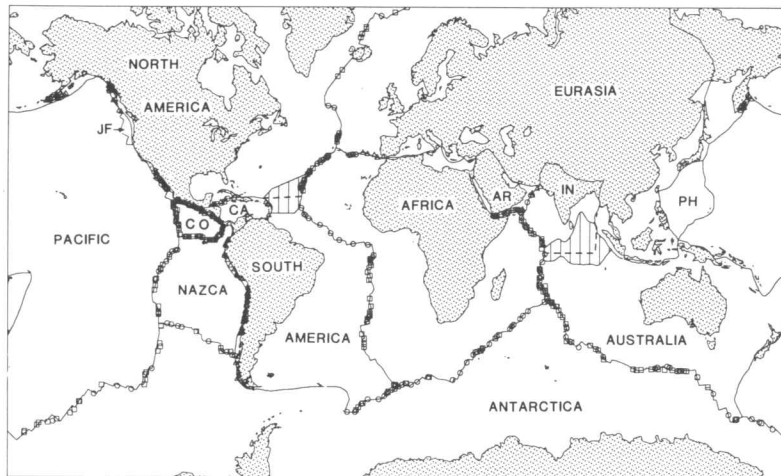
Figure 4. Data locations and plate geometry assumed for NUVEL-1. Regions with vertical lines mark diffuse plate boundaries between North and South America and between India and Australia. Within each of these diffuse boundaries a dashed line shows the discrete boundary assumed in NUVEL-1. Squares show locations of spreading rates, circles show locations of transform azimuths, and triangles show earthquake locations for slip vectors (except those along transform faults offsetting mid-ocean ridges, which are omitted for clarity). Also shown are two plates (Philippine and Juan de Fuca) omitted from NUVEL-1, but included in Table 1 for completeness. Plate name abbreviations: Cocos (CO), Caribbean (CA), Indian (IN), Arabian (AR), Philippine (PH), and Juan de Fuca (JF). Mercator projection.

setting and probably offset both continental and young oceanic crust. The other non-ridge–ridge transform faults used are the Gloria Fault along the Azores–Gibraltar ridge, the Swan and Oriente transforms along the Caribbean–North America boundary, the Panama transform fault along the Cocos–Nazca boundary, and the South Sandwich transform, which extends westward from the southern end of the American–Antarctic Ridge.

Many of the new data are more accurate than the typical data available a few years ago. In prior global plate motion models, transform azimuths were usually estimated from the trends of transform valleys, which are typically a few hundreds of kilometres long and 15–20 km wide. Side-scan and high resolution sonar systems such as GLORIA, Seabeam, and Seamarc resolve much narrower tectonic elements of transform faults. The widest of these elements is termed the transform tectonized zone, is defined as the zone on which all current and past strike–slip faulting has occurred, and is typically 3–10 km wide on slowly slipping transforms. Recent strike–slip motion is taken up in a narrower region, termed the transform fault zone, which is usually centred about the axis of maximum depth, is characterized by a narrow (500 m–2 km) belt of disrupted terrain, and can be traced along most transform valleys from one ridge-transform nodal basin to the other. Within several well-mapped transform fault zones, many fault strands appear to link up to form a single through-going strand, the principal transform displacement zone, along which most of the motion across the transform is taken up (Fox & Gallo, 1984, 1986; Searle 1986). Where transform tectonized zones, transform fault zones, or principal transform displacement zones have been mapped, the directions of plate motion are now known with improved accuracy, and in many places differ significantly from those adopted in prior models.

We also used undulations in the marine geoid measured with the Seasat altimeter to estimate the strikes of some transform faults in poorly sounded regions (Sandwell 1984; Haxby 1987). We used the geoidal signature of inactive

fracture zones to estimate the locations of ridge-transform intersections. The transform strike is estimated from the trend of the great circle connecting the estimated locations of ridge-transform intersections at the two ends of a transform fault. Because of Seasat's low spatial resolution and the obscure signature of the active traces of transform faults, transform strikes derived from only Seasat data typically are much more uncertain than those derived in whole or part from bathymetric data.

On isolated or widely separated magnetic profiles, the best-fitting spreading rate can be inaccurate because of unidentified fracture zones and propagating rifts. Recent aeromagnetic surveys consisting of many closely spaced profiles perpendicular to the strike of spreading ridges permit identification of propagating rifts and short-offset fracture zones, and permit anomalies to be confidently correlated.

Prior global plate motion models mainly used earthquake mechanisms based only on body-wave first motions. Many new mechanisms incorporate body and surface waveform modelling, as well as first-motion data, and give more accurate slip vectors. CMT solutions, derived using long-period body and surface waves (Dziewonski, Chou & Woodhouse 1981; Dziewonski & Woodhouse 1983) recorded on the Global Digital Seismic Network, provide thousands of earthquake focal mechanisms with nearly complete geographic coverage of the plate boundaries. We used 504 focal mechanisms selected from the ~5800 CMT mechanisms available in mid-1988.

OVERVIEW OF THE NUVEL-1 MODEL

NUVEL-1 describes the current motion of 12 assumed-rigid plates (Fig. 4). Because of the incommensurate time intervals averaged by the different types of data, we cannot define the interval averaged by NUVEL-1 precisely. Transform faults average the direction of plate motion over an unknown interval, which may be several million years

long, whereas earthquake slip vectors average plate motion directions over years, tens of years, and perhaps hundreds of years when the recurrence interval between earthquakes is long. Because we determined spreading rates consistently as 3.0-m.y. averages, we refer to the NUVEL-1 model as a 3-m.y.-average plate motion model.

The global circuit comprises a network of plate pairs with common boundaries along which plate motion data are available (Fig. 5). The NUVEL-1 plate geometry differs from that used to derive models P071 and RM2. The most important difference is the Indian Ocean plate geometry. Prior global models assumed that India and Australia lie on a single plate, which was divided from the Arabian plate by the Owen fracture zone. Wiens *et al.* (1985) proposed that India and Australia lie on separate plates divided by a diffuse equatorial plate boundary that extends eastward from the Central Indian Ridge, through Chagos Bank, to the Ninetyeast Ridge where it may continue northeastward to the Sumatra Trench. Wiens *et al.* (1985) further proposed that only negligible motion occurs along the Owen fracture zone and, therefore, India and Arabia are part of a single Indo-Arabian plate. Later analysis of magnetic anomaly profiles and bathymetric data along the Central Indian and Carlsberg ridges (Gordon *et al.* 1989) shows that motion between Australia and India was only about one third as fast as proposed by Wiens *et al.* (1985), and that motion along the Owen fracture zone is slow, about 2 mm yr^{-1} (Gordon & DeMets 1989). We thus adopt a plate geometry with separate Indian, Arabian, and Australian plates.

It is unclear whether to treat Nubia (West Africa) and Somalia (East Africa) as separate plates as in P071, or as a single plate, ignoring extension along the East African rift, as in RM2. We used no azimuths from Red Sea transforms because the transforms, if any exist, have very short offsets. We found that global models with distinct Nubian and Somalian plates predicted slow (~3 mm yr^{-1}), right-lateral slip along the East African rift. Because this unsuccessful

model disagrees with the observed E–W extension in the East African rift, we treat Africa as a single plate, and omit both azimuths and spreading rates from the Red Sea.

As in RM2, but differing from P071, we included a Caribbean plate, but not a Philippine plate. If we assume that North America and South America are divided by a discrete boundary, Mid-Atlantic Ridge plate motion data are best fit if the boundary intersects the Mid-Atlantic Ridge between 16 °N and 22 °N (Argus & Gordon 1989). Thus we divide the plate motion data at 19 °N, assigning data along the Mid-Atlantic Ridge north of 19 °N to North America–Africa, and data south of 19 °N to South America–Africa.

Table 2 lists the NUVEL-1 Euler vectors and their standard errors. Figs 6(a)–(c) show locations of the NUVEL-1 Euler vectors, best-fitting Euler vectors (Table 4), and the P071 and RM2 Euler vectors. Comparison of the standard errors of best-fitting Euler vectors with those of NUVEL-1 Euler vectors (Tables 2 and 4) shows that the latter are always equal to or smaller than the former, which is a direct consequence of the information added by plate circuit closures. The 3-D standard error ellipsoids are constructed from 3×3 matrices extracted from the 33 by 33 variance–covariance matrix, which describes the model uncertainties linearly propagated from the errors assigned to the data. The error regions listed in Table 2 are useful approximations to the model errors, which are fully described by the complete variance–covariance matrix (Table 5).

NUVEL-1 differs significantly from prior global models. One test of how much NUVEL-1 differs from prior models is whether a prior Euler vector lies within the 3-D 99 per cent confidence ellipsoid of the corresponding NUVEL-1 Euler vector. For the 30 pairs of plates sharing a common boundary, only one of the P071 Euler vectors and only five of the RM2 Euler vectors lie within the NUVEL-1 99 per cent confidence ellipsoids, and none of the P071 Euler vectors and only three of the RM2 Euler vectors lie within

GLOBAL PLATE CIRCUIT
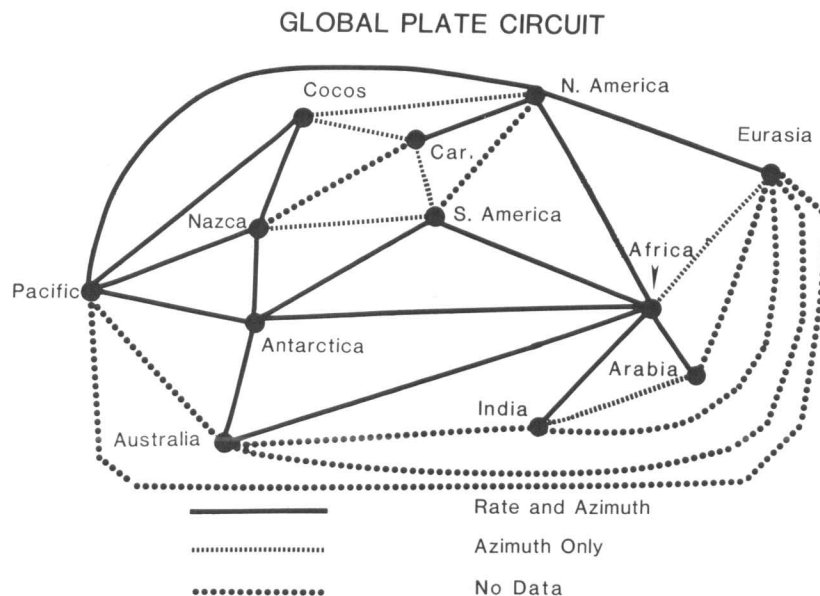
Figure 5. The NUVEL-1 network of plate circuit closures. The nodes (solid circles) represent the plates included in the model. The lines, which represent boundaries between plates, are coded by the types of data available along them.
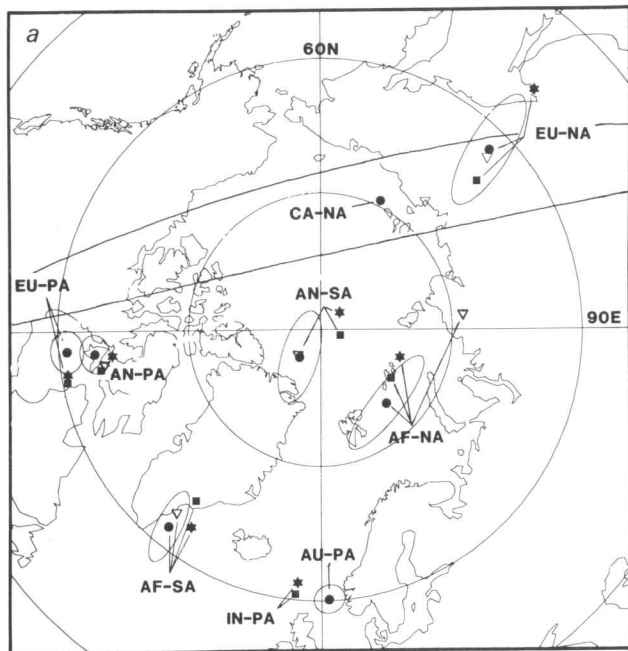
Figure 6(a). Location of some of the NUVEL-1 Euler poles (solid circles) and their 2-D 95 per cent confidence regions describing motion between the African (AF), Antarctic (AN), Australian (AU), Caribbean (CA), Eurasian (EU), Indian (IN), North American (NA), Pacific (PA), and South American (SA) plates. Best-fitting poles (open triangles), model P071 (Chase 1978) Euler poles (stars), and model RM2 (Minster & Jordan 1978) Euler poles (squares) are also shown. For each Euler pole, the first plate listed rotates counter-clockwise relative to the second plate.

the NUVEL-1 95 per cent confidence ellipsoids (Table 6a). The largest differences between NUVEL-1 and prior models are in the Pacific and Indian Ocean regions, where the biggest revisions to plate geometry and spreading rates were made.

The differences are not due solely to a general decrease or increase in spreading rates, however. A second test of how

much NUVEL-1 differs from prior models is whether a prior Euler pole lies within the 2-D 99 per cent confidence ellipse of the corresponding NUVEL-1 Euler pole, irrespective of the rate of rotation of the Euler vector. For the 30 pairs of plates sharing a common boundary, only one of the P071 Euler poles and only 10 of the RM2 Euler poles lie within the NUVEL-1 99 per cent confidence ellipses, and none of the P071 Euler poles and only eight of the RM2 Euler vectors lie within the NUVEL-1 95 per cent confidence ellipses (Table 6b).

A third test of how much NUVEL-1 differs from prior models is how well different models fit the NUVEL-1 data set. The fit improves with successive global models (Fig. 7). The misfits of prior models, however, are much larger than would be expected if the NUVEL-1 data were drawn from the same population of data used in prior studies: NUVEL-1 fits the data better than any other model at the 99 per cent confidence level. The misfits shown in Fig. 7 are further divided by data type. P071 and RM2 are nearly as good as NUVEL-1 at fitting slip vector data, but are worse at fitting transform azimuths, and much worse at fitting rates. We attribute the poor fit of prior models to some transform azimuths to systematic errors in previously used azimuths, now recognizable with improved seafloor mapping technology. Similarly, spreading rates used in prior models had systematic errors that have been recognized through our analysis of original data and from new dense surveys.

Figure 8 shows the average ratio of prior rates (i.e., for both P071 and RM2) to NUVEL-1 rates for the 15 spreading plate boundaries. Along 12 of these 15 spreading boundaries the prior rates are faster than NUVEL-1 rates, which agrees with the sense of change expected from the difference between Harland *et al.* (1982) time-scale we use and the Talwani *et al.* (1971) time-scale used in prior studies. However, the size of most of the changes are much larger than the 2 per cent change expected from the difference in age of the middle of chron 2A between the two time-scales. Only two plate pairs, Africa–North America and Australia–Antarctica, give an average change nearly
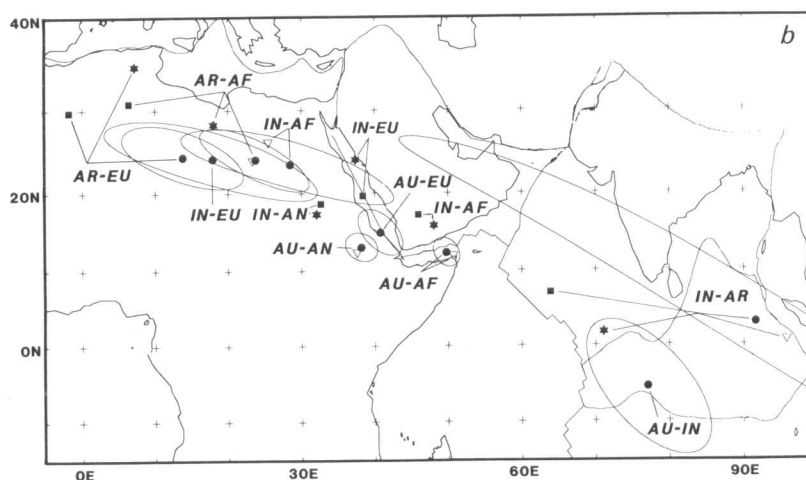
Figure 6(b). Location of some of the NUVEL-1 Euler poles (solid circles) and their 2-D 95 per cent confidence regions describing motion between the African (AF), Antarctic (AN), Arabian (AR), Australian (AU), Eurasian (EU), and Indian (IN) plates. Best-fitting poles (open triangles), model P071 Euler poles (stars), and model RM2 Euler poles (squares) are also shown. For each Euler pole, the first plate listed rotates counter-clockwise relative to the second plate. The India–Africa Euler pole shown for P071 is Chase's (1978) India–Somalia Euler vector. Unlike the NUVEL-1 Indian plate, the 'Indian' plate of P071 and of RM2 includes both India and Australia.
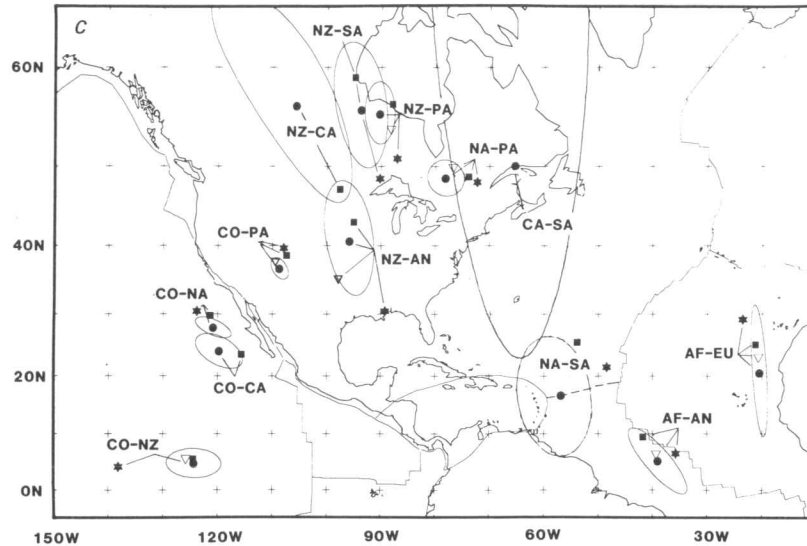
Figure 6(c). Location of some of the NUVEL-1 Euler poles (solid circles) and their 2-D 95 per cent confidence regions describing motion between the African (AF), Antarctic (AN), Caribbean (CA), Cocos (CO), Eurasian (EU), Nazca (NZ), North American (NA), Pacific (PA), and South American (SA) plates. Best-fitting poles (open triangles), model P071 Euler poles (stars), and model RM2 Euler poles (squares) are also shown. For each Euler pole, the first plate listed rotates counter-clockwise relative to the second plate.

Table 4. Best-fitting and closure-fitting Euler vectors.

Plate Pair	Best-fitting Vector Lat. °N	Long. °E	ω (deg-m.y.$^{-1}$)	Error Ellipse σ_{max}	σ_{min}	ζ_{max}	σ_{ω} (deg-m.y.$^{-1}$)	Closure-fitting Vector Lat. °N	Long. °E	ω (deg-m.y.$^{-1}$)
				Pacific Ocean						
na-pa	49.6	-76.7	0.74	3.1	1.5	66	0.05	48.3	-77.0	0.79
co-pa	34.4	-108.6	2.30	1.6	0.8	-12	0.11	37.3	-108.7	2.05
co-nz	5.2	-125.8	0.91	4.1	1.8	-88	0.06	4.9	-121.6	1.17
nz-pa	53.8	-88.2	1.42	8.2	2.6	19	0.03	55.8	-90.4	1.42
nz-an	35.0	-97.9	0.56	20.1	2.8	-2	0.04	40.3	-93.9	0.54
nz-sa	74.7	-106.3	----	62.1	2.1	-30	----	53.2	-97.5	0.77
an-pa	65.1	-80.6	0.93	2.3	1.6	34	0.02	64.6	-85.8	0.90
na-co	1.0	-73.2	----	107.5	1.8	-56	----	28.3	-120.3	1.42
ca-co	7.2	-79.9	----	3.3	0.4	-65	----	22.2	-119.2	1.35
				Atlantic Ocean						
eu-pa	63.2	134.5	0.23	4.8	1.4	-12	0.01	61.3	139.3	0.22
af-eu	22.7	-20.7	----	7.0	0.7	-04	----	19.5	-23.7	0.14
af-na	73.7	94.8	0.22	14.7	1.4	-40	0.01	74.3	17.2	0.27
af-sa	63.4	-39.4	0.32	3.0	0.8	-11	0.01	66.9	-43.8	0.37
an-sa	86.0	-40.5	0.30	8.9	1.4	-25	0.05	88.7	-36.1	0.27
ca-na	30.2	108.6	0.18	20.9	2.1	13	0.07			
ca-sa	70.3	-167.9	----	1193	10	79	----	63.1	-15.2	0.13
				Indian Ocean						
in-af	25.5	26.8	0.41	16.5	2.8	-67	0.11	23.4	26.9	0.41
ar-af	23.8	23.4	0.41	6.2	1.6	-68	0.06	24.7	-18.8	0.41
au-af	11.7	50.8	0.68	6.2	1.0	-34	0.07	11.1	49.0	0.66
au-an	12.1	37.7	0.68	1.7	1.6	-38	0.01	12.7	39.8	0.70
af-an	6.0	-39.3	0.14	6.7	1.4	-45	0.01	-1.8	-40.4	0.12
in-ar	0.8	95.0	----	33.1	2.7	-58	----	27.9	123.0	0.03

First plate moves counterclockwise relative to second plate. Plate abbreviations: pa, Pacific; na, North America; sa, South America; af, Africa; co, Cocos; nz, Nazca; eu, Eurasia; an, Antarctica; ar, Arabia; in, India; au, Australia; ca, Caribbean. One sigma-error ellipses are specified by the angular lengths of the principal axes and by the azimuths (ζ_{max}, given in degrees clockwise from north) of the major axis. The rotation rate uncertainty is determined from a one-dimensional marginal distribution, whereas the lengths of the principal axes are determined from a two-dimensional marginal distribution.

equal to that expected solely from the change in time-scale. Even so, this comparison obscures other differences between our rates and prior rates. For example, although the average change in rate along the Australia–Antarctica boundary is small, the gradient in rates along the boundary is very different in NUVEL-1 from that of P071 and RM2.

Therefore the change in time-scale accounts for only a very small portion of the differences between our spreading rates and those of prior models.

If the misfits to our 1122 data were normally distributed and their standard errors correctly estimated, χ^2 would be chi-squared distributed with 1089 (1122 less the 33 adjustable parameters) degrees of freedom. χ^2 would be expected to lie with 95 per cent probability in the interval 1013–1165. The value of χ^2 for NUVEL-1 is 262, about four times smaller than expected. Thus, like Chase (1978) and Minster & Jordan (1978), we have systematically overestimated the errors in the data, which is not surprising because we have tried to estimate errors consistent with those used in prior models. If the standard errors in the data were properly estimated, the sample standard deviation should be 1; the sample standard deviations for our data range from 0.43 for rates to 0.55 for the transforms (Fig. 9), showing that the data uncertainties were overestimated by a factor of 2, slightly larger than the $3^{1/2}$ overestimate reported by Minster & Jordan (1978). The factor of 2 overestimate suggests that the assigned data uncertainties are more like 95 per cent confidence limits than standard deviations. Thus the NUVEL-1 model errors are too conservative, and the accuracy of the model is probably better than implied by the model errors, perhaps by as much as a factor of 2. The distribution of normalized residuals for RM2 slip vectors is skewed toward negative values, owing to the negative residuals of slip vectors from the Aleutian and Kuril trenches (Minster & Jordan 1978). The mean of the NUVEL-1 residuals differs insignificantly from zero (Fig. 9), presumably because NUVEL-1 includes no slip vectors from the western Aleutian or Kuril trenches.

Summed data importances are listed by boundary and data type in Table 7. Although two thirds of the data are slip vectors, their summed importance is only 6.47; they contribute only 20 per cent of the information in the model. In contrast, transform azimuths are only 10 per cent of the

Table 5. NUVEL-1 variance-covariance matrix (Cartesian Pacific-fixed coordinates).

	North America			Cocos			Antarctica			Nazca			South America			Australia			Africa			Eurasia			India			Caribbean			Arabia		
North America	453	-45	7	248	93	42	296	2	4	257	96	27	352	2	-40	326	-26	-17	358	7	-37	457	-32	8	358	7	-37	475	-158	5	358	7	-37
	-45	512	-48	265	132	-20	107	322	179	101	159	-53	141	351	111	115	320	146	136	378	113	-51	457	-18	136	378	113	-65	661	-90	136	378	113
	7	-48	363	-20	-20	44	-21	39	217	29	-53	29	-67	26	275	-41	55	246	-67	10	273	6	-22	338	-67	10	273	60	-132	194	-67	10	273
Cocos	248	93	42	758	871	-172	344	376	-59	670	19	-60	366	26	99	341	35	109	339	39	107	247	76	52	339	39	107	199	233	144	339	39	107
	265	132	-20	871	877	-1960	376	60	3	793	227	-572	399	54	42	371	66	51	368	69	51	262	112	-11	368	69	51	186	305	186	368	69	51
	-20	-20	44	-172	-1960	653	-59	3	20	-157	107	269	-58	2	21	-56	0	0	-54	0	20	-20	-14	41	-54	0	20	-29	-49	108	-54	0	20
Antarctica	296	107	-21	344	376	-59	521	-9	86	369	28	110	459	15	100	494	10	102	469	25	116	292	11	14	469	25	116	268	13	18	469	25	116
	2	322	39	376	60	3	-9	318	116	50	160	-32	5	316	119	19	302	103	3	313	117	74	320	160	3	313	117	273	333	264	3	313	117
	4	179	217	-59	53	20	86	116	383	12	29	48	100	94	356	94	102	364	103	92	351	-2	62	259	103	92	351	-42	-19	75	103	92	351
Nazca	257	101	29	670	793	-157	369	50	12	728	-2	-69	394	22	97	365	33	108	364	37	106	255	81	41	364	37	106	211	255	100	364	37	106
	96	159	-53	19	227	107	28	160	29	-2	2743	847	149	137	-77	71	140	-43	92	162	-56	96	160	-53	92	162	-56	67	226	16	92	162	-56
	27	32	29	-60	-572	269	110	-32	48	-69	847	898	52	20	29	21	19	42	31	30	36	27	31	32	31	30	36	14	63	56	31	30	36
South America	352	141	-67	366	399	-58	459	5	111	394	149	52	673	-37	-39	485	-7	73	516	40	46	347	108	-52	516	40	46	301	456	-117	516	40	46
	2	351	26	26	54	2	15	316	94	22	137	20	-37	381	107	12	312	98	25	342	79	11	349	50	25	342	79	17	322	-18	25	342	79
	-40	111	275	99	42	21	100	119	356	97	-77	29	-39	107	620	103	96	388	84	42	420	-28	89	320	84	42	420	-13	129	136	84	42	420
Australia	326	115	-41	341	371	-56	494	19	94	365	71	21	485	12	103	611	-50	85	517	0	92	322	79	-22	517	0	92	299	276	-58	517	0	92
	-26	320	55	35	66	0	10	302	103	33	140	19	-7	312	96	-50	569	15	-22	322	98	-16	321	78	-22	322	98	-16	336	-6	-22	322	98
	-17	146	246	109	51	0	102	103	364	108	-43	42	73	98	388	85	15	559	95	84	381	-6	127	289	95	84	381	95	232	96	95	84	381
Africa	358	136	-67	339	368	-54	469	3	103	364	92	31	516	25	84	517	-22	95	562	13	73	352	97	-49	562	13	73	329	292	-79	562	13	73
	7	378	10	39	69	0	25	313	92	37	162	-56	40	342	42	0	322	84	13	380	51	16	379	32	13	380	51	14	393	-39	13	380	51
	-37	113	273	107	51	20	116	117	351	106	-56	36	46	79	420	92	98	381	73	51	409	-26	93	317	73	51	409	-20	199	116	73	51	409
Eurasia	457	-51	6	247	262	-20	292	11	14	255	96	27	347	11	-28	322	-16	-6	352	16	-26	612	-90	190	352	16	-26	480	-164	4	352	16	-26
	-32	457	-22	76	112	-14	74	320	160	81	160	31	108	349	89	79	321	127	97	379	93	-90	462	-82	97	379	93	-45	578	-73	97	379	93
	8	-18	338	52	-11	41	-2	62	259	41	-53	32	-52	50	320	-22	78	289	-49	32	317	190	-82	743	-49	32	317	56	-78	175	-49	32	317
India	358	136	-67	339	368	-54	469	3	103	364	92	31	516	25	84	517	-22	95	562	13	73	352	97	-49	4339	7080	1346	329	292	-79	4326	4165	1136
	7	378	10	39	69	0	25	313	92	37	162	-56	40	342	42	0	322	84	13	380	51	16	379	32	7080	14958	2709	14	393	-39	7021	8141	2197
	-37	113	273	107	51	20	116	117	351	106	-56	36	46	79	420	92	98	381	73	51	409	-26	93	317	1346	2709	1040	-20	199	116	1285	1417	911
Caribbean	475	-65	60	199	186	-29	268	13	18	211	67	14	301	17	-13	299	-16	-1	329	14	-20	480	-45	56	329	14	-20	847	-962	-513	329	14	-20
	-158	661	-132	233	305	-49	273	333	264	255	226	63	456	322	129	276	336	232	292	393	199	-164	578	-78	292	393	199	-962	4197	-188	292	393	199
	5	-90	194	144	186	108	-42	-19	75	100	16	56	-117	-18	136	-58	-6	96	-79	-39	116	4	-73	175	-79	-39	116	-513	-188	2622	-79	-39	116
Arabia	358	136	-67	339	368	-54	469	3	103	364	92	31	516	25	84	517	-22	95	562	13	73	352	97	-49	4326	7021	1285	329	292	-79	4551	4418	1243
	7	378	10	39	69	0	25	313	92	37	162	-56	40	342	42	0	322	84	13	380	51	16	379	32	4165	8141	1417	14	393	-39	4418	5420	1384
	-37	113	273	107	51	20	116	117	351	106	-56	36	46	79	420	92	98	381	73	51	409	-26	93	317	1136	2197	911	-20	199	116	1243	1384	921

Units are 10^{-10} radians^2/m.y.^{2} Each triple of rows or columns is listed in the following order of components: x (0°N, 0°E), y (0°N, 90°E), and z (90°N).

Table 6(a). Test of significance of the difference between NUVEL-1 Euler vectors and RM2 and P071 Euler vectors.

Euler Vector	χ^2 RM2	P071	Euler Vector	χ^2 RM2	P071
ar-in	7163	5340	au-eu	28	73
co-pa	191	189	in-eu	28	41
au-pa	106	155	ca-na	26	--
au-in	93	93	nz-sa	23	154
nz-pa	86	320	nz-an	19	138
au-an	76	69	ar-eu	18	48
au-af	48	53	nz-ca	16	--
in-af	47	123	af-ar	13	10^1, 68^2
ca-sa	46	--	af-na	12	22
an-sa	44	97	na-sa	12	25
pa-na	42	66	af-an	11	113^3, 327^4
af-sa	38	60	co-ca	9	--
an-pa	33	102	af-eu	7	22
co-na	32	34	co-nz	5	58
eu-pa	32	15	eu-na	2	31

The values of χ^2 at the 1% and 5% risk levels are 11.3 and 7.8, respectively. Values of χ^2 greater than 11.3 or 7.8 indicate that the Euler vector from the prior model falls outside the 99% or 95% confidence region, respectively, of NUVEL-1. Plate abbreviations: pa, Pacific; na, North America; sa, South America; af, Africa; co, Cocos; nz, Nazca; eu, Eurasia; an, Antarctica; ar, Arabia; in, India; au, Australia; ca, Caribbean.

1) Comparison to the P071 Arabia-Somalia Euler vector. 2) Comparison to the P071 Arabia-(West) Africa Euler vector. 3) Comparison to the P071 (West) Africa-Antarctica Euler vector. 4) Comparison to the P071 Somalia-Antarctica Euler vector.

Table 6(b). Test of significance of the difference between NUVEL-1 Euler poles and RM2 and P071 Euler poles.

Euler Vector	χ^2 RM2	P071	Euler Vector	χ^2 RM2	P071
ar-in	6620	4883	au-eu	16	67
co-pa	68	138	in-eu	89	109
au-pa	38	49	ca-na	24	--
au-in	-	-	nz-sa	2	18
nz-pa	6	34	nz-an	2	46
au-an	83	72	ar-eu	22	48
au-af	64	24	nz-ca	7	--
in-af	386	448	af-ar	162	37^1, 105^2
ca-sa	54	--	af-na	7	15
an-sa	29	33	na-sa	19	54
pa-na	12	24	af-an	4	86^3, 279^4
af-sa	16	26	co-ca	18	--
an-pa	5	9	af-eu	1	25
co-na	15	36	co-nz	1	469
eu-pa	19	10	eu-na	5	27

The values of χ^2 at the 1% and 5% risk levels are 9.2 and 6.0, respectively. Values of χ^2 greater than 9.2 or 6.0 indicate that the Euler pole from the prior model falls outside the 99% or 95% confidence region, respectively, of NUVEL-1.

Plate abbreviations and footnotes are the same as in Table 6a.

Figure 7. The weighted, squared misfit (χ^2) to NUVEL-1 data is shown for various global plate motion models: CH72 (Chase 1972), RM1 (Minster *et al.* 1974), P071 (Chase 1978), RM2 (Minster & Jordan 1978), and NUVEL-1. Each vertical bar showing total misfit is separated into three segments giving the misfit to each type of plate motion data: slip vector azimuths (S), transform fault azimuths (T), and spreading rates (R).
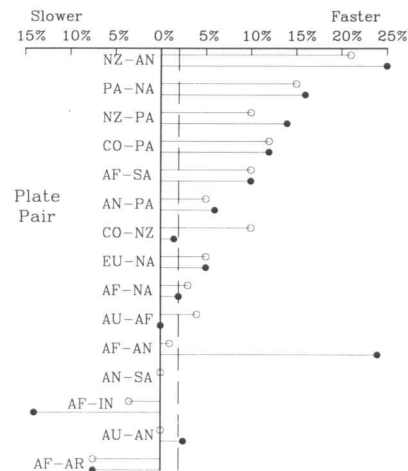
Figure 8. Comparison of the spreading rates used to derive NUVEL-1 with those used to derive P071 and RM2. Values to the right of the origin indicate that the rates used to derive prior models are faster on average than those used to derive NUVEL-1, whereas values to the left of the origin indicate that the rates used to derive prior models are slower. Most P071 (solid circles) and RM2 (open circles) rates are faster than those used to derive NUVEL-1. Along many spreading centres, especially those in the Pacific Ocean, the differences between NUVEL-1 rates and prior rates exceed the ~2 per cent difference (dashed line) attributable to differences between the Harland *et al.* (1982) time-scale used here, and the Talwani *et al.* (1971) time-scale used in determining prior global plate motion models.

data, but contribute one third of the information, owing to their smaller uncertainties. When all the data are considered, the 20 per cent with the highest importances contribute 72 per cent of the information, and 20 per cent of the information is contributed by the 74 per cent with the smallest importances.

DETAILED DESCRIPTION OF NUVEL-1

In this section we present detailed results. Differences between our data and prior data in many regions are

Figure 9. Histogram of the distribution of normalized errors [(observed − predicted)/σ] for rates, transform azimuths, and slip vector azimuths. The dashed curve shows the Gaussian distribution expected if the data uncertainties were properly estimated. The computed sample standard deviation is less than unity, showing that the data uncertainties were systematically overestimated.

Table 7. Data importances by plate boundary.

Plates	N_r	Rates	N_t	Transforms	N_s	S. Vectors	N	Total
af-sa	23	1.053	14	1.104	94	0.298	131	2.455
eu-na	20	1.580	5	0.696	14	0.083	39	2.359
af-ar	25	1.569	4	0.703	4	0.074	33	2.346
co-nz	29	1.557	3	0.537	16	0.236	48	2.330
ca-na	1	0.466	6	1.275	9	0.224	16	1.965
ar-in	0	0.000	2	0.992	6	0.927	8	1.919
af-an	12	0.534	18	1.066	39	0.270	69	1.870
au-an	38	1.435	13	0.207	78	0.214	129	1.856
af-in	18	1.318	2	0.251	7	0.159	27	1.728
af-na	20	0.886	4	0.739	12	0.067	36	1.692
co-pa	25	1.103	3	0.463	7	0.021	35	1.586
an-pa	21	1.118	8	0.233	54	0.203	83	1.554
af-eu	0	0.000	4	1.068	6	0.424	10	1.492
au-af	17	0.664	7	0.704	17	0.083	41	1.451
pa-na	5	0.565	6	0.291	66	0.559	77	1.415
an-sa	7	0.287	8	0.696	12	0.156	27	1.139
nz-an	4	0.529	8	0.178	51	0.369	63	1.076
nz-pa	12	0.590	6	0.080	27	0.064	45	0.734
ca-sa	0	0.000	0	0.000	6	0.648	6	0.648
co-ca	0	0.000	0	0.000	56	0.621	56	0.621
nz-sa	0	0.000	0	0.000	99	0.492	99	0.492
co-na	0	0.000	0	0.000	44	0.288	44	0.288
Total	277	15.254	121	11.283	724	6.470	1122	33.007

N_r is the number of rates, N_t the number of transform fault azimuths, N_s the number of slip vector azimuths, and N the total number of data. Plate abbreviations: pa, Pacific; na, North America; sa, South America; af, Africa; co, Cocos; nz, Nazca; eu, Eurasia; an, Antarctica; ar, Arabia; in, India; au, Australia; ca, Caribbean.

documented elsewhere (DeMets *et al.* 1988; Stein *et al.* 1988; Argus *et al.* 1989; Argus & Gordon 1989; Gordon & DeMets 1989), but the differences between NUVEL-1 and prior Pacific basin data are documented below.

The Arctic and Atlantic regions

Eurasia–North America

We use 20 rates, five transform azimuths, and 14 slip vectors well distributed along the Arctic Ridge system and the mid-Atlantic Ridge north of the Azores triple junction. Few data north of 70 °N along the Arctic ridge system were available to prior global plate motion studies. We use 11 rates determined from 160 aeromagnetic profiles north of Iceland and nine rates determined from 20 surface magnetic profiles south of Iceland. Magnetic profiles collected just north of the Azores triple junction give rates 2–4 mm yr^{-1} slower than used in prior models. The trends of the Jan Mayen and Spitsbergen transforms, and the GLORIA-surveyed northern and southern Charlie-Gibbs transforms, give the direction of Eurasian–North American motion. Eurasia–North America data are fit well by the best-fitting and NUVEL-1 Euler vectors (Fig. 10).

Africa–North America

Surveys with GLORIA side-scan sonar have measured the azimuths of the Oceanographer, Hayes, Atlantis, and Kane transforms, giving accurate estimates of the direction of Africa–North America motion. The Kane has also been surveyed by Seabeam, giving an azimuth nearly identical to that from the GLORIA survey. Unlike Minster & Jordan (1978), we used no azimuths from short-offset transforms such as transforms A and B in the FAMOUS region. The active fault traces within short-offset (<~25–35 km) transforms in many places appear not to parallel the direction of plate motion (Searle & Laughton 1977; Collette & Slootweg 1978; Macdonald 1986; Searle 1986; Argus *et al.* 1989).

Rates along the boundary are typically 1–2 mm yr^{-1} slower than those used by Minster & Jordan (1978) and Chase (1978) (Fig. 11). Argus *et al.* (1989) determined 13 rates from surface magnetic and aeromagnetic profiles compiled by Rabinowitz & Schouten (1985). Deep-tow magnetics from the FAMOUS region give spreading rates near the Azores triple junction (Macdonald 1977), and profiles from Rona & Gray (1980) give the rates along the southern part of the plate boundary.

Africa–Eurasia

Plate motion data from the Azores–Gibraltar line include four azimuths from the GLORIA-surveyed Gloria Fault and six slip vectors from the eastern Azores–Gibraltar Ridge. Africa–Eurasia focal mechanisms vary from strike–slip faulting near the Gloria Fault to thrust faulting near Gibraltar. We excluded data east of Gibraltar because they reflect continent–continent thrusting. Slip vectors in the Mediterranean that may record Africa–Eurasia motion are discussed by Argus *et al.* (1989). The four azimuths along the 400-km-long, E–W trending Gloria Fault strongly

EURASIA – NORTH AMERICA
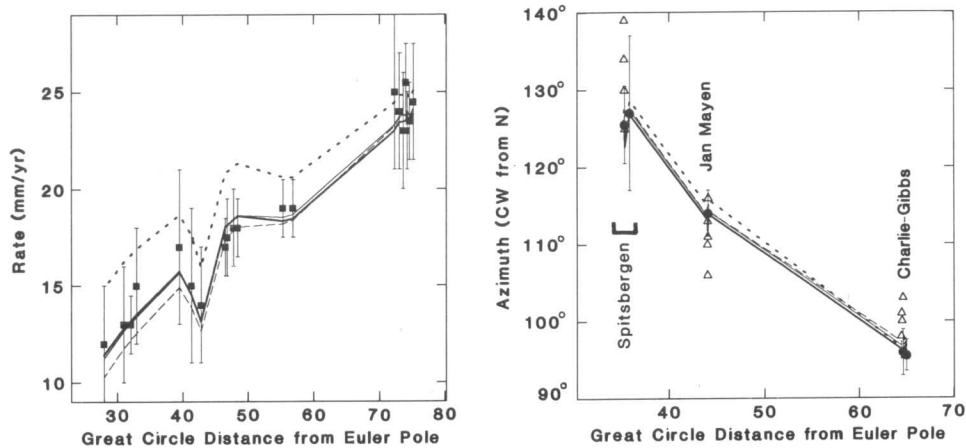
Figure 10. Spreading rates (squares), transform fault azimuths (circles), and slip vector azimuths (triangles) observed along the Arctic Ridge and northern Mid-Atlantic Ridge are compared with directions and rates from the NUVEL-1 (bold solid), best-fitting (thin solid), RM2 (long dashed), and P071 (short dashed) Eurasia–North America Euler vectors. The horizontal axis shows the angular distance from the best-fitting Euler vector (Table 4). Vertical error bars show 1-σ errors assigned to rates and transform fault azimuths.

constrain the longitude of the Africa–Eurasia Euler vector. Argus *et al.* (1989) found that the strike of the Gloria is consistent with it being an active Africa–Eurasia transform fault and with closure of the Africa–Eurasia–North America plate circuit.

The NUVEL-1 Africa–Eurasia Euler vector fits the Gloria Fault azimuths within their uncertainties and is consistent with the scattered thrust-faulting earthquake slip vectors east of the Gloria Fault (Fig. 12). The NUVEL-1 Africa–Eurasia Euler vector predicts motion along the Gloria Fault of 4 ± 1 mm yr^{-1}, faster than the 2 mm yr^{-1} predicted by RM2 and P071. The model predicts 6 ± 1 mm yr^{-1}, N29 $\pm$ 8 °W convergence in the Mediterranean (at 35 °N, 2 °E), slightly faster than the 4 mm yr^{-1} predicted by RM2. (Confidence limits in this paper

following a ' $\pm$ ' sign are plus or minus one standard error, calculated by linear propagation of errors.)

Africa–South America

The extent and accuracy of data measuring Africa–South America motion have improved greatly. No transform azimuths south of 7.5 °S were used in P071 and RM2, leaving about 5000 km of the Mid-Atlantic Ridge unrepresented. The new data include Seabeam surveys of the Meteor (34.2 °S), Cox (32.3 °S), Boda Verde (11.5 °S), and Ascension (7.0 °S) transform faults. Other accurate new data include GLORIA surveys of the Fifteen-Twenty and Romanche transforms and deep tow surveys of the Vema

AFRICA – NORTH AMERICA
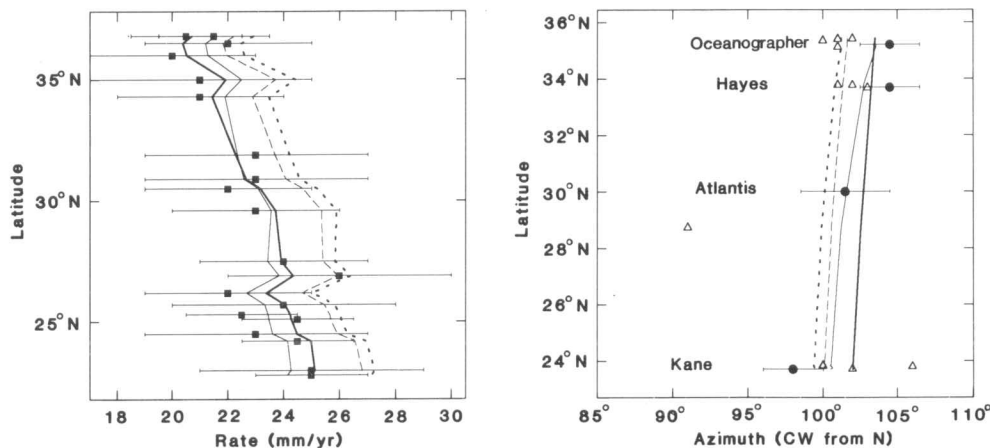
Figure 11. Spreading rates (squares), transform fault azimuths (circles), and slip vector azimuths (triangles) observed along the central Mid-Atlantic Ridge are compared with directions and rates from the NUVEL-1 (bold solid), best-fitting (thin solid), RM2 (long dashed), and P071 (short dashed) Africa–North America Euler vectors. The four transform azimuths were determined from GLORIA and Seabeam surveys. Horizontal error bars show assigned 1-σ errors.

EURASIA – AFRICA
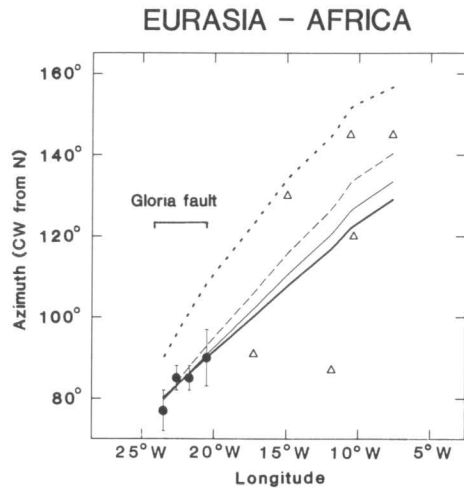
Figure 12. Transform fault azimuths (circles), and slip vector azimuths (triangles) observed along the Azores–Gibraltar ridge are compared with directions from the NUVEL-1 (bold solid), best-fitting (thin solid), RM2 (long dashed), and P071 (short dashed) Eurasia–Africa Euler poles. The four transform azimuths were determined from GLORIA surveys. Vertical error bars show assigned 1-σ errors.

transform. The direction of motion is further described by 94 slip vectors (Table 3).

NUVEL-1 incorporates rates from 9 °S to 25 °S, where prior global plate motion models had none, and from 38 °S to 54 °S, where RM2 had none. These new data include five rates determined from 60 closely spaced aeromagnetic profiles from 10 °S to 17 °S and four rates from ~32 °S. We also determined 11 rates from published profiles and three rates from profiles from the NGDC that cross the ridge just north of the Bouvet triple junction. Gaps remain in the rate coverage, mainly in equatorial latitudes (15 °N–6 °S), where magnetic anomalies are of low amplitude, and from 43 °S to 54 °S. The rates we estimated are typically 2–4 mm yr^{-1} (~8–10 per cent) slower than those used in P071 and RM2. Rates calculated from the NUVEL-1 Africa–South America

Euler vector and best-fitting vector are similar (Fig. 13). As expected from the slower observed rates, the model gives rates 3–4 mm yr^{-1} slower than P071 and RM2. NUVEL-1 gives a direction of motion 2°–4° counter-clockwise of prior models, but agreeing well with the many accurate transform azimuths (Fig. 13).

Antarctica–South America

Before 1978, the South American–Antarctic Ridge had been surveyed only near the Bouvet triple junction. Recent cruises have surveyed the rest of the ridge (Lawver & Dick 1983; Barker & Lawver 1988). From magnetic and bathymetric data compiled by Barker & Lawver (1988), we estimated four rates and seven transform azimuths from the western 90 per cent of the ridge. These include trends from the Bullard and Vulcan transforms, which were unmapped before 1980. We also determined three rates near the Bouvet triple junction from data from the NGDC. Our slip vectors also differ from those used before. RM2 included two slip vectors from the western end of the South Sandwich fracture zone (Forsyth 1975). We excluded these slip vectors because their slip direction and the nearby trend of the fracture zone are anomalous with respect to the rest of the fracture zone. Diffuse seismicity north of the western end of the fracture zone suggests that this tiny triangle of presumed South American lithosphere may be deforming. Slip vectors derived from two small ($M_0 = 2$–4×10^{24} dyne cm) shallow thrusting earthquakes south of the Chile (Nazca–Antarctic–South America) triple junction are included, but are poorly fit (Fig. 14).

NUVEL-1 gives a direction of motion along the South American–Antarctic Ridge that differs significantly from prior models (Fig. 14), which systematically misfit the new transform fault azimuths. NUVEL-1 gives rates 1–3 mm yr^{-1} slower than observed. An inversion of only South America–Africa, Antarctic–South America, and Africa–Antarctica plate motion data suggests the small misfit is caused by non-closure of this three-plate circuit. The non-closure may be due to deformation within one of these
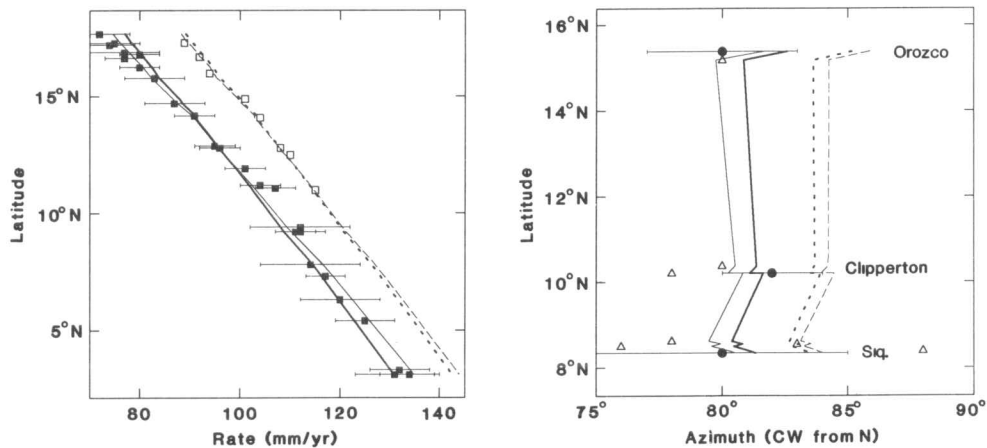
AFRICA – SOUTH AMERICA
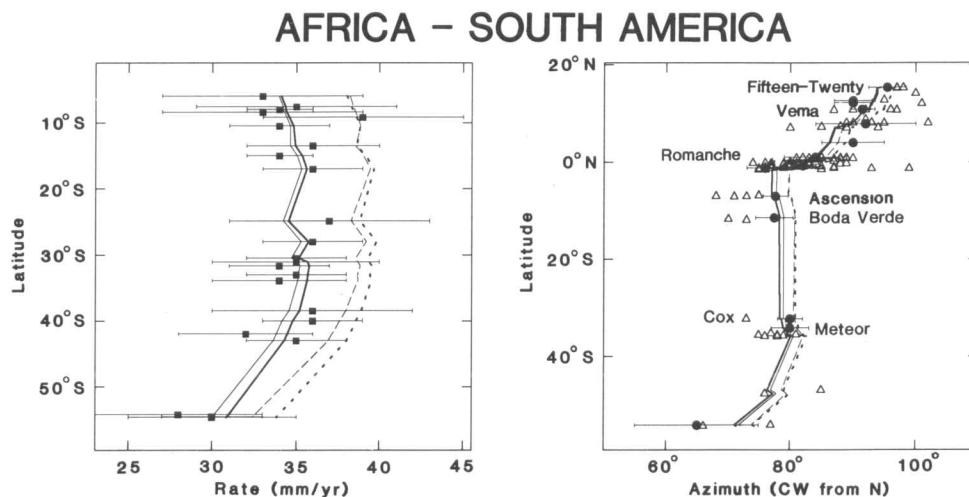
Figure 13. Spreading rates (squares), transform fault azimuths (circles), and slip vector azimuths (triangles) observed along the southern Mid-Atlantic Ridge are compared with directions and rates from the NUVEL-1 (bold solid), best-fitting (thin solid), RM2 (long dashed), and P071 (short dashed) Africa–South America Euler vectors. Horizontal error bars show assigned 1-σ errors.

ANTARCTICA – SOUTH AMERICA
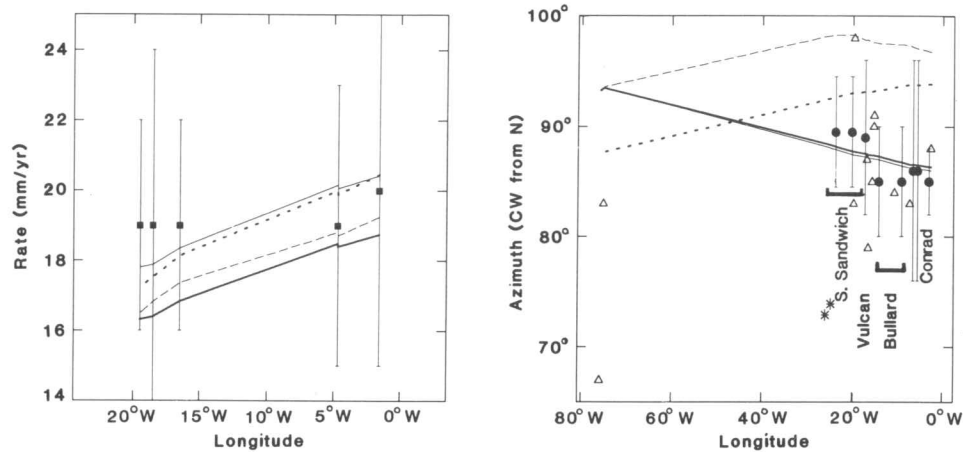
Figure 14. Spreading rates (squares), transform fault azimuths (circles), and slip vector azimuths (triangles) observed along the American–Antarctic Ridge are compared with directions and rates from the NUVEL-1 (bold solid), best-fitting (thin solid), RM2 (long dashed), and P071 (short dashed) Antarctica–South America Euler vectors. Vertical error bars show assigned 1-σ errors. Asterisks show two South Sandwich fracture zone slip vectors used to derive RM2, but omitted from NUVEL-1 because their slip direction and the nearby trend of the fracture zone are anomalous with respect to the rest of the fracture zone.

three plates, for example, motion between East and West Africa or within the zone of diffuse seismicity north of the American–Antarctic Ridge. Alternatively, the small misfit may be caused by systematic errors in some of the data. For example, many of the magnetic profiles along the slowly spreading Southwest Indian Ridge are hard to correlate and our rate estimates may be systematically in error by a few millimetres per year. Many closely spaced ship tracks would be needed to obtain spreading rates accurate enough to resolve these equations.

The Indian Ocean

Models P071 and RM2 systematically misfit plate motion data in the Indian Ocean. Here these misfits have been eliminated through incorporation of new data, reanalysis of old data, and by use of separate Indian and Australian

plates divided along an E–W trending diffuse equatorial plate boundary (Fig. 4) (Wiens *et al.* 1985; Gordon *et al.* 1989). Except for a 1–2 mm yr^{-1} difference in spreading rates along the Southwest Indian Ridge (due to closure constraints about the South America–Africa–Antarctica plate circuit), NUVEL-1 differs insignificantly from and is nearly identical to three and five-plate models for the motion of the Antarctic, Australian, African, Indian, and Arabian plates discussed in detail elsewhere (DeMets *et al.* 1988; Gordon & DeMets 1989; Gordon *et al.* 1989).

Australia–Antarctica

The fit of the NUVEL-1 Australia–Antarctica Euler vector to Southeast Indian Ridge data is better than that of prior models, which systematically misfit spreading rates (Fig. 15). The misfit of prior models is in part due to the plate

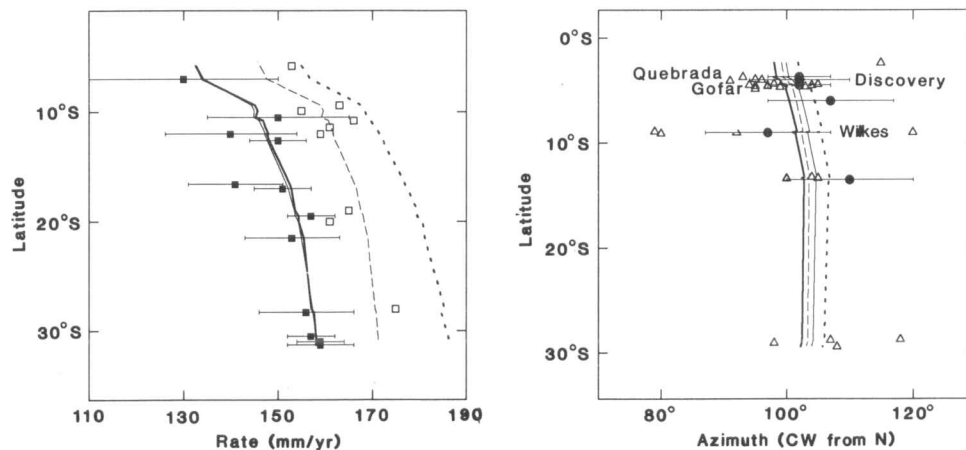## AUSTRALIA – ANTARCTICA
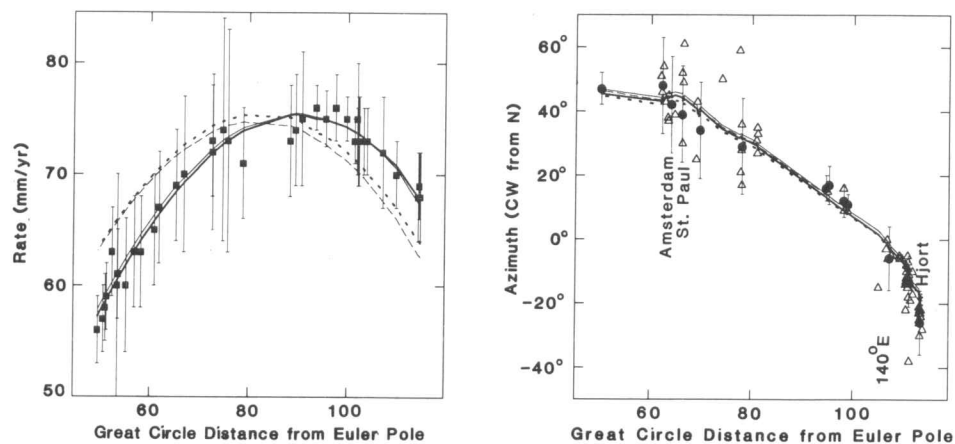
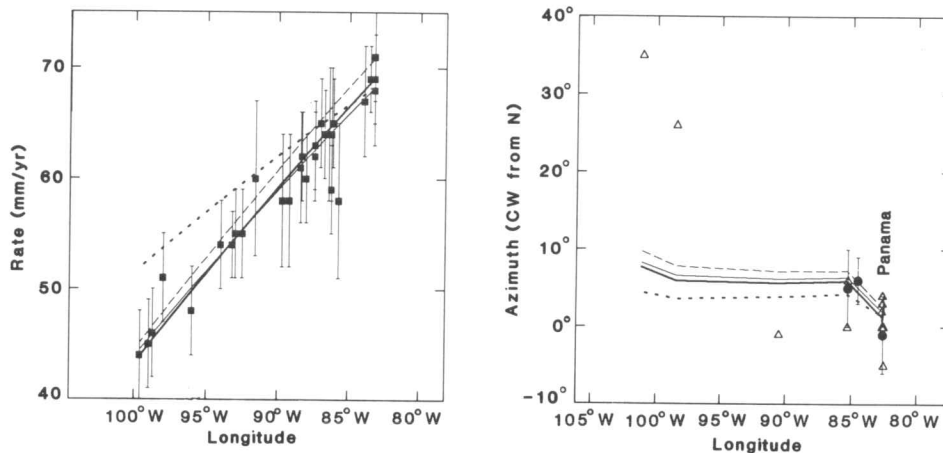**Figure 15.** Spreading rates (squares), transform fault azimuths (circles), and slip vector azimuths (triangles) observed along the Southeast Indian Ridge are compared with directions and rates from the NUVEL-1 (bold solid) and best-fitting (thin solid) Australia–Antarctica Euler vectors, and the RM2 (long dashed) and P071 (short dashed) India–Antarctica Euler vectors. The horizontal axis shows the angular distance from the best-fitting Euler vector (Table 4). Vertical error bars show assigned 1-σ errors.

AFRICA - ANTARCTICA
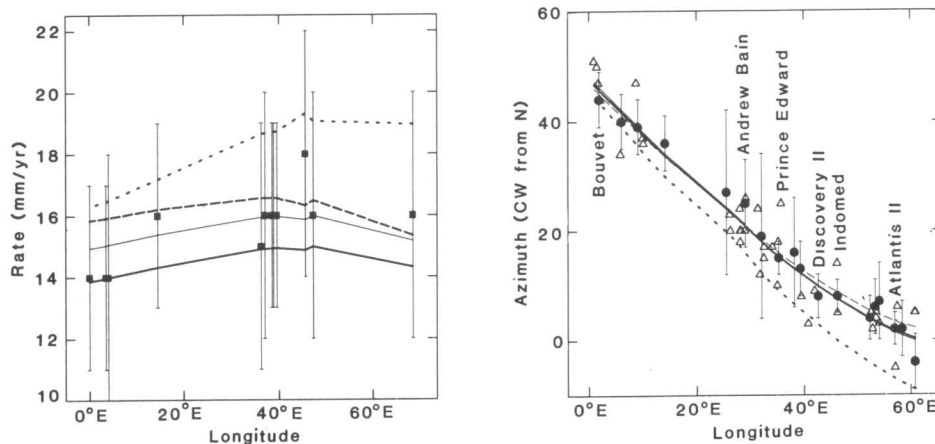
Figure 16. Spreading rates (squares), transform fault azimuths (circles), and slip vector azimuths (triangles) observed along the Southwest Indian Ridge are compared with directions and rates from the NUVEL-1 (bold solid), best-fitting (thin solid), RM2 (long dashed), and P071 (short dashed) Africa–Antarctica Euler vectors. Vertical error bars show assigned 1-σ errors.

geometry assumed and, in RM2, to the use of spreading rates that were systematically too fast along the Central Indian Ridge (DeMets *et al.* 1988). On the other hand, the new azimuths along the Southeast Indian Ridge are systematically misfit east of 140 °E. The observed azimuths tend to be 2°–10° counter-clockwise of the predicted direction of plate motion, which is similar for our best-fitting vector, NUVEL-1, P071, and RM2 (Fig. 15). There are several possible causes of this misfit. Internal deformation of the southeastern corner of the Australian plate, the corresponding part of the Antarctic plate, or both is suggested by intraplate seismicity west of the Macquarie Ridge (Stewart 1983). Because the systematic misfit is small, we cannot exclude the alternative explanation of small systematic errors in the azimuths (DeMets *et al.* 1988).

Africa–Antarctica

Data along the Southwest Indian Ridge, including many new slip vectors and new surveys of several long transform faults (Sclater *et al.* 1981; Fisher & Sclater 1983), are fit well by a single Euler vector (Fig. 16). Although any southern continuation of the East African rift system should intersect the Southwest Indian Ridge, the data suggest that motion near the ridge is negligible (DeMets *et al.* 1988). Observed spreading rates along the Southwest Indian Ridge are 1–2 mm yr^{-1} faster than calculated from NUVEL-1. This small misfit probably reflects the non-closure of the Antarctic–African–South American circuit discussed above.

Australia–Africa

Rates and azimuths from the Central Indian Ridge south of 5 °S are fit well by NUVEL-1 (Fig. 17). Observed and modeled rates are similar to those of P071, but systematically slower than those of RM2 (DeMets *et al.* 1988).

India–Africa

Motion between India and Africa is recorded by 14 spreading rates along the Carlsberg Ridge and four along the Central Indian Ridge north of 3 °S. Four magnetic profiles cross the northern Central Indian and Carlsberg ridges near the equator where only one was available before. These profiles are noisy and do not give high-quality rates, but are used here with large assigned errors because better data are unavailable. The India–Africa data are fit well except the trend of the easternmost transform along the Carlsberg Ridge, which is poorly known and disagrees with nearby slip vectors (Fig. 18).

P071 and RM2 predict rates along the Carlsberg Ridge 8–12 mm yr^{-1} slower than observed. Wiens *et al.* (1985) and Gordon *et al.* (1989) have shown that these misfits result from treating India and Australia as part of the same plate, and fitting data from the Carlsberg and Central Indian ridges with a single Euler vector.

Arabia–Africa

Arabia–Africa motion is recorded by 25 spreading rates along the Sheba Ridge. New azimuths include four transform trends from a GLORIA survey in the Gulf of Aden and slip vectors from three CMT solutions. We use no magnetic profiles west of 44.25 °E in the Gulf of Aden to avoid any biases from rift propagation (Courtillot, Galdeano & Le Mouël 1980). Because we neglect Nubia–Somalia motion, we omit spreading rates from the Red Sea.

The Arabia–Africa data are fit well (Fig. 19) except for the westernmost transform trend. Some seafloor lineaments picked from GLORIA sonographs of the westernmost transform (Tamsett & Searle 1988) suggest that the transform trend may be several degrees clockwise of the trend of the dominant lineaments, which would resolve most of the 5° misfit. Except for rates at the western end of the Sheba ridge, P071 and RM2 predict spreading rates

AUSTRALIA - AFRICA
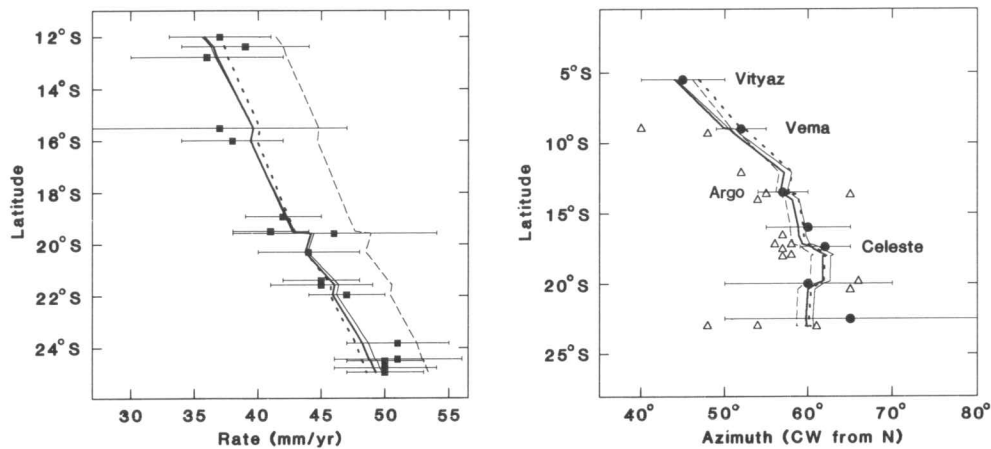
Figure 17. Spreading rates (squares), transform fault azimuths (circles), and slip vector azimuths (triangles) observed along the Central Indian Ridge are compared with directions and rates from the NUVEL-1 (bold solid) and best-fitting (thin solid) Australia–Africa Euler vectors, the RM2 (long dashed) India–Africa Euler vector, and the P071 (short dashed) India–Somalia Euler vector. Horizontal error bars show assigned 1-σ errors.

2–3 mm yr^{-1} slower than observed, and azimuths ~5° clockwise of those observed.

Arabia–India

Along the Owen fracture zone and Dalrymple trough NUVEL-1 gives a velocity of 2 mm yr^{-1}, several times slower than the 9 and 13 mm yr^{-1} predicted by RM2 and P071 at 15 °N, 58 °E (Gordon & DeMets 1989). The Arabia–India Euler vector gives directions that agree with azimuths along the Owen fracture zone and Dalrymple trough (Fig. 20). Models P071 and RM2 predict a component of convergence across the boundary, in disagreement with evidence for active extension along the Dalrymple trough (Quittmeyer & Kafka 1984; White 1984; Gordon & DeMets 1989).

The Caribbean

Determining the motion between the Caribbean and neighbouring plates is challenging because data are sparse. The only rate is from the Cayman Rise. Azimuths can be derived from slip vectors at the Middle America and Lesser Antilles trenches, and from the azimuths of transform faults and slip vectors along the Caribbean plate's northern boundary. We previously found that plate motion data supported Jordan's (1975) model in which the observed Cayman spreading rate is assumed to record North America–Caribbean motion (Stein *et al.* 1988). However, we were unable to reconcile the E–W direction of North America–Caribbean motion recorded by focal mechanisms and morphology along the Motagua, Swan Island, and Oriente faults with the more northerly (~N70 °E) direction of slip vectors from the Lesser Antilles trench.

INDIA - AFRICA
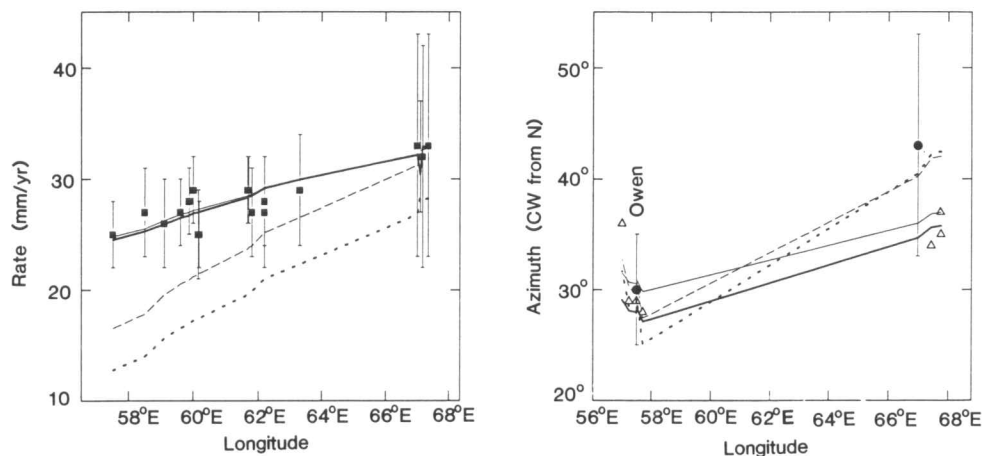
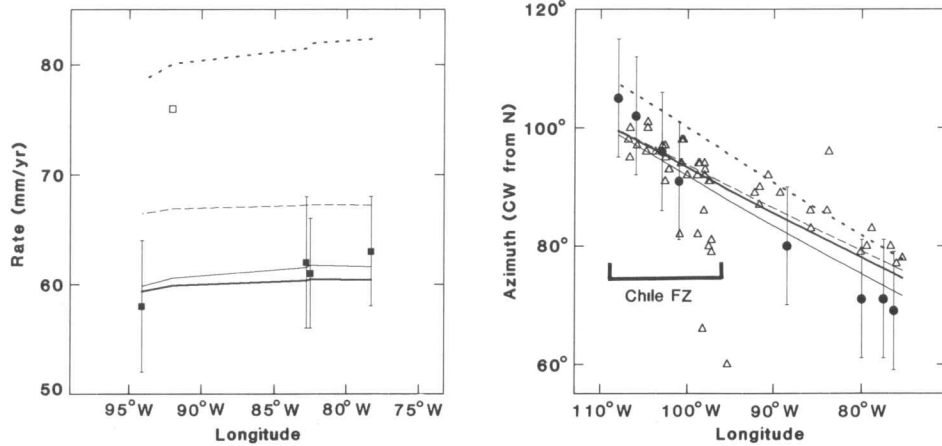**Figure 18.** Spreading rates (squares), transform fault azimuths (circles), and slip vector azimuths (triangles) observed along the Carlsberg Ridge and northernmost Central Indian Ridge are compared with directions and rates from the NUVEL-1 (bold solid), best-fitting (thin solid), and RM2 (long dashed) India–Africa Euler vectors, and the P071 (short dashed) India–Somalia Euler vector. Vertical error bars show assigned 1-σ errors.

ARABIA − AFRICA
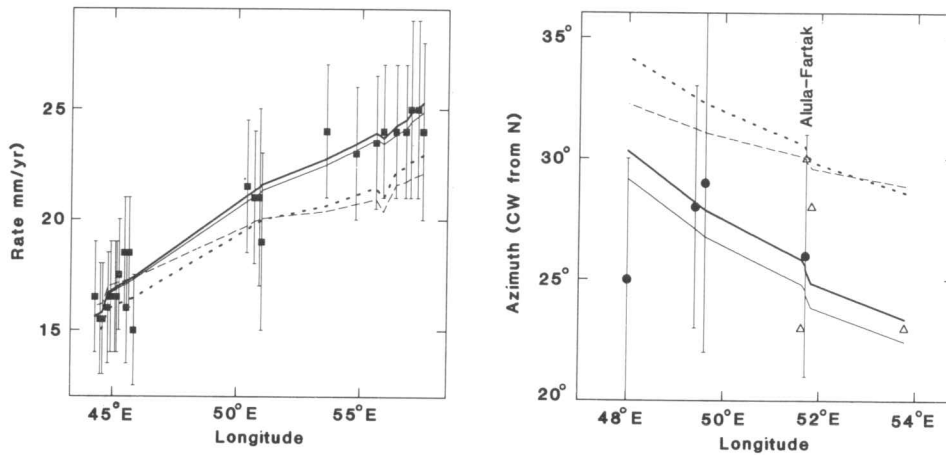
Figure 19. Spreading rates (squares), transform fault azimuths (circles), and slip vector azimuths (triangles) observed along the Sheba Ridge are compared with directions and rates from the NUVEL-1 (bold solid), best-fitting (thin solid), and RM2 (long dashed) Arabia–Africa Euler vectors, and the P071 (short dashed) Arabia–Somalia Euler vector. Vertical error bars show assigned 1-σ errors.

ARABIA − INDIA
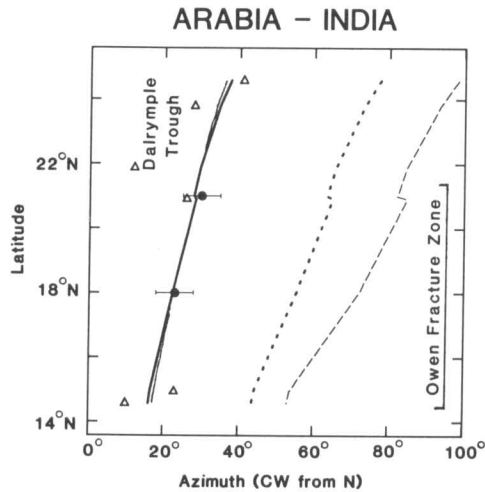
Figure 20. Transform fault azimuths (circles) and slip vector azimuths (triangles) observed along the Owen fracture zone and Dalrymple trough are compared with directions and rates from the NUVEL-1 (bold solid), best-fitting (thin solid), RM2 (long dashed), and P071 (short dashed) Arabia–India Euler vectors. Horizontal error bars show assigned 1-σ errors of transform fault azimuths.

Using more data and a different location for the North America–South America boundary, we update the prior analysis here. Although some thrust faulting occurs as far south as Jamaica (Goreau 1983), we treat the Oriente Fault as a transform fault, as we did before. Excluding the Oriente worsens the fit to the Swan Island transform azimuths (Stein *et al.* 1988), but improves the fit to Lesser Antilles slip vectors (Sykes *et al.* 1982). Prior studies followed Minster & Jordan's (1978) suggestion that the North America–South America plate boundary intersects the Lesser Antilles trench at ∼15 °N, where the Mid-Atlantic ridge is closest to the trench. Here, following Argus & Gordon (1989), we assume the boundary intersects the Lesser Antilles farther north, near 19 °N, and hence treat Lesser Antilles slip vectors as if they record Caribbean–South America motion. Numerical experiments

showed that the calculated motion of the Caribbean relative to neighbouring plates is insensitive to the assumed location along the Lesser Antilles trench of the Caribbean–North America–South America triple junction.

The NUVEL-1 error ellipses include the Euler vectors of our prior study (Figs 6a and c). The NUVEL-1 rate $(12 \pm 3 \text{ mm yr}^{-1})$ at the Cayman spreading centre is similar to our prior estimate and to the $15 \pm 5 \text{ mm yr}^{-1}$ rate derived from magnetic anomalies and subsidence rates (Rosencrantz, Ross & Sclater 1988). The convergence rate predicted near the Lesser Antilles (16 °N, 60 °W) for Caribbean–South America or Caribbean–North America motion is $12 \pm 4 \text{ mm yr}^{-1}$. The fit to Caribbean–North America azimuths is worse than in prior models because of the greater number of Lesser Antilles slip vectors now available (Fig. 21). Furthermore, the Lesser Antilles slip vectors are fit poorly (Fig. 22). In contrast, the Caribbean–North American best-fitting vector, which is unaffected by the Lesser Antilles slip vectors, gives a better fit to the Caribbean–North America azimuths (Fig. 21). We previously noted that the few Lesser Antilles slip vectors available were inconsistent with the northern boundary data, and that their incorporation biases plate motion models (Stein *et al.* 1988). The present data now include enough Lesser Antilles slip vectors to exclude the possibility that the discrepancies are due to random errors.

The poor fit to the Lesser Antilles slip vectors, observed whether compared with Caribbean–South America or Caribbean–North America motion (Fig. 22), has several possible explanations. First, it could be caused by noisy data, but there seem to be just enough data to make such a coincidence seem unlikely. Second, the slip directions may not reflect the long-term slip direction in the trench. Subduction appears to be mainly aseismic with most instrumentally recorded earthquakes, including the two largest, suggesting not interplate thrust faulting but intraplate deformation (Dorel 1981; Stein *et al.* 1982, 1986a). The remaining slip vectors (Fig. 22) are from small $(M_S < 7)$ possibly unrepresentative earthquakes. Third, the misfit may be due to deformation within or behind the arc or

CARIBBEAN – NORTH AMERICA
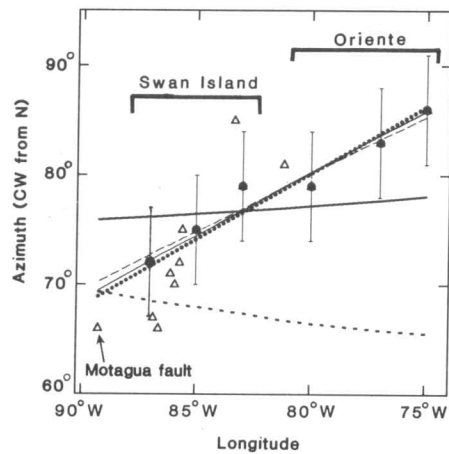
Figure 21. Transform fault azimuths (circles) and slip vector azimuths (triangles) observed along the Motagua fault, Swan Island fracture zone, and Oriente fracture zone are compared with directions from the NUVEL-1 (bold solid), best-fitting (thin solid), RM2 (long dashed), and Sykes *et al.* (1982) (short dashed) Caribbean–North America Euler vectors. The dotted curve shows what NUVEL-1 Caribbean–North America motion would be if Lesser Antilles slip vectors had been deleted.

forearc, as suggested by focal mechanisms in the Lesser Antilles arc and forearc regions (Stein *et al.* 1982), and by seismic reflection data (Torrini & Speed 1989). Where the Caribbean plate overrides the South American plate east of the El Pilar Fault, Speed (1985) infers a southeasterly transport direction, which also disagrees with the Lesser Antilles slip vectors. The systematic misfit to Lesser Antilles slip vectors may be part of a global pattern of a systematic misfits to trench slip vectors (Fitch 1972; Jarrard 1986a) discussed in detail below. All in all, these observations suggest that the Lesser Antilles slip vectors reliably record neither the Caribbean–North America nor Caribbean–South America direction.
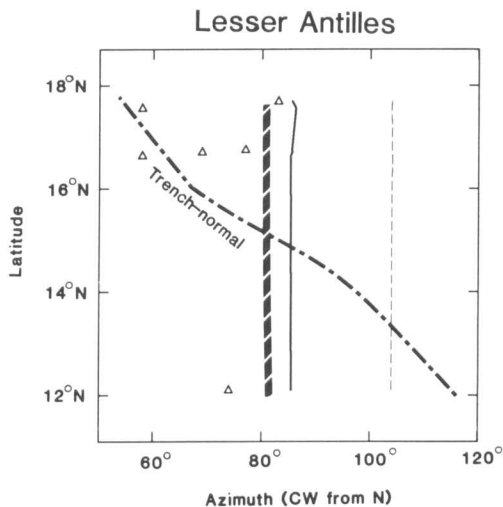
Lesser Antilles

Figure 22. Slip vector azimuths (triangles) observed along the Lesser Antilles trench are compared with directions from the NUVEL-1 (solid) and RM2 (thin dashed) Caribbean–South America Euler vectors and to the NUVEL-1 Caribbean–North America Euler vector (bold dashed).

To obtain alternative Euler vectors free of biases in the Lesser Antilles data, we also inverted the NUVEL-1 data without them. The resulting Caribbean–South America Euler vector (63.1 °N, 15.2 °W, 0.13° m.y.$^{-1}$) gives 13 ± 3 mm yr^{-1}, S68 ± 10 °E motion near the El Pilar Fault (11 °N, 62 °W), consistent with geologic evidence. In the Lesser Antilles (16 °N, 60 °W), the Caribbean–South America Euler vector gives convergence (12 ± 4 mm yr^{-1}, S67 ± 10 °E) about 30° clockwise of the mean azimuth of the trench slip vectors. The Caribbean–North America Euler vector (28.6 °N, 108.2 °E, 0.14° m.y.$^{-1}$) is similar to the best fitting vector and gives convergence of 11 ± 4 mm yr^{-1}, S76 ± 12 °E in the Lesser Antilles, closer to, but still 20° clockwise of, the slip vector azimuths. Along the northern boundary, azimuths and rates are fit better than by the NUVEL-1 Euler vector, which was affected by the incorporation of Lesser Antilles slip vectors into the Caribbean–South America data set (Fig. 21). Although not a full description of Caribbean tectonic complexities, this alternative model may be the best we can do with a rigid plate model and the available plate motion data.

The Pacific Ocean

Although no inconsistencies of Pacific basin plate motion data were reported in prior global plate motion studies, the largest differences between NUVEL-1 and prior models are in the Pacific. Spreading rates along the Pacific–Antarctic Rise, the East Pacific Rise, the Chile Rise, and in the Gulf of California are 5–25 per cent (up to 20 mm yr^{-1}) slower in NUVEL-1 than in prior models. Our Pacific spreading rates are based mainly on analysis of original data, encompass many more magnetic profiles than used in prior studies, and have wider geographic coverage. The new rates give Pacific Basin Euler vectors that exclude nearly all Euler vectors of prior models (Table 6; Fig. 6c).

A key problem addressable with a global plate motion model, but not with local plate motion studies, is the motion of the Pacific basin plates relative to the surrounding continental plates. Except for the Pacific–Antarctic Rise and the Gulf of California, the plate boundaries linking the Pacific basin plates to the global circuit are trenches. As is discussed further below, trench slip vectors have biases that are only partly understood.

Plate motions about the Galapagos triple junction

Spreading rates along the East Pacific Rise, which we determined from nearly 100 magnetic profiles from the NGDC, are systematically slower than used in P071 and RM2. These systematic differences range from 8 to 16 mm yr^{-1} along the Pacific–Cocos boundary and from 10 to 20 mm yr^{-1} along the Nazca–Pacific boundary. The Cocos–Nazca–Pacific plate circuit has small but significant non-closure, which is partly reflected by a systematic misfit of ~3 mm yr^{-1} to Pacific–Cocos rates north of the Orozco transform fault.

Many of our Pacific–Cocos rates came from the same profiles used for P071 and RM2 rates (Figs 23 and 24). The systematic difference between our rates and prior rates is
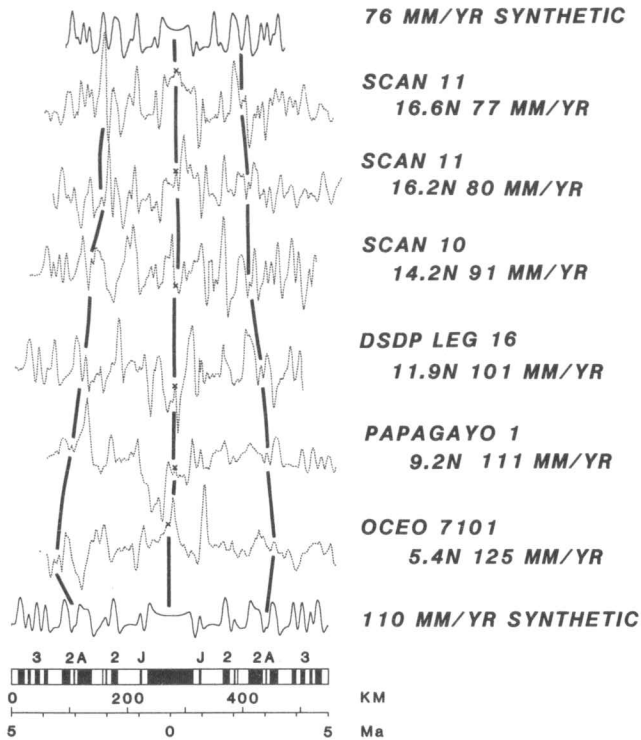
Figure 23. Cocos–Pacific magnetic profiles from the NGDC archives (dashed lines). The uppermost and lowermost profiles (solid lines) are computed synthetic profiles. The shape of the central anomaly in the lower four observed profiles poorly matches the shape of the central anomaly in the computed profiles, but the rise crest (marked with crosses) was easily located from the along-track bathymetry. All profiles are projected on to ridge-normal directions.

puzzling. Differences between the Harland *et al.* (1982) time-scale that we used and the Talwani *et al.* (1971) time-scale that Chase (1978) and Minster & Jordan (1978) used are far too small to explain the differences in spreading rates (Figs 1 and 8). When we estimate rates from the

figures shown in Sclater, Anderson & Bell (1971), we get rates similar to those used in P071 and RM2. However, when we model the same profiles from more recent papers (Klitgord & Mammerickx 1982; Mammerickx 1985), we find rates similar to the slower rates we estimated from profiles from the NGDC. Thus, a plotting error in Sclater *et al.* (1971) may have affected the Pacific–Cocos rates adopted in prior models, but we do not know what caused the differences in rates along the Pacific–Nazca boundary.

Detailed studies of near-ridge morphology and magnetics near 6 °S, 9 °S–12 °S, 20 °S and 31 °S give spreading rates and ridge orientations along much of the Nazca–Pacific boundary (Rea 1976a,b, 1977, 1978). We determined three rates from ~35 profiles from the NGDC between 17 °S and 22 °S and used dense magnetic surveys near 10.5 °S and 7 °S to correlate the low-amplitude, poor quality profiles from these regions. As the magnetic anomalies from 6 °S to 12 °S are poor and the profiles cross only part of anomaly 2A, the estimated spreading rates may be systematically in error. The best anomalies are on profiles near 31 °S, just north of the Juan Fernandez (Pacific–Nazca–Antarctic) triple junction, where prior global studies had no rates. The 157–$159\ \mathrm{mm\ yr^{-1}}$ rates we determined (Fig. 25) are 16–$20\ \mathrm{mm\ yr^{-1}}$ slower than a nearby rate (28 °S) used in P071 and RM2. Except for rates along the Chile Rise, this is the largest difference from P071 and RM2 rates.

Azimuths of the Orozco, Clipperton, and Siquieros transforms were determined from Seabeam data, and azimuths of the Quebrada, Discovery, and Gofar transforms (~4 °S) were determined from GLORIA data. We assigned 10° errors to the latter three azimuths because Searle (1983) suggests that the direction of motion has changed since 1 Ma, within the interval (0–3 Ma) over which we average spreading rates. The directions of motion are further constrained by 40 new slip vectors. We include 11 slip vectors along the Panama transform fault south of 5.8 °N because its trend parallels the predicted Cocos–Nazca direction, suggesting it is the eastern Cocos–Nazca boundary (Chase 1978; Minster & Jordan 1978). However,

**Figure 24.** Spreading rates (solid squares), transform fault azimuths (circles), and slip vector azimuths (triangles) observed along the East Pacific Rise are compared with directions and rates from the NUVEL-1 (bold solid), best-fitting (thin solid), RM2 (long dashed), and P071 (short dashed) Cocos–Pacific Euler vectors. Horizontal error bars show assigned 1-σ errors. The observed spreading rates, which we estimated from data we obtained from the NGDC, are systematically slower than those used to derive P071 and RM2 (open squares). 'Siq.' labels the Siquieros transform fault.

OCEO 7303
157 MM/YR

YAQUINA 7304
159 MM/YR

YAQUINA 7304
159 MM/YR
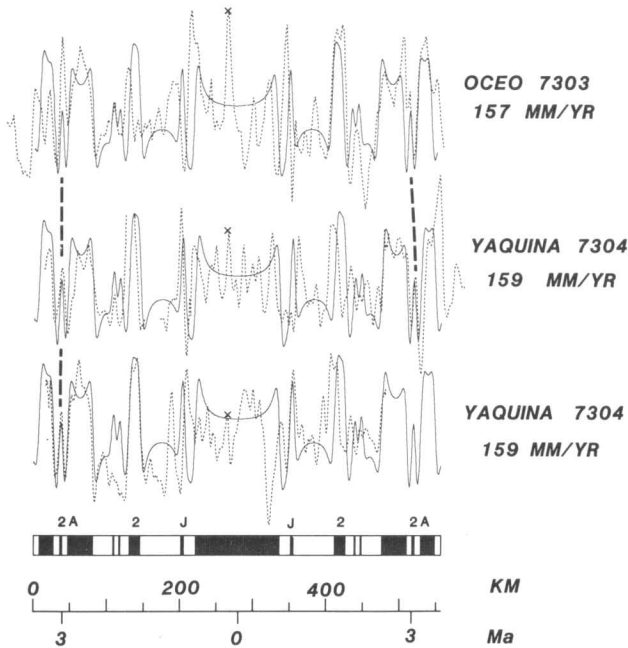
Figure 25. Nazca–Pacific magnetic profiles (obtained from the NGDC archives) from ~31 °S. Observed anomaly profiles are dashed, whereas computed synthetic anomaly profiles are solid. The best-fitting rates vary from 157 to 159 mm yr^{-1}, ~10 per cent slower than rates used to derive P071 and RM2. All profiles have been projected on to the ridge-normal directions listed in Table 3. The profiles are marked with crosses where they intersect the rise crest. No attempt has been made to model asymmetric spreading, ridge jumps, or variable spreading rates. Thus the computed profiles, which were computed using a constant spreading rate, generally fit only anomaly 2A precisely.

we omit Panama transform fault slip vectors north of 5.8 °N because bathymetric contours and epicentres suggest the fault is splayed (Adamek, Frohlich & Pennington 1988).

The many good data along the three spreading centres are fit well (Figs 24, 26, and 27). The new Pacific–Cocos Euler vector gives azimuths that differ systematically from RM2 and P071, which misfit the three transform trends determined from Seabeam data (Fig. 24). Azimuths of slip vectors both north and south of 5.8 °N along the Panama transform fault agree with the new Cocos–Nazca plate motion directions: the mean azimuth (N1.5 °E) of 11 slip vectors south of 5.8 °N, as well as the mean azimuth (N1 ± 2 °W) of 13 slip vectors north of 5.8 °N, are within 1° of the predicted direction of motion. The slip vectors therefore give no evidence of deformation of the NE Nazca plate.

Although nearly all the data along the three ridges are fit within their errors, a test for closure of the Pacific–Cocos–Nazca plate circuit gave $F = 7.0$, showing non-closure significant at the 1 per cent risk level. Part of the non-closure appears as a 3 mm yr^{-1} systematic misfit of NUVEL-1 to the Pacific–Cocos rates north of 16 °N. The consistency with closure of the Nazca–Antarctic–Pacific circuit suggests the Nazca–Pacific data do not cause the Galapagos non-closure. Possibly one or more of the three plates has deformed since 3 Ma, but no region of seismicity suggestive of deformation occurs within them. Alternatively, what we take to be the northernmost Cocos plate may really be part of a diffuse boundary between the Cocos and Rivera plate. Possibly systematic errors contaminate some plate motion data, e.g., the noisy near-equatorial profiles from the southern Pacific–Cocos and northern Nazca–Pacific boundaries.

The circuit non-closure could also result from a change in plate velocity since 3 Ma. For example, Searle (1983) has suggested that the direction of Pacific–Nazca plate motion has changed since 1 Ma. Thus, the transform trends may reflect motion over an interval shorter than the 3 m.y. over which spreading rates are averaged. This hypothesis could be tested by examining plate circuit closure using rate data with shorter averaging intervals.

The data may have tectonically induced biases. For example, north of the Orozco transform, Pacific–Cocos motion was split 4 Ma between the dual Mathematician and
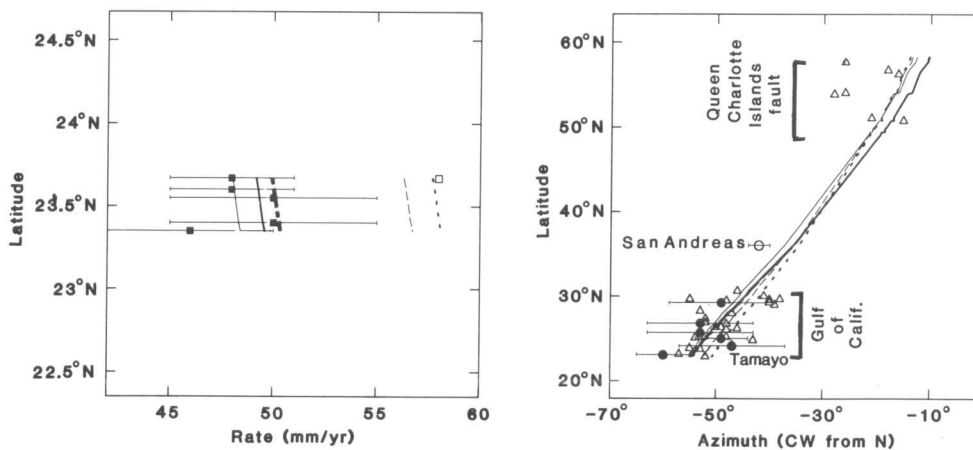
NAZCA – PACIFIC

Figure 26. Spreading rates (solid squares), transform fault azimuths (circles), and slip vector azimuths (triangles) observed along the East Pacific Rise are compared with directions and rates from the NUVEL-1 (bold solid), best-fitting (thin solid), RM2 (long dashed), and P071 (short dashed) Nazca–Pacific Euler vectors. Horizontal error bars show assigned 1-σ errors. The observed spreading rates, which we estimated from data we obtained from the NGDC, are systematically slower than those used to derive P071 and RM2 (open squares).

COCOS – NAZCA

Figure 27. Spreading rates (squares), transform fault azimuths (circles), and slip vector azimuths (triangles) observed along the Galapagos spreading centre are compared with directions and rates from the NUVEL-1 (bold solid), best-fitting (thin solid), RM2 (long dashed), and P071 (short dashed) Cocos–Nazca Euler vectors. Vertical error bars show assigned 1-σ errors.

northward-propagating East Pacific Rise spreading centres. Spreading along the Mathematician Ridge ceased by 3.0–3.5 Ma, and all Pacific–Cocos motion was transferred to the East Pacific Rise (Mammerickx 1984; Mammerickx, Naar & Tyce 1988). If slow spreading on the Mathematician Ridge continued to take up some of the motion between the Pacific and Cocos plates during chron 2A (2.48–3.40 Ma), the profiles north of the Orozco transform (15.2 °N) may reflect not Cocos–Pacific, but Cocos–Mathematician spreading over part of this interval. The East Pacific Rise spreading rate would thus be slower than the total Pacific–Cocos rate. If we exclude the eight rates north of the Orozco transform, the value of F (2.1) indicates only insignificant non-closure of the circuit.

None of these explanations is compelling enough to justify eliminating any of the data to resolve the circuit non-closure. We thus use all the data from these three boundaries to obtain a model with the best least-squares compromise fit.

Plate motions about the Juan Fernandez triple junction

Chile Rise magnetic data are of poor quality because most ship tracks cross the closely spaced fracture zones offsetting the rise. Nevertheless the data seem good enough to show that spreading is 25 per cent slower than assumed by Chase (1978) and Minster & Jordan (1978) (Fig. 28). We reduced the available magnetic data to four rates [two rates from data obtained from the NGDC and two rates from the many profiles shown in Herron, Cande & Hall (1981)] varying from 58 to 63 mm yr^{-1}. Because it crosses two fracture zones near the rise crest, we omitted the South Tow 2 profile used in prior global plate motion models (Klitgord *et al.* 1973; Herron *et al.* 1981). The direction of motion is described by 51 slip vectors (41 from the CMT solutions). In contrast to most oceanic transform faults, along which slip vectors contribute little information to our plate motion model, slip vectors along the transform faults offsetting the Chile Rise contribute more information to the model than do the transform azimuths (Table 7). Slip vectors agree with

transform azimuths west of 100 °W, but differ systematically east of 100 °W (Fig. 28) (Anderson–Fontana *et al.* 1987).

The NUVEL-1 Nazca–Antarctic Euler vector gives a spreading rate of ~60 mm yr^{-1} along the Chile Rise, ~15 mm yr^{-1} slower than the rate included in prior global data sets (Fig. 28), and 7 mm yr^{-1} slower than the rate calculated from RM2. The directions given by the NUVEL-1 and RM2 models are similar, but both differ systematically from those determined from the best-fitting vector. Unlike the best-fitting vector, the NUVEL-1 Euler vector fits the many slip vectors along the Chile Rise, but misfits the transform azimuths. That the azimuths from the slip vectors are more consistent with plate circuit closure than are the mapped transform azimuths suggests that the latter may be systematically in error, but other explanations are possible. A GLORIA, Seabeam, or Seamarc survey of the Chile Rise transforms, particularly those east of 95 °W, could help determine the cause of the discrepancy between the slip vectors and transform azimuths.

The Pacific–Antarctic Rise is the key spreading centre linking the Pacific basin to the global circuit. We determined 17 rates from magnetic profiles from the NGDC and four from published figures. Near the NE end of the ridge, anomalies are easily correlated and give rates of 90–100 mm yr^{-1} (Fig. 29a). Although magnetic profiles are less clear as the spreading rate decreases to the southwest (Fig. 29b), anomaly 2A is unambiguous in the better profiles. Profiles from the SW end of the Pacific–Antarctic Rise give spreading rates of ~55 mm yr^{-1}. Our Pacific–Antarctic rates, which are as much as 5–8 mm yr^{-1} slower than those used to derive P071 and RM2 (Fig. 30), contribute to the differences between the NUVEL-1 estimate and prior estimates of Pacific–North America motion.

The bathymetric and magnetic data along the Pacific–Antarctic Rise (Molnar *et al.* 1975) are too sparse to give accurate estimates of the azimuths, and in some cases, the locations of many of the transform faults. We determined transform azimuths from bathymetric data, epicentre distributions, and the along-track first derivative of

NAZCA – ANTARCTIC

Figure 28. Spreading rates (solid squares), transform fault azimuths (circles), and slip vector azimuths (triangles) observed along the Chile Rise are compared with directions and rates from the NUVEL-1 (bold solid), best-fitting (thin solid), RM2 (long dashed), and P071 (short dashed) Nazca–Antarctic Euler vectors. Vertical error bars show assigned 1-σ errors. The observed spreading rates, which we estimated from data we obtained from the NGDC, are slower than the rate used in RM2 (open square).

ascending and descending Seasat altimetry profiles (Fig. 31). Where the transforms we include coincide with those of Minster & Jordan (1978), the azimuths were similar. The dense bathymetric data crossing a seismically inactive

transform fault near the western end (173.8 °E) of the rise define two segments with distinctly different trends. We used an azimuth of N31 °W, paralleling the more northerly trending segment (Fig. 31).

Earthquake slip vectors contribute nearly as much information to the direction of Pacific–Antarctic motion as the transform azimuths contribute (Table 7). Fifty-four slip
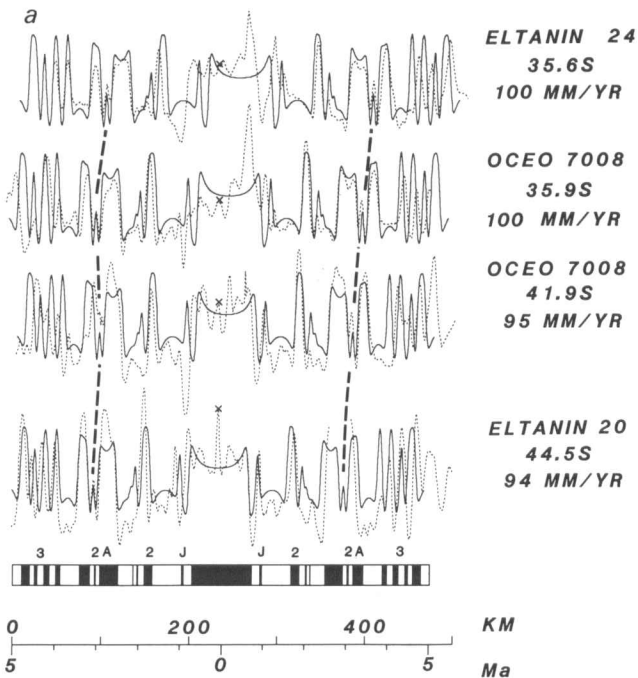
Figure 29(a). Antarctic–Pacific magnetic profiles (obtained from the NGDC archives) from 35° to 45 °S, 110° to 112 °W. Observed anomaly profiles are dashed, whereas computed synthetic anomaly profiles are solid. No attempt has been made to model asymmetric spreading, ridge jumps, or variable spreading rates. Thus the computed profiles, which were computed using a constant spreading rate, generally fit only anomaly 2A precisely. The rates that best fit the observed profiles are ~10 mm yr^{-1} slower than those used to derive P071 and RM2. Profiles are projected on to the ridge-normal direction (Table 3). The profiles are marked with crosses where they intersect the rise crest.
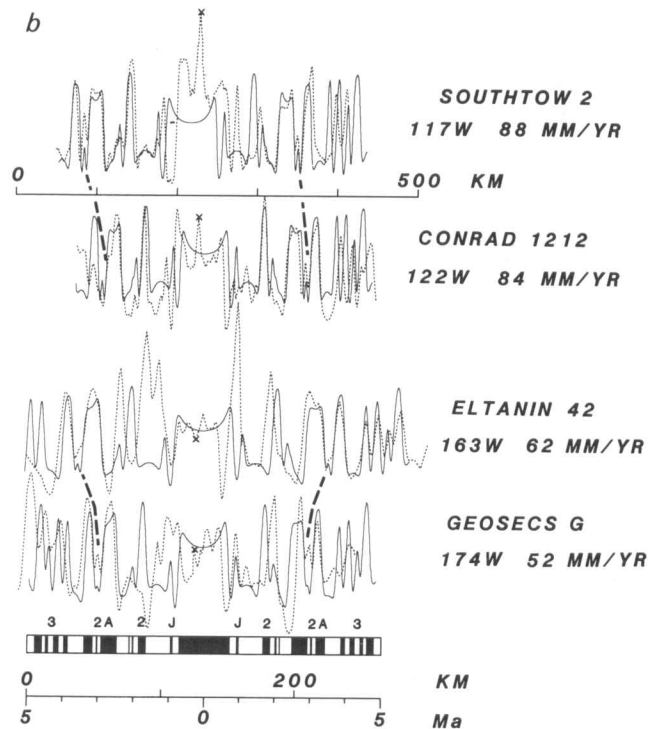
Figure 29(b). Antarctic–Pacific magnetic profiles (obtained from the NGDC archives) from 45° to 65 °S, 117° to 174 °W. The South Tow and *Conrad* profiles, which use the upper distance scale, give rates ~10 per cent slower than used in P071 and RM2. Profiles are projected on to the ridge-normal direction (Table 3). The profiles are marked with crosses where they intersect the rise crest.

ANTARCTIC – PACIFIC
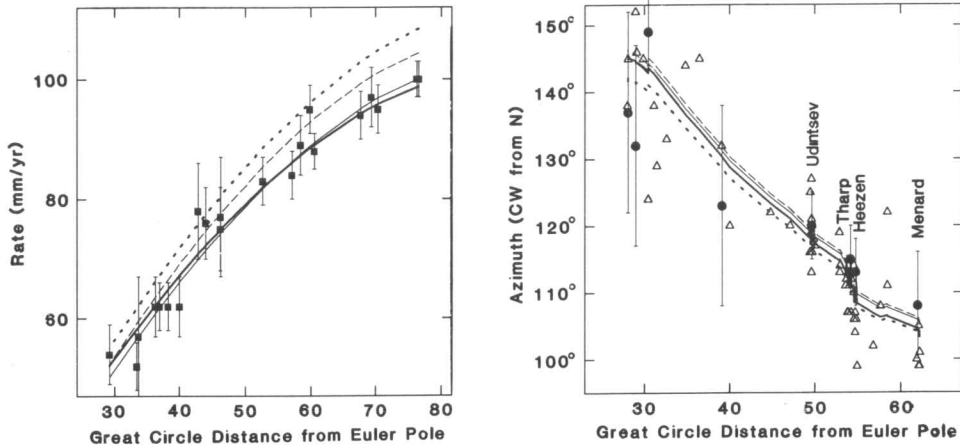
Figure 30. Spreading rates (squares), transform fault azimuths (circles), and slip vector azimuths (triangles) observed along the Pacific–Antarctic Rise are compared with directions and rates from the NUVEL-1 (bold solid), best-fitting (thin solid), RM2 (long dashed), and P071 (short dashed) Antarctic–Pacific Euler vectors. Vertical error bars show assigned 1-σ errors.

vectors (50 from the CMT solutions), including several along previously unidentified transforms, are well distributed along the Pacific–Antarctic Rise. Especially useful are the slip vectors near the western end of the rise, where transform trends are uncertain.

NUVEL-1 fits nearly all the Pacific–Antarctic rates within their uncertainties despite the small 3–4 mm yr^{-1} errors we assigned to the better rates (Fig. 30). P071 and RM2 give rates systematically faster than given by NUVEL-1. All three models adequately fit the scattered azimuthal data. The inconsistency in the observed trends of the western transforms may be caused by the lack of detailed bathymetric surveys.

Middle America Trench

To determine the directions of Cocos–Caribbean and Cocos–North America motion along the Middle America Trench, we use 100 slip vectors (56 from CMT solutions)

evenly distributed along the trench (Fig. 32). The location of the Caribbean–North America boundary along the Middle America Trench is poorly defined by seismicity; we arbitrarily place it at 96 °W, about where an extrapolation of the Motagua Fault would intersect the coast. Slip vectors from 88 °W to 96 °W may be biased by E–W extension in Nicaragua and Honduras south of the Motagua and Cuilco–Chixoy–Polochic faults (Manton 1987).

The NUVEL-1 Cocos–North America Euler vector fits the Cocos–North America slip vectors better than do prior models, but misfits slip vectors west of 100 °W by ~5°–10° (Fig. 33). Cocos–Caribbean slip vectors are also fit well, although the NUVEL-1 and best-fitting Cocos–Caribbean Euler vectors give directions that differ systematically by 5°–10°. The good fit to slip vectors from 88 °W to 96 °W suggests that any E–W extension within El Salvador and Honduras is much slower than the trench convergence rate, in the same direction as convergence, or both.
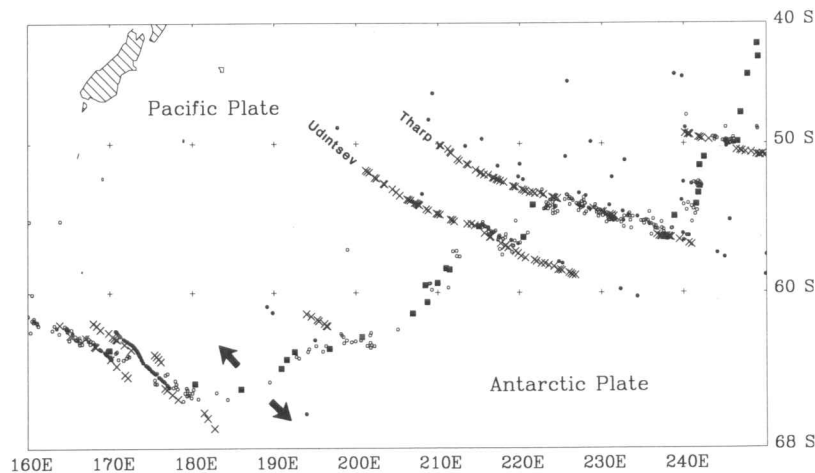
Figure 31. Earthquake epicentres (open circles), Seasat fracture zone crossings ('x'), ship-board fracture zone crossings (solid circles), and ridge locations from magnetic profiles (solid squares) along the Pacific–Antarctic rise. The epicentre, bathymetric, and Seasat data were used to estimate the strikes of transform faults along the rise.
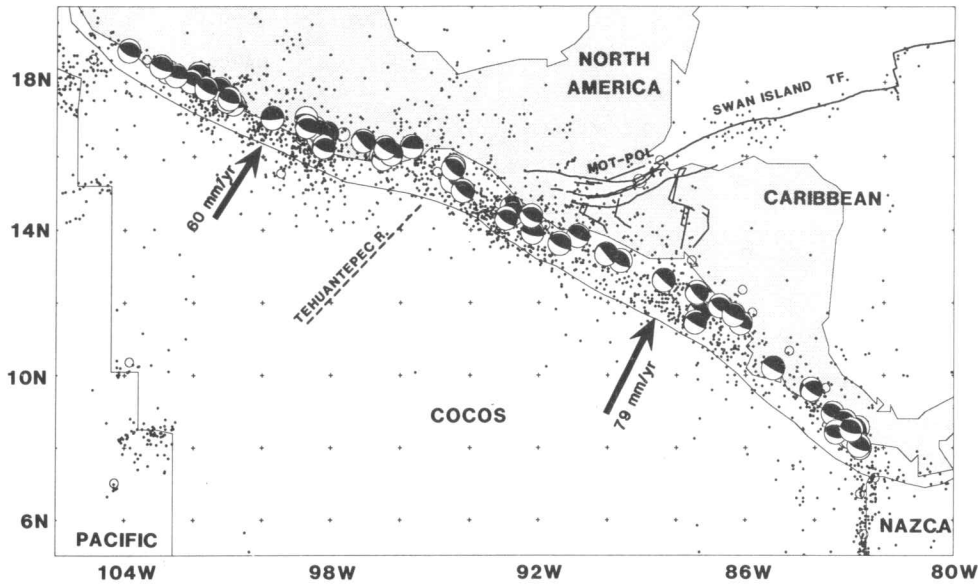
Figure 32. Focal mechanisms along the Middle America trench from the Harvard centroid-moment tensor solutions. The focal mechanisms give even slip vector coverage along the trench. Open circles and black dots show epicentres of earthquakes from 1963 to 1985 with depths shallower than 60 km. The black dots mark events with magnitudes less than 5.5, the small open circles mark events with magnitudes between 5.5 and 7.0, and the larger open circles mark events with magnitudes greater than 7.0. 'MOT-POL' labels the Motagua–Polochic fault system.

Nazca–South America

Nazca–South America motion is described by 99 slip vectors from the Peru–Chile and Ecuador trenches. Slip vectors from the Colombia–Ecuador trench north of 1 °N are omitted because seismicity within NW South America and Panama suggest deformation is diffuse (Pennington 1981; Mann & Burke 1984). The 99 slip vectors (68 from CMT solutions) are widely but non-uniformly distributed along the trench. Many earthquakes cluster near 33 °S where the Juan Fernandez ridge enters the trench (Figs 34–36). From 15 °S to 20 °S, where the Peru–Chile trench changes from a N–S to a NW–SE strike, the fault planes rotate but the slip

vectors maintain their E–W orientation, despite the expected oblique convergence (Fig. 34). South of 39 °S, in the rupture zone of the great 1960 earthquake, the only available thrust slip vector lies near the Chile triple junction.

The directions given by the NUVEL-1 Nazca–South America Euler vector nowhere differ by more than 5° from the directions from the best-fitting vector (Fig. 37). The fit to the slip vectors is similar to that given by RM2 and P071, but the convergence rate predicted by NUVEL-1 is significantly slower than predicted by prior Euler vectors. The 84 ± 2 mm yr^{-1} convergence rate at 40 °S, 74 °W, near the location of the great 1960 Chilean earthquake, is 7 mm yr^{-1} slower than predicted by RM2, and 24 mm yr^{-1}
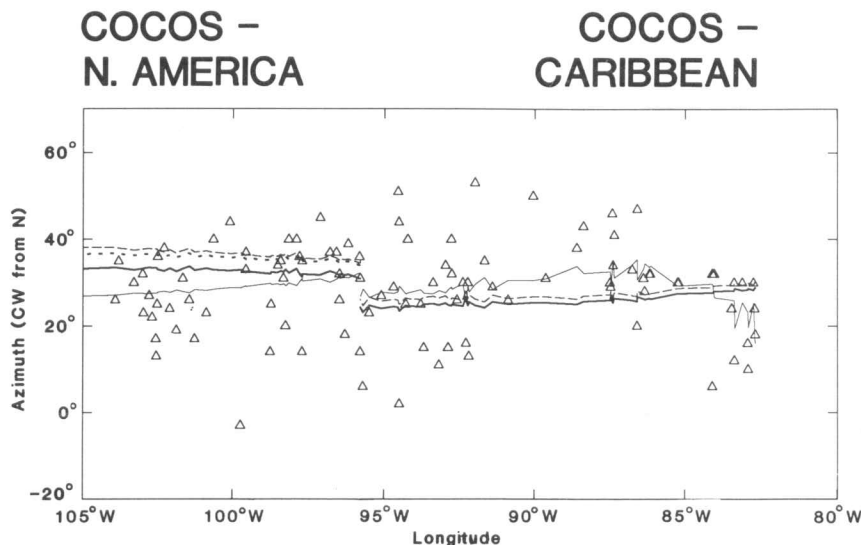
Figure 33. Slip vector azimuths (triangles) observed along the Middle America trench are compared with directions from the NUVEL-1 (bold solid), best-fitting (thin solid), RM2 (long dashed), and P071 (short dashed) Cocos–North America (west of 96 °W) and Cocos–Caribbean (east of 96 °W) Euler vectors. Because P071 did not include a Caribbean plate, no P071 model is shown east of 96 °W.
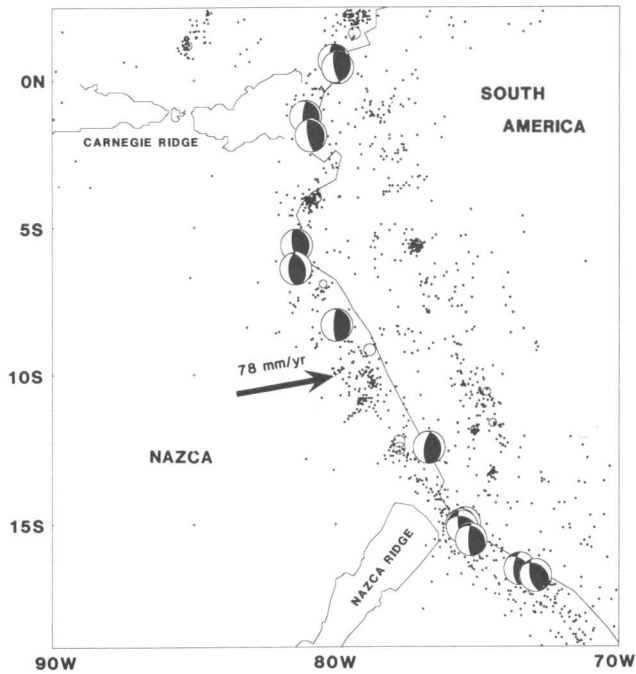
Figure 34. Harvard centroid-moment tensor focal mechanisms along the Ecuador and Peru–Chile trenches from 2.5 °N to 19 °S. Black dots show epicentres of earthquakes from 1963 to 1985 with depths shallower than 60 km. South of 15 °S, the strikes of the fault planes are counter-clockwise of those farther north, mirroring the counter-clockwise change in the strike of the trench. However, the auxiliary planes of the earthquakes south of 15 °S strike N–S giving E–W slip vectors similar to those from the equator to 15 °S and from 20 °S to 45 °S.
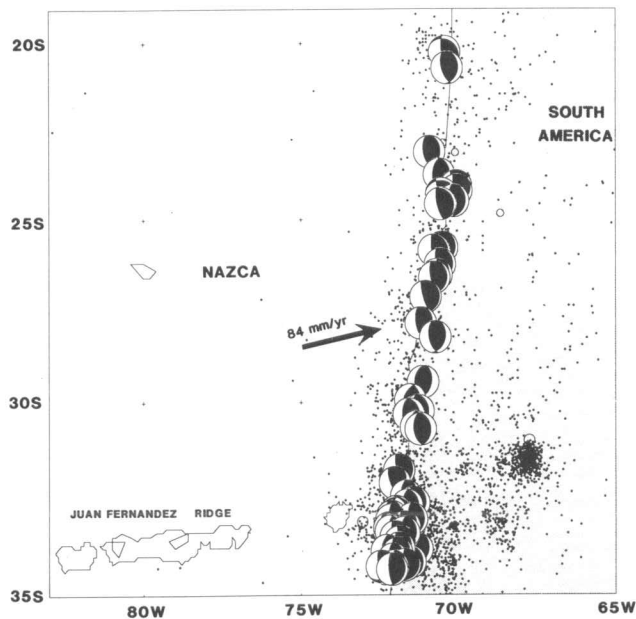
Figure 35. Harvard centroid-moment tensor focal mechanisms along the Peru–Chile trench from 19° to 35 °S. Black dots show epicentres of earthquakes from 1963 to 1985 with depths shallower than 60 km.
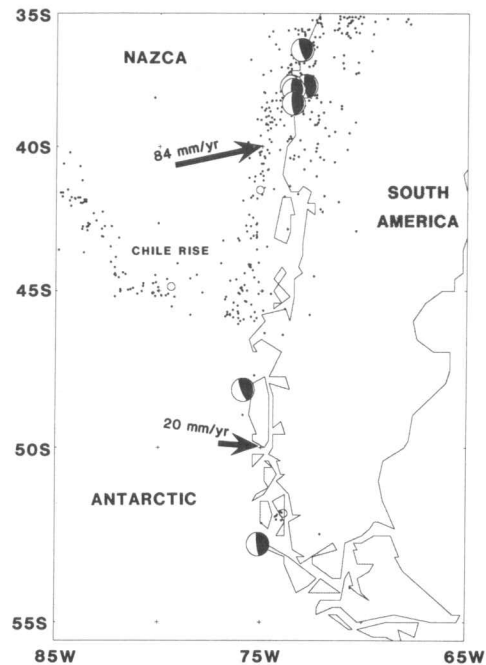
Figure 36. Harvard centroid-moment tensor focal mechanisms along the Peru–Chile trench from 35 °S to 56 °S. Black dots show epicentres of earthquakes from 1963 to 1985 with depths shallower than 60 km.

slower than predicted by P071. The slower convergence rate implies that the characteristic Chilean subduction zone earthquake is smaller than the 1960 earthquake, that the average recurrence interval is longer than in the past 400 yr, or both (Stein *et al.* 1986b).

Pacific–North America

The only direct observations of the rate of Pacific–North America motion come from five magnetic profiles that cross the Gulf Rise, the only Gulf of California ridge segment
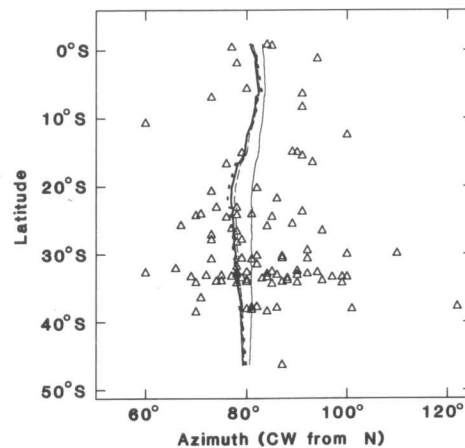
Figure 37. Slip vector azimuths (triangles) observed along the Peru–Chile trench are compared with directions from the NUVEL-1 (bold solid), best-fitting (thin solid), RM2 (long dashed), and P071 (short dashed) Nazca–South America Euler vectors.
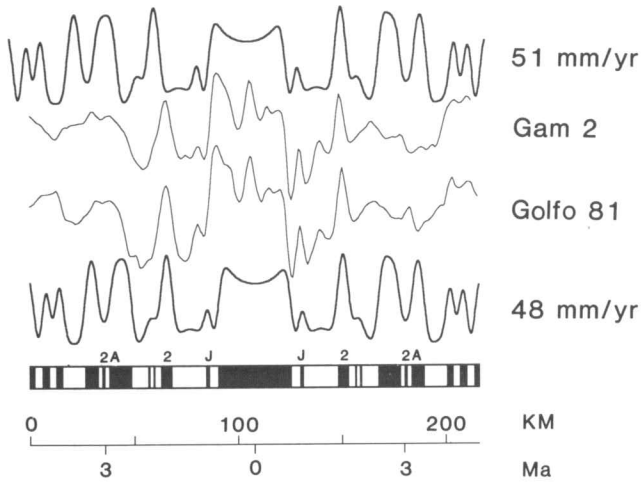
Figure 38. Magnetic anomaly profiles from the Gam-2 and Golfo-81 cruises across the Gulf Rise in the southern Gulf of California. Profiles are shown along-track (ship-tracks trend within 5° of N60 °W, the ridge-normal direction) and are reduced to the pole by a phase shift of 83° determined from the 1976 IGRF for the present magnetic field and an axial geocentric dipole for the remanent magnetization of the seafloor. Although the central anomaly and Jaramillo anomaly suggest an average rate of 51 mm yr^{-1} (upper synthetic magnetic anomaly profiles) since 1 Ma, the best fit to anomaly 2 or 2A is given by a rate of 48 mm yr^{-1} (lower synthetic magnetic anomaly profile).

with correlatable anomalies. The central and Jaramillo anomalies are fit by rates of 51–53 mm yr^{-1}, whereas anomaly 2 and a possible anomaly 2A are fit by 48 mm yr^{-1} (Fig. 38), 10 mm yr^{-1} slower than assumed in P071 and RM2 (DeMets *et al.* 1987). The direction of Pacific–North America motion was estimated from six Gulf transform azimuths and 26 Gulf slip vectors. The azimuth of the Tamayo transform is the most heavily weighted because it was estimated from detailed deep-tow surveys (Kastens,

Macdonald & Becker 1979; Macdonald *et al.* 1979; CYAMEX Scientific Team & Pastouret 1981) and because the Tamayo is the only Pacific–North America transform fault that offsets oceanic crust along its entire length. We determined trends of transforms located north of the Tamayo transform from a detailed bathymetric map (Dauphin & Ness 1989). These Gulf transforms, which are suspect because they partly or entirely offset continental crust, trend 7°–13° clockwise of the Tamayo (Fig. 39). Our Gulf transform trends are similar to those used by Minster & Jordan (1978), but are systematically ~5° clockwise of those estimated from the same data by Humphreys & Weldon (1989). New slip vectors (Goff, Bergman & Solomon 1987) are oriented 2°–5° counter-clockwise of those used in RM2, but are also clockwise of the trend of the Tamayo (Fig. 39). Any bias in the Gulf of California transform azimuths is important because the direction of Pacific–North America motion predicted by rigid-plate models along the San Andreas Fault in central California depends strongly on these azimuths. If Humphreys & Weldon's (1989) estimates are more appropriate than ours, then the Pacific–North America direction would be predicted to be closer to the trend of the San Andreas Fault, reducing the San Andreas discrepancy (Minster & Jordan 1984, 1987; DeMets *et al.* 1987).

Many other data may reflect the direction of Pacific–North America motion. How well these data do so, however, is unclear: the Pacific–North America boundary is in many places broad (e.g., the western US) and many trench slip vectors may be biased indicators of plate motion. Because slip vectors along the Aleutian and Kuril trenches were inconsistent with Pacific–North America motion estimated from other data, Minster *et al.* (1974) postulated that a distinct Bering plate moved independently of the North American plate. Because Engdahl, Sleep & Lin (1977) showed that Aleutian slip vectors may be biased by lateral seismic velocity heterogeneities reflecting the presence of cold subducting slab and because newer slip

PACIFIC – NORTH AMERICA

Figure 39. Spreading rates (solid squares), transform fault azimuths (solid circles), and slip vector azimuths (triangles) observed within the Gulf of California and along the Queen Charlotte Islands fault are compared with directions and rates from the NUVEL-1 (bold solid), best-fitting (thin solid), closure-fitting (bold dashed), RM2 (long dashed), and P071 (short dashed) Pacific–North America Euler vectors. The observed spreading rates, which we estimated from data from the NGDC archives and from G. Ness (personal communication, 1987), are slower than the rate used in RM2 (open square). An open circle shows the strike of the San Andreas fault along the Carrizo Plain. Horizontal error bars show assigned 1-σ errors.

vectors along the Kuril trench agreed with independently estimated Pacific–North America motion, Minster & Jordan (1978) eliminated the Bering plate and reassigned the trench slip vectors to the Pacific–North America boundary, although the Aleutian slip vectors were still systematically misfit. Part of the misfit may be caused by neglect of lateral heterogeneity of seismic velocities due to the cold subducting slab when earthquake focal mechanisms are determined (Toksoz, Minear and Julian 1971; Engdahl *et al.* 1977), but growing evidence suggests that the systematic misfits along many trenches, including the Aleutian trench, are partly or mainly caused by deformation of the leading edge of the overriding plate. Strike–slip motion occurs along many faults behind trenches and within forearcs (Fitch 1972; Zonenshain & Karasik 1981; Jarrard 1986a). Seismological evidence for deformation behind trenches includes strike–slip focal mechanisms with one nodal plane parallel to the volcanic arc (Fitch 1972; Ekstrom & Engdahl 1989) and volcanic arc eruptions preceded by such earthquakes (Sylvester 1988).

Given the complexities along the Pacific–North America boundary, it is difficult to decide which Pacific–North America plate motion data to accept and which to reject. One approach would be to include all data, but if some data are systematically in error, the resulting estimates of Pacific–North America motion could be biased. Alternatively, we could exclude all data that may have systematic errors, leaving a very small, but possibly unbiased set of data. However, the smaller the final data set, the more influenced it is by biases about the 'right' answer or by unrecognized systematic errors. We chose an approach closer to the latter than the former: we excluded data having strong independent evidence of biases, but we tried to retain enough data that biases would be averaged out.

From 30 °N to 58 °N, the Pacific–North America boundary consists of two disjoint segments: the San Andreas Fault system and the Queen Charlotte Islands Fault. Between these segments, from Cape Mendocino to Vancouver Island, the Pacific and North American plates are not in contact, and are instead separated by the Juan de Fuca and Explorer plates. We, like prior workers, omitted San Andreas Fault azimuths because extension in the Basin and Range shows that lithosphere east of the fault is moving relative to stable North America. The Queen Charlotte Islands Fault is a NNW-trending offshore fault extending from Vancouver Island to SE Alaska (Fig. 40). We use seven slip vectors along the Queen Charlotte Islands Fault north of 50 °N, but omit slip vectors north of 57.8 °N because earthquake focal mechanisms show tectonic complexities adjacent to the Fairweather Fault (Chandra 1974).

In the Gulf of Alaska, the interaction of the Pacific and North American plates is complex. At least one independent block, the Yakutat block, and perhaps two additional blocks, the St. Elias and Wrangell blocks, buffer Pacific–North America motion. These blocks are bounded to the south by the Aleutian trench and the Aleutian transition zone, an offshore zone of oblique thrusting (Lahr & Plafker 1980; Perez & Jacob 1980). On land, the Fairweather, Denali, Totschunda, and other strike–slip and thrust faults take up part of Pacific–North America motion. We therefore omit slip vectors between 137 °W, the postulated eastern limit of the St. Elias and Yakutat blocks, and 155 °W, the postulated western limit of the Wrangell block (Lahr & Plafker 1980).

We omitted Aleutian trench slip vectors west of ~165 °W (i.e., the Alaska Peninsula) because geological and seismological (Ekstrom & Engdahl 1989) data suggest the
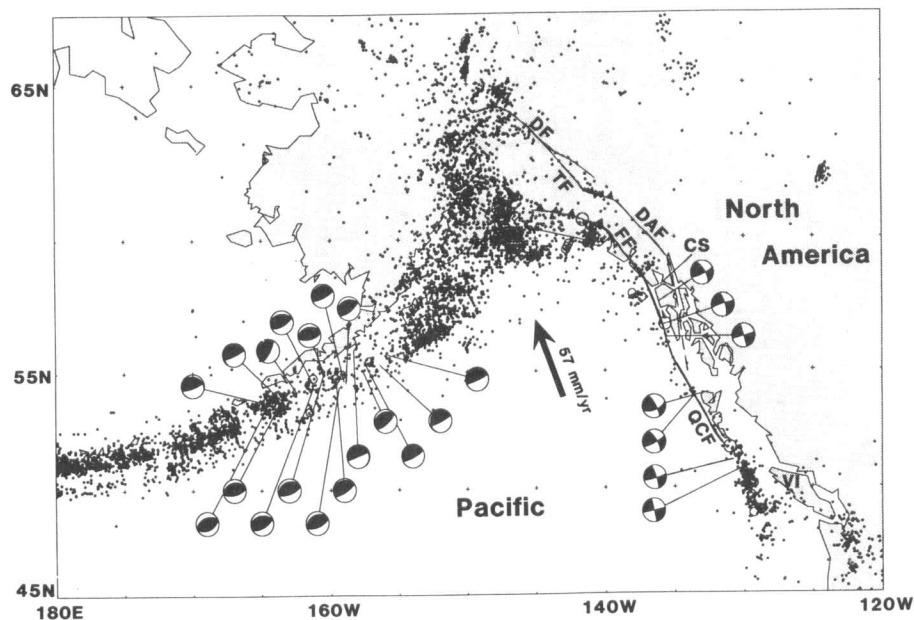
Figure 40. Focal mechanisms along the Queen Charlotte Islands fault and Alaska Peninsula used to derive slip vectors to estimate Pacific–North America motion. Black dots show epicentres of earthquakes from 1963 to 1985 with depths shallower than 50 km. The major active faults discussed in the text are the Denali fault (DF), Dalton fault (DAF), Queen Charlotte Islands fault (QCF), Totschunda fault (TF), and Fairweather fault (FF). The Queen Charlotte Islands fault, extending from northern Vancouver Island (VI) to Cross Sound (CS), is mainly a strike–slip fault, but may also take up some convergence. Seismicity between ~145 °W and 155 °W extends far inland from the trench, suggesting that convergence is taken up over a broad region.

PACIFIC – NORTH AMERICA
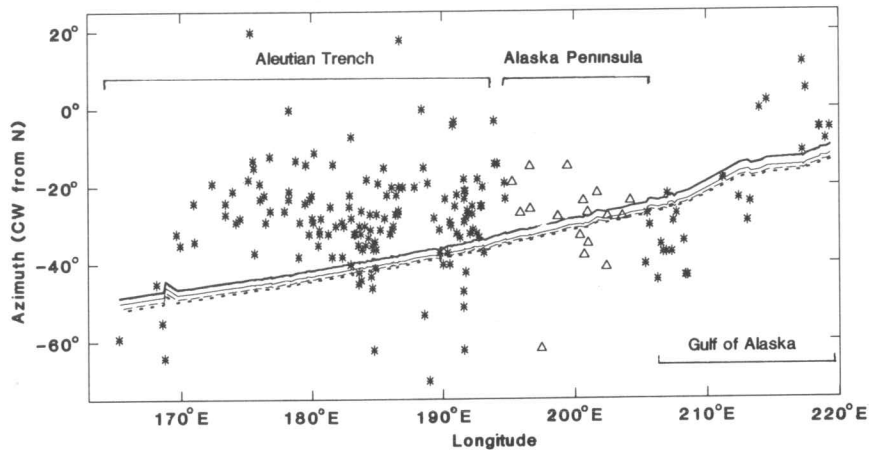
Figure 41. Slip vector azimuths (triangles) observed along the Aleutian Trench and in the Gulf of Alaska are compared with directions from the NUVEL-1 (bold solid), best-fitting (thin solid), RM2 (long dashed), and P071 (short dashed) Pacific–North America Euler vectors. Asterisks show slip vectors not used in deriving NUVEL-1. The NUVEL-1 and closure-fitting vectors give directions that are indistinguishable in this figure.

Aleutian forearc moves independently of the North American plate. Reflection seismic data from intra-arc basins near 172 °W suggest intra-arc extension related to rotations of forearc blocks (Geist, Childs & Scholl 1987). Palaeomagnetic data and the trends of the fault scarps bounding these blocks suggest that several independent blocks west of 168 °W are rotating clockwise and translating westward, probably as a result of oblique convergence along the trench (Harbert 1987; Geist, Childs & Scholl 1988).

P071 and RM2 include slip vectors from the Kuril–Kamchatka trench to describe Pacific–North America motion. In the absence of evidence for strike–slip faulting in Kamchatka (Jarrard 1986a,b), we include 15 slip vectors from earthquakes along the Kamchatka trench. However, Seno (1985) cites seismological and geological evidence for a collision between Hokkaido and a southwestward translating Kuril forearc. We thus omit slip vectors along the Japan trench and the Kuril trench south of Kamchatka.

NUVEL-1 fits Gulf of California rates and azimuths within their uncertainties, except for the Tamayo transform (which is fit just outside its assigned uncertainty) (Fig. 39). NUVEL-1 gives a rate of 49 mm yr^{-1} in the Gulf of California, close to the rate previously determined from a slightly different set of data (DeMets *et al.* 1987). Only two of 66 Pacific–North America slip vectors are fit outside their uncertainties (Figs 39, 41, and 42). The only systematic misfit occurs along the Queen Charlotte Islands Fault, where six of seven vectors are counter-clockwise of NUVEL-1, suggesting unmodelled contraction perpendicular to the Queen Charlotte Islands Fault, a bias in NUVEL-1, or a bias in the slip vectors, possibly due to the strong horizontal seismic velocity gradients of the ocean–continent transition. These seven slip vectors have little effect on NUVEL-1; their summed importance is only 0.04.

The best-fitting Euler vector for our set of 77 data is 49.6 °N, 76.7 °W, 0.74° m.y.$^{-1}$. Adding the 340 slip vectors

PACIFIC – NORTH AMERICA
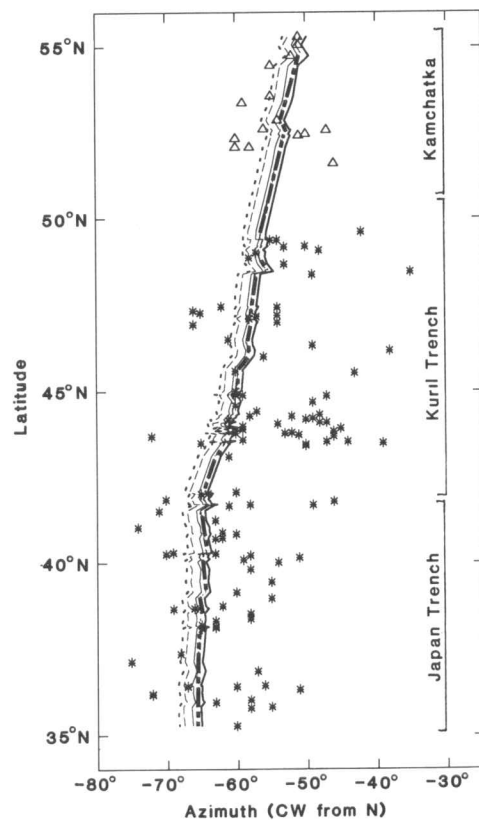
Figure 42. Slip vector azimuths (triangles) observed along the Kamchatka, Kuril, and Japan trenches are compared with directions from the NUVEL-1 (bold solid), best-fitting (thin solid), closure-fitting (bold dashed), RM2 (long dashed), and P071 (short dashed) Pacific–North America Euler vectors. Asterisks show slip vectors not used in deriving NUVEL-1.

omitted along the Japan and Kuril trench, the Aleutian arc, and the Gulf of Alaska, the best fitting Euler vector shifts to 46.3 °N, 84.9 °W, 0.88° m.y.$^{-1}$, a 6° shift in pole location and a 19 per cent increase in rotation rate. The larger data set is less well fit with χ^2 equaling 253.4 with 414 degrees of freedom ($\chi^2_v = 0.61$), compared with χ^2 of 15.3 with 74 degrees of freedom ($\chi^2_v = 0.21$) for the smaller data set. An *F*-ratio test shows that the hypothesis that the 77 selected data and the 340 omitted data are drawn from the same population can be rejected at the 1 per cent risk level; the systematic misfit to the omitted data is much too large. This test suggests that the smaller data set gives us a better estimate of Pacific–North America motion than would the larger data set. Encouragingly, the smaller data set also gives an Euler vector in better agreement with the closure-fitting vector than does the larger data set.

We also examined the effect on the global model of adding the 340 omitted data. The NUVEL-1 Pacific–North America Euler vector is 48.7 °N, 78.2 °W, 0.78° m.y.$^{-1}$. With the 340 slip vectors added to the global data set, this Euler vector shifts to 46.9 °N, 81.8 °W, 0.79° m.y.$^{-1}$, a 3° shift in pole location and a 1 per cent increase in rotation rate. Thus, NUVEL-1 would be only modestly altered by adding these 340 slip vectors.

CLOSURE OF PLATE CIRCUITS

The many redundancies in the NUVEL-1 plate circuit network (Fig. 5) allow the mutual consistency of the data to be tested. An inconsistency may be indicated by plate circuit non-closure, which could be caused by systematic errors in the data, intraplate deformation, or the existence of a previously unrecognized diffuse plate boundary, such as the boundary between India and Australia. Here we systematically test for plate circuit closure in two different ways. First we test the closure of all three-plate circuits with enough data on each boundary to estimate a best-fitting Euler vector or pole. Second we test plate circuit closure globally by comparing each best-fitting vector or pole with its closure-fitting vector.

Closure of three-plate circuits

A statistical test for plate circuit non-closure based on an *F*-ratio test (Gordon *et al.* 1987) was applied to the nine possible three-plate circuits having enough data along each boundary. Only the Bouvet and Galapagos triple junctions fail the closure test at the 1 per cent risk level (Fig. 43). Non-closure about the Galapagos triple junction causes a systematic misfit of ~3 mm yr^{-1} to Pacific–Cocos rates north of 16 °N (Fig. 24). Non-closure about Bouvet causes a 1–2 mm yr^{-1} misfit to the Antarctic–South America (Fig. 14) and Africa–Antarctic rates (Fig. 16). These misfits are small enough to be caused by systematic errors, but may reflect intraplate deformation adding up to a few mm yr^{-1}. Despite the small, significant, systematic misfits, the absence of larger misfits testifies to the accuracy of the rigid plate hypothesis when applied to the plate boundaries (mainly in oceanic lithosphere) represented by the NUVEL-1 data. Applying the same test for closure to the same triple junctions, but using the RM2 data, three (Azores, Bouvet,
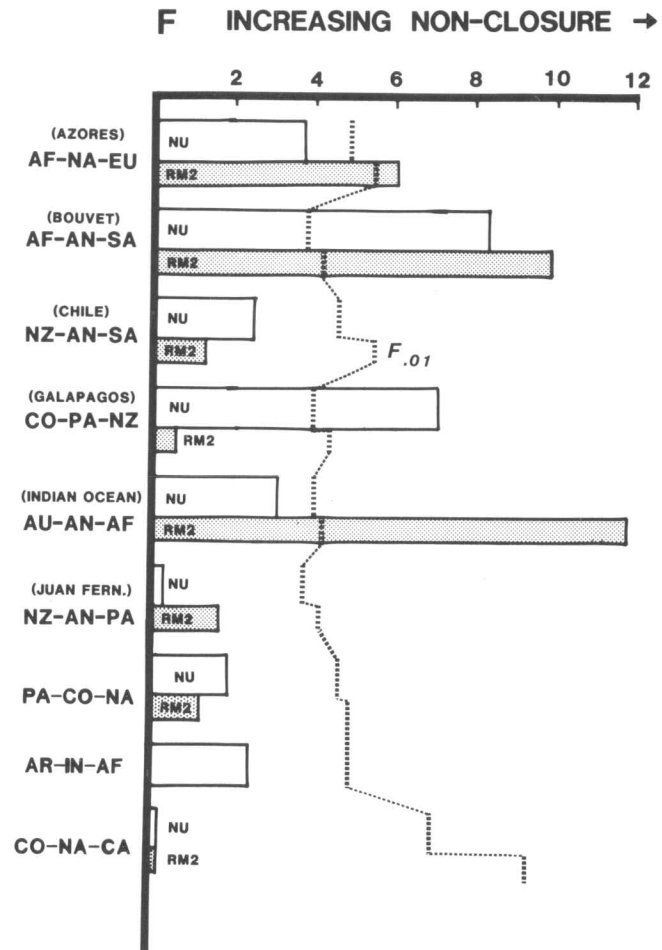
Figure 43. Test for closure of nine three-plate circuits. Values of *F* exceeding the 1 per cent risk level show significant non-closure of a plate circuit (Gordon *et al.* 1987). Open bars show results using NUVEL-1 data, and shaded bars show results using RM2 data. Abbreviations: Africa (AF), Antarctica (AN), Australia (AU), Cocos (CO), Eurasia (EU), Nazca (NZ), Pacific (PA), North America (NA), India (IN), Caribbean (CA), Arabia (AR), and South America (SA).

and Indian Ocean) of the nine three-plate circuits fail closure (Fig. 43).

Global closure: comparison of best- and closure-fitting Euler vectors

The mutual consistency of the data can also be tested globally, through comparison of each best-fitting vector or pole with the closure-fitting vector calculated from the rest of Earth. In a test for closure of a three-plate circuit, the possible cause of the systematic misfit is restricted to the plate boundaries analysed. In global closure tests, however, systematic errors anywhere could cause non-closure. Thus, a global closure test is a stronger test, more likely to indicate significant non-closure, but it is a less specific test because it is harder to isolate the data causing the non–closure. The tests we use are straightforward extensions of previously described tests for closure (Gordon *et al.* 1987).

Global closure tests for all 22 plate boundaries for which we could determine a best-fitting vector or pole give two

significant (at the 1 per cent risk level) non-closures based on a chi-square test and nine significant non-closures based on an F-ratio test (Table 8, Fig. 44). We focus on the results of the F-ratio tests, because the chi-square test underestimates non-closure if, as we believe, errors have been systematically overestimated (Gordon *et al.* 1987). All four best-fitting poles determined only from trench slip vectors (Caribbean–South America, Cocos–Caribbean, Cocos–North America, and Nazca–South America) systematically differ from their closure-fitting vectors (Fig. 44), again suggesting that trench slip vectors in many places are biased measures of plate motion.

The other five significant misfits are from plate boundaries consisting of spreading centres and the transform faults that offset them. As discussed above, the Cocos–Nacza and Cocos–Pacific misfits may have a local cause, as suggested by the significant non-closure of the Cocos–Nazca–Pacific plate circuit. Similarly, the Africa–Antarctica and Africa–South America misfits may have a local cause as suggested by the significant non-closure of the Africa–Antarctica–South America plate circuit. The remaining discrepancy, Africa–North America, is not easily related to local non-closure, because the only relevant three-plate circuit (Africa–Eurasia–North America) is consistent with closure. NUVEL-1 gives an excellent fit to all Africa–North America plate motion data except the azimuth of the Kane transform (Fig. 11), which has been mapped with both GLORIA and Seabeam (Roest, Searle & Collette 1984; Pockalny, Detrick & Fox 1988). These surveys give azimuths that agree within

Figure 44. Test for consistency between each best-fitting Euler vector and its corresponding closure-fitting Euler vector. 'F' is determined from an F-ratio test for plate circuit closure (Gordon *et al.* 1987). The curves labeled '$F_{.05}$' and '$F_{.01}$' respectively show the 5 and 1 per cent risk levels for the F-ratio test. Where a horizontal bar extends to the right of only one curve (i.e., the '$F_{.05}$' curve), the best- and closure-fitting vector differ at the 5 per cent risk (95 per cent confidence) level; where a horizontal bar extends to the right of both curves, the best- and closure-fitting vector differ at the 1 per cent risk (99 per cent confidence) level. Composite plate boundaries include data from spreading ridges, transform faults, and trenches.

0.5°. We think our estimate of a 2° uncertainty is conservative, yet the misfit by NUVEL-1 exceeds 4°.

One plausible explanation for the misfit is that non-closures of circuits that connect the Pacific basin plates to the North American plate are taken up in NUVEL-1 along the short Africa–North America boundary. Argus & Gordon (1989) find that the fit to the Kane improves if only Atlantic plate circuit closures, and not all global closures, are enforced. Argus & Gordon (1989) also propose that the Kane transform fault separates the African plate from lithosphere within a diffuse plate boundary dividing North America from South America. In their model, the azimuth of the Kane suggests that the American seafloor adjacent to it moves with a velocity roughly midway between the velocity expected if the seafloor were part of a rigid North American plate and if the seafloor were part of a rigid South American plate. We suspect that both global closures and the proximity of a diffuse North America–South America boundary are responsible for at least part of the misfit of NUVEL-1 to the azimuth of the Kane transform fault.

Table 8. Test of significance of the difference between best- and closure-fitting Euler vectors.

Euler Vector	Degrees of Freedom	χ^2_v	F
Spreading Centers and Transform Faults			
af-na	3	2.6	10.9
co-nz	3	2.2	9.2
af-an	3	1.7	7.0
co-pa	3	1.6	6.9
af-sa	3	1.4	6.0
an-pa	3	0.7	2.9
nz-an	3	0.6	2.5
au-af	3	0.6	2.5
au-an	3	0.6	2.5
eu-na	3	0.4	1.5
nz-pa	3	0.3	1.2
ar-af	3	0.2	1.0
in-af	3	0.2	1.0
Transform Only			
ar-in	2	0.4	1.5
Composite			
af-eu	2	0.5	2.2
pa-na	3	0.5	2.1
an-sa	3	0.5	2.1
Trenches			
ca-sa	2	6.3	27.4
co-ca	2	4.2	18.0
nz-sa	2	3.6	15.4
co-na	2	1.9	8.0

The values of χ^2_v and F for two and three degrees of freedom at the 1% risk level are 4.6 and 3.8 (at the 5% risk level: 2.6 and 3.0). Plate abbreviations: pa, Pacific; na, North America; sa, South America; af, Africa; co, Cocos; nz, Nazca; eu, Eurasia; an, Antarctica; ar, Arabia; in, India; au, Australia; ca, Caribbean.

Despite these discrepancies, nearly all the data used to derive NUVEL-1 are fit well, with no systematic misfits to rates exceeding ~3 mm yr^{-1}. In particular, discrepancies are small in the Indian Ocean, where prior global models had large misfits.

PREDICTIONS AND IMPLICATIONS

Although rigid plate models poorly describe the deformation within a diffuse plate boundary, they predict the motion of the major plates bounding the deforming zone. Owing to the complexity of these deformation zones, data from them were not used in constructing NUVEL-1. Here we compare NUVEL-1's predictions for some of these complex regions with geodetic data, seismicity and earthquake focal mechanisms, and other data.

Western North America

The concept of western North America as a wide, soft, boundary between rigid Pacific and North American plates was advocated by Atwater (1970) following pre-plate tectonic concepts of Carey (1958), Wise (1963), and Hamilton & Myers (1966). The broad seismic zone distributed over the western US contrasts sharply with the narrow seismic belts that delineate the oceanic transform faults and mid-ocean ridges. Several recent papers have attempted to quantify how this deformation is distributed (Minster & Jordan 1984, 1987; Weldon & Humphreys 1986). A critical constraint on these models is the velocity of the Pacific relative to the North American plate. NUVEL-1 predicts motion 8–10 mm yr^{-1} slower than predicted by prior global plate motion models. The different predictions for Pacific–North America motion in central California at 36 °N, 120.6 °W [the 'fiducial point' of Minster & Jordan (1984)] are 56 mm yr^{-1} at N36 °W (RM2), 58 mm yr^{-1} at N35 °W (P071), and 48 ± 1 mm yr^{-1} at N36 ± 2 °W (NUVEL-1).

Recent data from very-long-baseline interferometry (VLBI) provide the first geodetic measurements of Pacific–North America motion (Clark *et al.* 1987; Kroger *et al.* 1987). In a reference frame where six stations on stable North America are held fixed, VLBI sites near the California coastline (Vandenberg and Fort Ord) are moving 50–51 mm yr^{-1} in a direction similar to all three global plate motion models (Clark *et al.* 1987). If these sites are moving with the Pacific plate, NUVEL-1 predicts that Vandenberg moves 49 ± 1 mm yr^{-1} directed N38 ± 2 °W and that Fort Ord moves 48 ± 1 mm yr^{-1} directed N35 ± 2 °W relative to stable North America. The good agreement with the NUVEL-1 model is consistent with the joint hypotheses that the VLBI measurements can be compared with plate motion averaged over several million years and that the slip rate on offshore faults west of Vandenberg is negligible.

The measured slip along the San Andreas Fault is too slow (~35 mm yr^{-1}) (Prescott, Lisowski & Savage 1981; Sieh & Jahns 1984) to take up all the motion between the Pacific and North American plates. Moreover, the strike of the San Andreas Fault, N41 °W, is 5° counter-clockwise of the direction predicted by NUVEL-1. Unless NUVEL-1, P071, and RM2 give significantly biased estimates of the direction of plate motion, the San Andreas Fault trends

the wrong direction to take up all Pacific–North America motion.

This 'San Andreas discrepancy' can be quantified as a vector difference: the Pacific–North America velocity predicted at the fiducial point minus the observed San Andreas slip (Minster & Jordan 1984, 1987; DeMets *et al.* 1987). The discrepancy vector determined using NUVEL-1 (14 mm yr^{-1} directed N23 °W) (top of Fig. 45) is smaller than the discrepancy vector determined from RM2 (22 mm yr^{-1} directed N27 °W). Until a few years ago, it was widely assumed that the San Andreas discrepancy could be explained by extension within the Basin and Range. Minster & Jordan (1984) argue, however, that Basin and Range spreading is too slow (~10 mm yr^{-1}) and in the wrong direction (~N60 °W) to explain the discrepancy. Their kinematic model fit to extension directions in the Basin and Range gives a direction at the fiducial point of N69 °W, respectively 52° and 56° CCW of the RM2 and NUVEL-1 discrepancy vectors.

A modified discrepancy vector can be found by subtracting from the Pacific–North America velocity both
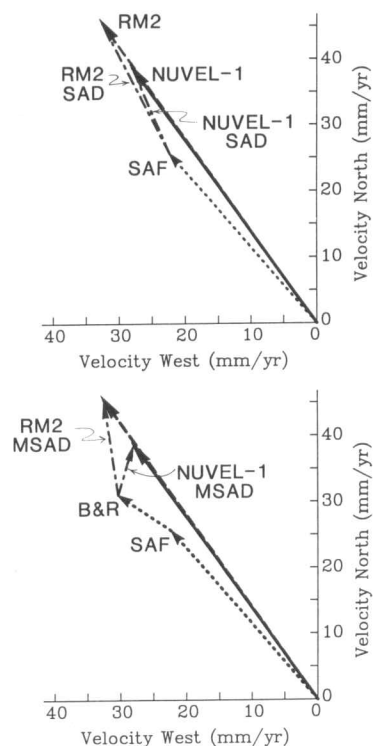
Figure 45. Linear velocity vectors showing the observed and predicted motions at 36 °N, 120.6 °W along the San Andreas fault in central California. In the top half of the figure the Pacific–North America velocity predicted from NUVEL-1 (solid line) and RM2 (long-dashed line) are compared with the slip observed along the San Andreas Fault (short-dashed line labelled 'SAF'). The vector difference between observed and predicted motion gives the San Andreas discrepancy (dot–dashed lines labelled 'NUVEL-1 SAD' and 'RM2 SAD'). In the bottom half of the figure the predicted velocities are compared with the sum of the slip observed along the San Andreas Fault (short-dashed line labelled 'SAF') and the motion attributed to Basin and Range spreading (short-dashed line labelled 'B&R'). The vector difference between observed and predicted motion gives the modified San Andreas discrepancy (dot–dashed lines labeled 'NUVEL-1 MSAD' and 'RM2 MSAD').

San Andreas slip and the effect of Basin and Range expansion at the fiducial point. From model RM2, Minster & Jordan (1987) obtain a modified discrepancy vector of 14 mm yr^{-1} directed N08 °W, which can be resolved into components of 12 mm yr^{-1} parallel and 8 mm yr^{-1} perpendicular to the San Andreas Fault (bottom of Fig. 45). The modified San Andreas discrepancy from NUVEL-1 is 8 mm yr^{-1} directed N18 °E, which can be resolved into components of 4 mm yr^{-1} parallel and 7 mm yr^{-1} perpendicular to the San Andreas fault. The NUVEL-1 modified discrepancy vector is smaller than, but rotated clockwise of the RM2 modified discrepancy vector, and is thus even farther from the assumed direction of Basin and Range extension.

The smaller fault-parallel component of the NUVEL-1 modified discrepancy vector implies that less motion need be explained by strike–slip faulting on northwest-striking faults other than the San Andreas Fault. The component of the discrepancy perpendicular to the San Andreas Fault is little changed from the RM2 estimates, however, and suggests significant contraction perpendicular to the fault. Considerable evidence, from the orientations of folds and thrust faults in the Coast Ranges (Aydin & Page 1984; Page & Engebretson 1984; Stein & King 1984) and from the pattern of stress in central California (Mount & Suppe 1987; Zoback

et al. 1987; Oppenheimer, Reasenberg & Simpson 1988), suggests contraction in the correct sense in coastal and near-coastal California. How to reconcile the small observed shortening with the geologically large 7 mm yr^{-1} shortening deduced from the modified discrepancy vector remains puzzling.

Australia–Pacific motion: Tonga–Kermadec, New Zealand, and the Macquarie ridge

The Australia–Pacific plate boundary includes the Solomon, Kermadec, and Tonga trenches, the Alpine Fault system in New Zealand, and the Macquarie ridge complex, which extends southwards from New Zealand to the Australia–Pacific–Antarctic triple junction. Because NUVEL-1 includes no data along the Australia–Pacific plate boundary, the Australia–Pacific Euler vector is predicted from data along other plate boundaries. The predicted directions are ~5°–15° counter-clockwise of those of P071 and RM2 along most of the plate boundary (Fig. 46). The convergence rate predicted by NUVEL-1 at 35 °S, 181 °E, north of New Zealand, is 53 ± 1 mm yr^{-1}, ~15 per cent slower than the 61 and 65 mm yr^{-1} rates predicted by RM2 and P071. Unlike Minster & Jordan (1978), we use no slip vectors from earthquakes along the Tonga–Kermadec trench because of
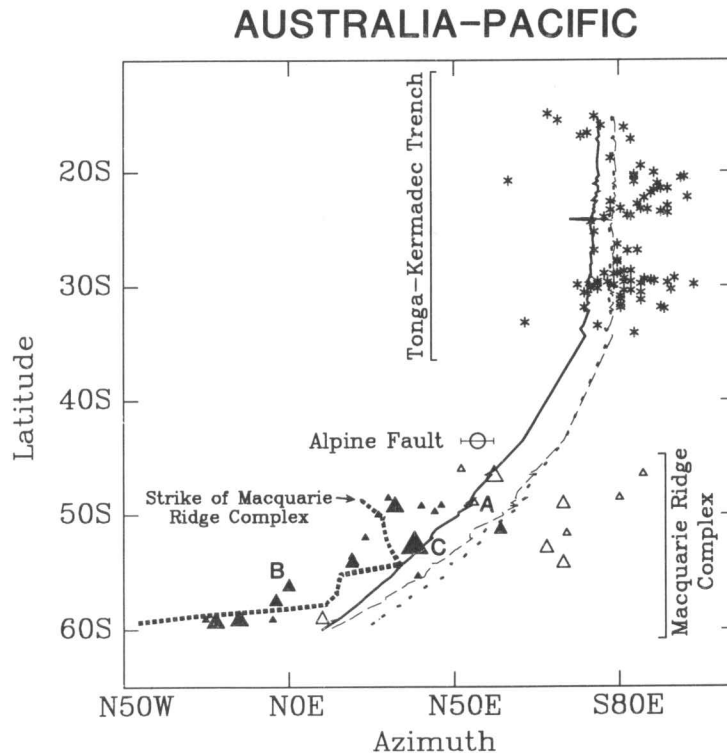
Figure 46. The strike of the Alpine fault (South Island, New Zealand) (open circle), and slip vector azimuths (asterisks north of 40 °S; solid triangles for strike–slip mechanisms and open triangles for thrust mechanisms south of 40 °S) observed along the Macquarie ridge, Tonga trench, and Kermadec trench are compared with the strike of the Macquarie ridge complex (bold dashed curve) and to the directions from the NUVEL-1 (bold solid) Australia–Pacific Euler vector and the RM2 (long dashed) and P071 (short dashed) India–Pacific Euler vectors. The symbol size for slip vectors from earthquakes south of New Zealand increases with increasing seismic moment: the smallest symbols show the slip from events with $M_0 < 10^{26}$ dyne cm, the second smallest show events with $10^{26} < M_0 < 10^{27}$ dyne cm, the third smallest show events with $10^{27} < M_0 < 10^{28}$ dyne cm, and the largest symbol shows an event with $M_0 > 10^{28}$ dyne cm. The slip vectors labelled 'A', 'B' and 'C' are respectively from the 1964 November 8, 1965 August 2, and 1989 May 23 events mentioned in the text. We used no slip vectors shown in this figure (or elsewhere along the Australia–Pacific boundary) in deriving NUVEL-1.

seafloor spreading behind the arc (Weissel, Hayes & Herron 1977; Malahoff, Feden & Fleming 1982). Along the Tonga–Kermadec trench, the direction of motion predicted by NUVEL-1 is N87–89°W, which is ~17° counter-clockwise of the mean slip direction, N71 ± 1°W, of 185 slip vectors. The sense of the discrepancy suggests that the lithospheric sliver or slivers overriding the trench move southeast relative to the Australian plate. At 41.5°S, 172.0°E, in northern South Island, the Australia–Pacific Euler vector predicts 42 ± 1 mm yr^{-1} directed N75 ± 2°E, consistent with velocities calculated from triangulation data (Bibby 1981; Walcott 1984). At 43.5°S, 170°E, along the Alpine Fault in South Island, New Zealand, the predicted motion is 39 mm yr^{-1} directed N71°E, ~16° clockwise of the N55°E trend of the fault, suggesting oblique convergence with an 11 mm yr^{-1} component perpendicular to the fault, and a 37 mm yr^{-1} component parallel to the fault. Along the short segment of the boundary north of 48°S and southwest of New Zealand, only thrust events have been observed and the direction of slip, while counter-clockwise of that predicted by P071 and RM2, is close to that predicted by NUVEL-1 (Fig. 46).

Chase (1978) used no slip vectors from earthquakes south of New Zealand and Minster & Jordan (1978) used only two, one from the 1964 November 8 thrust earthquake near 49°S ('A' in Fig. 46) and the 1965 August 2 strike–slip event near 56°S ('B' in Fig. 46). Both P071 and RM2 give directions of slip 10° or more clockwise of these two slip vectors, and many tens of degrees clockwise of the strike of the Macquarie ridge complex (Fig. 46), which Falconer (1973) proposed to be a strike–slip fault. Minster & Jordan (1978) suggested that the non-parallelism of RM2 with earthquake slip vectors and the strike of the boundary was caused by deformation within the Indian (i.e., Indo-Australian) plate. Because NUVEL-1 explicitly models motion between India and Australia and agrees well with the data along the Southeast Indian Ridge, we can now test this hypothesis. Fig. 46 shows that NUVEL-1 predicts a direction of motion typically many tens of degrees clockwise of the strike of the Macquarie ridge complex, except along a short segment near 53°S, which nearly parallels the predicted direction of motion. NUVEL-1 thus predicts that the Macquarie ridge complex is not a strike–slip boundary and instead accommodates oblique convergence, if the Australian and Pacific plates are both rigid.

A test of whether NUVEL-1 is consistent with the observed slip vectors is more complex. South of 48°S along the Macquarie ridge complex, both strike–slip and thrust faulting events occur. Nearly all the strike–slip events give slip vectors ~15–25° counterclockwise of the predicted direction of motion. All but one of the thrust events occur north of ~55°S and typically give slip vectors about 40° clockwise of the predicted direction (Figs 46–47). Thus along the segment of the boundary where many events with both types of mechanisms are observed (i.e., from 48°S to 55°S), the predicted direction tends to lie between the group of slip vectors from strike–slip events and the group of slip vectors from thrust events. Although the predicted slip is therefore consistent with the plate motion direction, the spread in slip directions is too large to give a strong test. The occurrence of two distinct types of mechanisms and slip directions suggests that earthquakes along this boundary
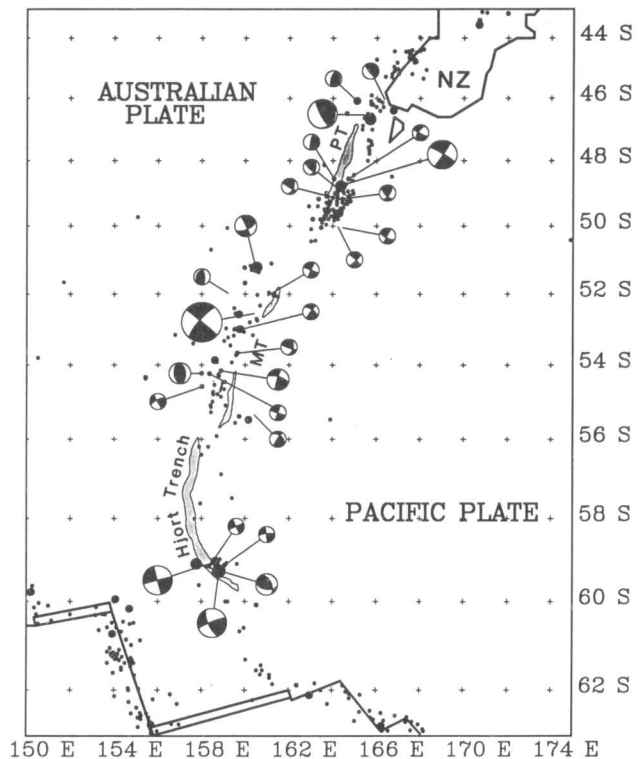
Figure 47. Earthquake focal mechanisms along the Australia–Pacific plate boundary south of New Zealand from CMT solutions [those cited in Table 3 plus Dziewonski *et al.* (1988e)], Banghar & Sykes (1969), Sykes (1967), P. Lundgren (personal communication, 1988), and Romanowicz & Ekstrom (1989). The size of the plotted mechanism increases monotonically with seismic moment: the smallest mechanisms show events with $M_0 < 10^{26}$ dyne cm, the second smallest show events with $10^{26} < M_0 < {}^{27}$ dyne cm, the third smallest show events with $10^{27} < M_0 < 10^{28}$ dyne cm, and the largest shows an event with $M_0 > 10^{28}$ dyne cm. The Australia–Pacific plate boundary south of New Zealand follows the Macquarie ridge complex, which includes the Puysegur trench (PT), Macquarie trench (MT), and Hjort trench (trenches are shaded).

segment do not occur along a single discrete fault. After this paper was submitted, a large earthquake occurred along the Macquarie ridge at 52.5°S, 161°E. With a seismic moment release of ~2×10^{28} dyne cm, it dominates the instrumentally recorded moment release. Romanowicz & Ekstrom (1989) determined a mechanism of pure strike–slip with a slip vector nearly parallel to the direction predicted by NUVEL-1 ('C' in Fig. 46), consistent with the joint hypotheses of rigid Australian and Pacific plates, and the accuracy of NUVEL-1 in describing their motion along the Macquarie ridge, at least near 52.5°S.

Along the segment of the Macquarie ridge complex south of 55°S (along the Hjort trench), the mechanisms of all but one earthquake are strike–slip. If we choose the fault plane for each of these strike–slip events to be the nodal plane nearest the local strike of the Hjort trench, then the slip vectors are ~30–40° counter-clockwise of the predicted direction of motion, suggesting that the real direction of slip differs significantly from NUVEL-1. Conflicting with this pattern is the occurrence of one thrust event with a seismic moment of ~2×10^{26} dyne cm. Which of its nodal planes is the fault plane is ambiguous (Fig. 47); the south-dipping,

east-striking plane gives a slip vector of N64 °E, while the NE dipping, NNW-striking plane gives a slip vector of N10 °E, which is the direction shown in Fig. 46. Whichever is the correct slip vector, this earthquake appears to be too small to account for the difference between the direction of slip observed in strike–slip earthquakes and that predicted by NUVEL-1. The geoid anomaly from this region also suggests that strike–slip dominates the long-term mode of slip. Ruff & Cazenave (1985) analysed Seasat profiles along the Macquarie ridge complex and found geoid anomalies characteristic of subduction along the latitudes where many thrust slip vectors are shown in Figs 46 and 47. However, south of 55 °S the Seasat profiles show little or no evidence of subduction and instead resemble profiles over active transform faults. The slip vectors along at least the southernmost part of the Macquarie ridge complex thus appear inconsistent with the predictions of the rigid plate model. The differences are too large to be explained by small systematic differences between fault azimuths and slip vectors, like those observed along Atlantic transform faults (Argus *et al.* 1989). A more likely explanation may be deformation or independent motion of the SE corner of the Australian plate, as suggested from systematic misfits to azimuth data along the eastern Southeast Indian Ridge (DeMets *et al.* 1988).

Motion between India and Australia

Because no data from the diffuse boundary dividing India and Australia are used in deriving NUVEL-1, the observed deformation within the boundary zone provides an independent test of the plate motion model. NUVEL-1 India–Australia motion is similar to that found by Gordon *et al.* (1989) from an analysis of data only in the Indian Ocean. With India arbitrarily held fixed, Australia rotates counter-clockwise about an Euler pole at 6 °S, 77 °E (Fig. 6b), i.e., the distance between the Australian and Indian continents is decreasing. Deformation observed within Indian Ocean lithosphere east and northeast of the Euler vector is consistent with the predicted shortening: basement folds and reverse faults are oriented roughly E–W west of the Ninetyeast ridge (Weissel, Anderson & Geller 1980; Stein, Cloetingh & Wortel 1989) and earthquakes with strike–slip mechanisms consistent with left-lateral slip on N–S striking fault planes occur along and near the Ninetyeast ridge (Stein & Okal 1978; Bergman & Solomon 1985). Moreover, west of the Euler vector, large normal faulting earthquakes showing N–S extension occur near Chagos Bank (Stein 1978; Wiens & Stein 1984; Wiens 1986). The model predicts that the distance between Calcutta and Sydney is decreasing at a rate of $12 \pm 3 \, \text{mm yr}^{-1}$, a rate measurable by VLBI or satellite laser ranging. Predictions and observations are compared more extensively by Gordon *et al.* (1989).

Motion between North and South America

Although motion between North and South America has long been resolvable from plate motion data (Minster *et al.* 1974; Chase 1978; Minster & Jordan 1978; Stein & Gordon 1984), predictions of the sense of motion along the assumed location of the North America–South America boundary

have not been robust. From RM1, Minster *et al.* (1974) predicted mainly left-lateral strike–slip motion along a boundary they assumed extended westward from the Mid-Atlantic Ridge at 15 °N. RM2 predicts right-lateral strike–slip along this same boundary, and P071 predicted N–S contraction. Given these prior predictions it seems only fitting that NUVEL-1 predicts mainly extension along most of the same assumed boundary. The wide range of predictions of the sense of motion is misleading, however, in how much the various Euler vectors differ. Because all the Euler vectors are located close to one another and to the assumed location of the North America–South America boundary (or boundary zone) (Fig. 6c), modest shifts in the Euler pole lead to changes in the sense of predicted motion. Both the RM2 and P071 Euler poles lie within the 95 per cent confidence limits of the NUVEL-1 Euler pole, although the P071 Euler vector differs significantly from the NUVEL-1 Euler vector because of its significantly different rotation rate.

The strikes of well-mapped transform faults along the Mid-Atlantic Ridge have small, systematic, significant departures from the predictions of a model with a discrete North America–South America plate boundary. From these observations, Argus & Gordon (1989) propose that the boundary is diffuse, and that its intersection with the Mid-Atlantic Ridge is not centred at 15 °N, as previously assumed, but farther north. The pole of rotation they find from only Atlantic and Arctic data lies a few degrees from the NUVEL-1 pole. The sense of deformation predicted by the NUVEL-1 North America–South American pole can be compared with the principal stress axes of earthquake mechanisms within the diffuse plate boundary. *P* axes for two earthquakes (at 19.8 °N, 56.1 °W and 17.3 °N, 54.9 °W) (Bergman 1986) suggest that the instantaneous North America–South America Euler pole lies slightly east of the NUVEL-1 pole, but within its confidence limits.

Direction of Africa–Eurasia convergence in the Mediterranean

Seismicity in the western Mediterranean lies within a narrow band (~200 km wide) that runs east of Gibraltar, across North Africa, to Sicily. Because NUVEL-1 was determined from data outside the Mediterranean, its predictions can be compared with slip vectors from earthquakes between Gibraltar and Sicily, which may reflect motion between Eurasia and Africa. NUVEL-1 predicts northwest (~N45 °W) convergence at Gibraltar and N–NW (~N20 °W) convergence near Sicily. These predictions are ~10° counter-clockwise of RM2 and 15°–25° counter-clockwise of P071. Five slip vectors from strike–slip mechanisms and nine from thrust mechanisms agree reasonably with the predicted direction of motion (Argus *et al.* 1989). Moreover, *P*-wave modelling of the 1980 October 10 El Asnam earthquake (Yielding 1985) and geodetic survey results (Ruegg *et al.* 1982) suggest that the African plate moves northwest relative to the Eurasian plate. NUVEL-1, along with CMT slip vectors and the El Asnam studies, suggests Africa–Eurasia motion systematically counter-clockwise of prior models. The predicted rate ($5–8 \, \text{mm yr}^{-1}$) is similar (within $2 \, \text{mm yr}^{-1}$) to RM2 and P071.

East of Sicily, earthquakes may reflect motion of microplates or zones of distributed deformation (McKenzie 1972; Dewey & Sengor 1979; Jackson & McKenzie 1988). NUVEL-1 predicts the motion of the bounding African and Eurasian plates to be N19 °W at 8 mm yr^{-1} at Sicily and N07 °W at 10 mm yr^{-1} at Crete. These are ~2 mm yr^{-1} faster, and ~6° counter-clockwise of RM2, and within 1 mm yr^{-1} but ~15° counter-clockwise of P071.

Motion of Arabia and India relative to Eurasia

Along the Zagros and Himalayan collision belts, where Arabia and India are colliding with Eurasia (Fig. 48), deformation is distributed over a zone that is in places wider than 1000 km. Since no data from the Arabia–Eurasia and India–Eurasia boundaries are used to derive NUVEL-1, their Euler vectors are derived indirectly through plate circuits. The non-closures of Indian Ocean plate circuits in P071 and RM2 biased their Arabia–Eurasia and India–Eurasia Euler vectors. Because these non-closures are eliminated, NUVEL-1 provides an improved description of India–Eurasia and Arabia–Eurasia motion.

Along the Zagros fold and thrust belt and Makran subduction zone (Figs 48–50), the NUVEL-1 Arabia–Eurasia Euler vector predict directions 10°–15° counter-clockwise of RM2 and P071. Three slip vectors from the Makran subduction zone, the only place along the collision zone where oceanic lithosphere is being subducted, are better fit by NUVEL-1 (Fig. 50), but the earthquakes are small ($M_0 \cong 10^{24}$ dyne cm) and may be unrepresentative of the long-term convergence direction. Thrust faulting occurs along the southern and central Zagros, and right-lateral strike–slip motion occurs along the Main Recent Fault. The NUVEL-1 Arabia–Eurasia Euler vector systematically misfits slip vectors from thrust-faulting mechanisms west of

~54 °E along the Zagros Mountains (Fig. 50). If the slip vectors are unbiased estimates of the direction of plate motion, they are inconsistent with the Zagros being the boundary between rigid Arabian and Eurasian plates. One possible explanation is that additional deformation occurs along a curved belt of faults and earthquakes that extends from the SW margin of the Caspian Sea to southeastern Iran (Fig. 48). From summed seismic moments, Jackson & McKenzie (1988) estimate a deformation rate along this belt comparable with or greater than that along the Zagros.

Along the Main Recent Fault (Fig. 48), seismologic and field evidence suggest right-lateral strike–slip with some thrusting (Tchalenko & Braud 1974; Berberian 1981). The predicted direction of motion (N11 °W) at 35 °N, 47 °E is 34° clockwise of the strike of the fault. As along the Macquarie ridge, the direction predicted along the fault is between the directions determined from slip vectors derived from strike–slip earthquakes and those from thrust earthquakes on or near the fault (Fig. 50).

Along the India–Eurasia boundary (Fig. 51), NUVEL-1 predicts convergence 7°–20° clockwise of directions predicted from P071 and RM2. The mean direction of slip vectors from strike–slip earthquakes along the Ornach-Nal Fault (Fig. 48) is N07° ± 3 °E, in good agreement with the NUVEL-1 predictions. Thrust earthquakes along the Himalayan frontal thrust from 75° to 80 °E give slip vectors clockwise of NUVEL-1, whereas thrust earthquakes from 85° to 95 °E give slip vectors counter-clockwise of NUVEL-1. Similar to the pattern of slip vectors from trench earthquakes, the slip vectors tend to track the perpendicular to the front thrust, reflecting some of the complexities of the India–Eurasia collision (Baranowski et al. 1984; T. Seno, personal communication, 1988). Fig. 51 also shows the scattered azimuths of slip vectors from the Pamir thrust, which have an average direction of slip close to that
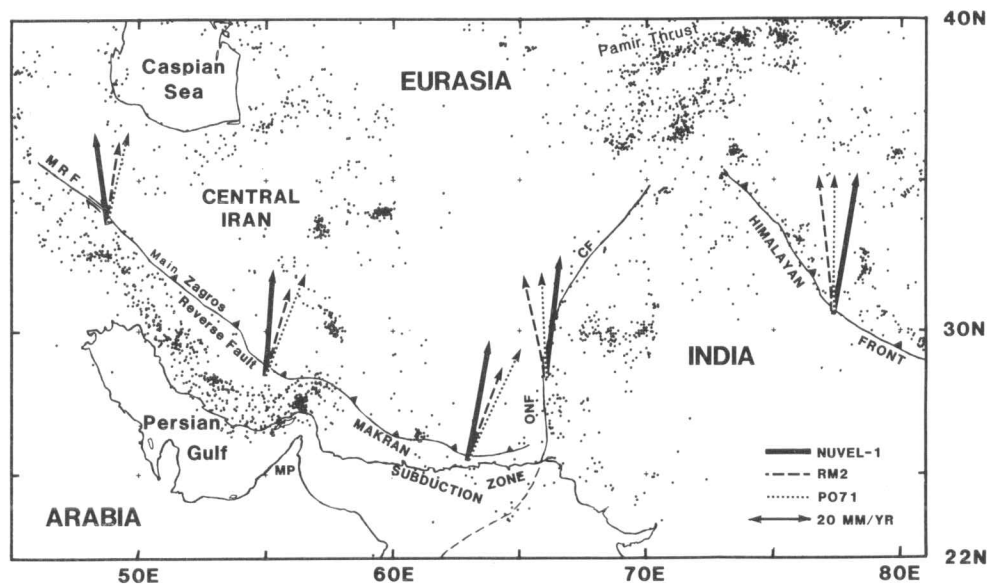
Figure 48. India–Eurasia and Arabia–Eurasia linear velocities predicted by P071 (short dashed), RM2 (long dashed), and NUVEL-1 (solid) and 1963–1986 seismicity shallower than 40 km. Deformation associated with the collision between Arabia and Eurasia extends northeast over 1000 km from the Zagros fold and thrust belt. The Main Zagros Reverse Fault marks the NE limit of the Zagros Fold and Thrust Belt, but may itself be inactive (Jackson & McKenzie 1984). Abbreviations: ONF, Ornach-Nal Fault; CF, Chaman Fault; MP, Mussandam peninsula; MRF, Main Recent Fault.
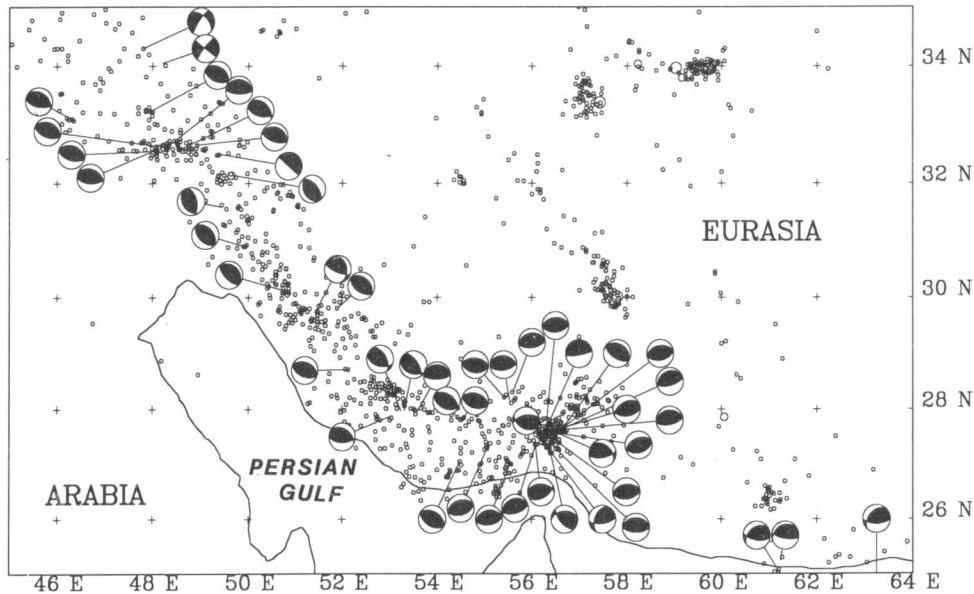
Figure 49. Earthquake focal mechanisms from Jackson & McKenzie (1984) and the Harvard centroid-moment tensor solutions are shown along the Main Recent fault, Zagros fold and thrust belt, and Makran subduction zone. The horizontal slip vectors derived from these focal mechanisms are shown in Fig. 49. Focal depths are no deeper than 50 km.

predicted by NUVEL-1. Given the tectonic complexities of the region, this agreement is likely fortuitous.

Strike–slip motion of Aleutian forearc slivers relative to the North American plate

The systematic misfit between the NUVEL-1 direction of motion and the azimuths of slip vectors along the Aleutian trench may be caused by motion of crustal or lithospheric forearc slivers relative to the North American plate. Aleutian trench slip vectors from earthquakes west of 195 °E that were omitted from the NUVEL-1 data set can be used to estimate the motion of the forearc slivers assuming that the entire azimuthal discrepancy is caused by such motion.
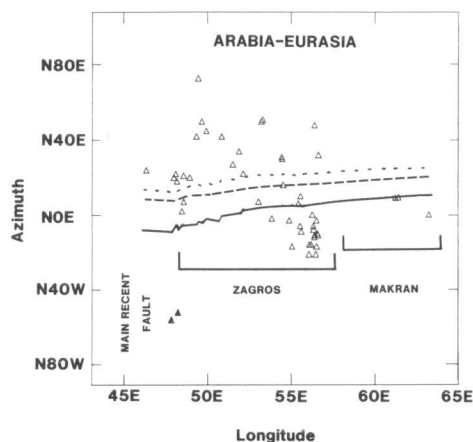
Figure 50. Thrust slip vectors (open triangles) from the Makran subduction zone, Zagros fold and thrust belt, and strike–slip slip vectors (solid triangles) from the Main Recent Fault are compared with predictions of the NUVEL-1 (bold solid), RM2 (long dashed), and P071 (short dashed) Arabia–Eurasia Euler vectors. Slip vectors are determined from CMT solutions and mechanisms given by Jackson & McKenzie (1984).

The rate of forearc strike–slip faulting, V_s, can be computed from

$$V_s = \frac{V_c \sin(\theta)}{\cos(\psi - \theta)} \tag{5}$$

where V_c is the NUVEL-1 Pacific–North America convergence rate, θ is the angle between the observed and predicted convergence directions, and ψ is the angle between the predicted direction of motion and the trench-normal. Equation (5), simplified from Jarrard (1986a), assumes that the component of sliver-North America motion perpendicular to the trench is zero. The difference (θ) between the slip directions along the Aleutian trench and the predicted Pacific–North America direction was estimated by averaging 198 slip vector directions at regular intervals along the trench from 164 °E to 195 °E (Fig. 52). The average slip directions lie between the predicted direction of plate motion and the trench-normal direction, even where the sense of oblique convergence reverses. If we simplistically divide the forearc into an eastern block located between 180° and 195 °E, and a western block located between 165° and 180 °E, the average rate of westward motion is ~15 mm yr^{-1} for the eastern block and ~35 mm yr^{-1} for the western block. This suggests up to 20 mm yr^{-1} extension may be distributed between several semi-rigid forearc blocks (Spence 1977; Geist *et al.* 1988; Ekstrom & Engdahl 1989).

Juan de Fuca–North America motion

The Juan de Fuca and Explorer plates subduct beneath North America along the Cascadia subduction zone, where no large underthrusting earthquakes, which describe the convergence direction in other subduction zones, have been instrumentally recorded. Plate models predict North America–Juan de Fuca motion by adding a North

INDIA–EURASIA
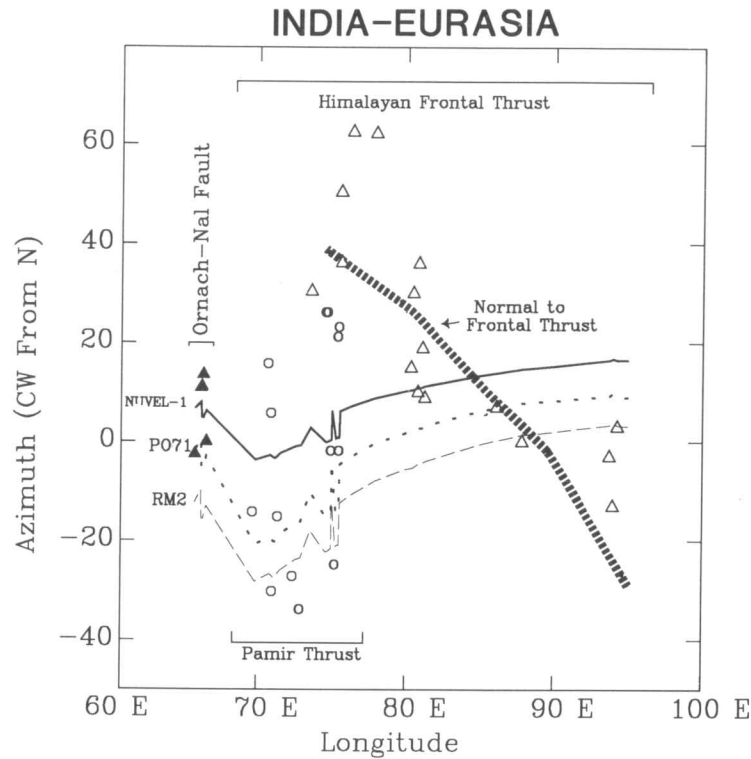
Figure 51. Strike–slip (solid triangles) slip vectors along the Ornach-Nal fault of southern Pakistan and thrust slip vectors along the Pamir Thrust (open circles) and along the Himalayan frontal thrust (open triangles) are compared with predictions of the NUVEL-1 (bold solid), RM2 (long dashed), and P071 (short dashed) India–Eurasia Euler vectors. All slip vectors shown are from CMT solutions. The variation in slip vector azimuths along the Himalayan frontal thrust tend to coincide not with the predicted direction of plate motion, but with the normal to the strike of the thrust (heavy dashed line).

America–Pacific Euler vector to a Pacific–Juan de Fuca Euler vector estimated from spreading rates and transform azimuths along the Juan de Fuca Ridge (Silver 1971; Riddihough 1977; 1984; Wilson 1988). Prior models predict E–NE convergence of ~40 mm yr^{-1} with the predicted rate decreasing from north to south along the trench.

Because the NUVEL-1 Pacific–North America Euler vectors differs significantly from P071 and RM2, our prediction of Juan de Fuca–North America motion differs from prior predictions. Using an anomaly 2A Pacific–Juan de Fuca Euler vector (Wilson 1988), we obtain a North America–Juan de Fuca Euler vector (20.7 °N, 112.2 °W,
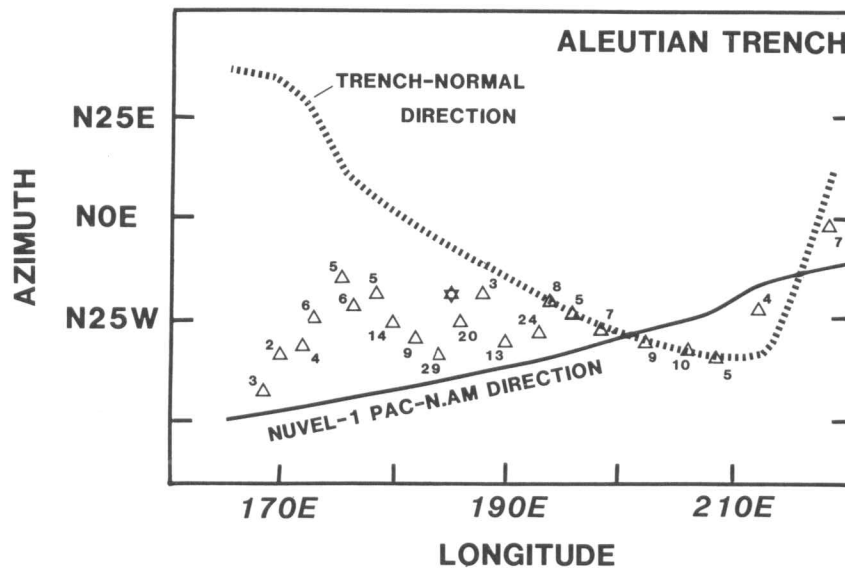
Figure 52. Mean slip vectors along the Aleutian trench are compared with the trench-normal direction and to the direction of Pacific–North America motion predicted by NUVEL-1. The mean slip vectors, which were computed by averaging weighted slip vectors at regular intervals along the trench, nearly always lie between the trench-normal direction and the predicted direction of motion. The small numerals next to each mean slip vector direction gives the number of slip vectors averaged. The star shows the azimuth of the magnitude 8 event of 1986 May 17.

0.80° m.y.$^{-1}$) that predicts motion (42 mm yr^{-1} directed N69 °E) at Seattle (47.5 °N, 122.5 °W) 10° clockwise of the motion (42 mm yr^{-1} directed N59 °E) predicted from the corresponding vector derived from RM2, and 14° clockwise of the motion (47 mm yr^{-1} directed N55 °E) predicted by the Euler vector given by Riddihough (1984).

The predicted convergence direction is similar to the average ENE trend of *T* axes of downdip extension events within the slab (Taber & Smith 1985), but these directions may not parallel the convergence direction. Geodetic results indicate shortening of the North American plate along N66° ± 5° E (Savage, Lisowski & Prescott 1981; Lisowski *et al.* 1987), similar to the directions inferred from both NUVEL-1 and RM2.

Red Sea spreading and African rifting

Although no data from the Red Sea, which separates Africa from Arabia in the NUVEL-1 plate geometry (Fig. 4), are used to derive NUVEL-1, a comparison of spreading rates from the Red Sea with the opening rate predicted by the NUVEL-1 Africa–Arabia Euler vector is useful in assessing the accuracy of NUVEL-1 and in placing limits on the rate of extension between Nubia and Somalia. The Red Sea has several distinct regions of seafloor spreading within a bisecting axial trough. The short spreading segments are well surveyed (Allan 1970; Roeser 1975; Bicknell *et al.*

RED SEA

Figure 53. Spreading rates (solid squares) observed in the Red Sea are compared with rates from the NUVEL-1 Arabia–Africa (bold solid) and P071 Arabia–Nubia [short dashed, referred to as Arabia–Africa by Chase (1978)] Euler vectors. The observed spreading rates, which we estimated from published profiles (Allan 1970; Roeser 1975; LaBrecque & Zitellini 1985; Miller *et al.* 1985), are 2–4 mm yr^{-1} faster than expected from NUVEL-1 if motion between Nubia (west Africa) and Somalia (east Africa) is neglected. However, the observed rates also are 2–4 mm yr^{-1} slower than calculated from the P071 Arabia–Nubia Euler vector, suggesting that P071 predicts Nubia–Somalia motion that is too fast by about a factor of 2. Horizontal error bars show assigned 1-σ errors.

1986) and have correlatable magnetic anomalies. We reduced published magnetic profiles (Allan 1970; Roeser 1975; LaBrecque & Zitellini 1985; Miller *et al.* 1985) to 20 spreading rates averaged over anomaly 2A. These profiles suggest a spreading rate of 15 ± 1 mm yr^{-1}, in good agreement with the interpretations from Allan (1970), Roeser (1975), and Miller *et al.* (1985), but slower than the 20 mm yr^{-1} spreading rate favoured by LaBrecque & Zitellini (1985).

The NUVEL-1 Africa–Arabia Euler vector predicts Red Sea spreading rates 2–4 mm yr^{-1} slower than the observed 15 mm yr^{-1} rate (Fig. 53). If we assume rifting in eastern Africa is roughly normal to the N–NNE trend of the rift valleys, the difference between the observed Red Sea opening rate and the rate predicted by NUVEL-1 implies 2–4 mm yr^{-1} extension in the Afar region. The P071 Nubia–Somalia Euler vector predicts 6 ± 4 mm yr^{-1} E–W extension in the Afar region (11 °N, 41 °E), several mm yr^{-1} faster than we infer from this analysis.

DISCUSSION

After 20 years, the model of Earth's surface consisting of rigid plates divided by discrete boundaries continues to be useful. That so many (1122) data are so well described by so few (33) adjustable parameters strongly supports this claim. That the largest systematic misfits of prior models seem best explained not by pervasive intraplate deformation, but by inappropriate data (i.e., FAMOUS area fracture zones A and B) or an inappropriate plate geometry (i.e., in the Indian Ocean), suggests that the assumption of plate rigidity is more accurate than widely believed a few years ago.

Nevertheless, small systematic misfits of NUVEL-1 to its data, between different types of data, and between the NUVEL-1 and prior data sets remain. Most evident is the misfit of NUVEL-1 to azimuths of slip vectors from earthquakes along trenches; these misfits appear to be due not to deformation far from plate boundaries, but to deformation confined to a plate boundary zone that is ~100–500 km wide. The best example of misfits between different types of data is the unexplained, systematic difference between slip vectors and the strike of the Chile fracture zone (Anderson–Fontana *et al.* 1987), which may be similar to small systematic differences between slip vectors and strikes along Atlantic transform faults (Argus *et al.* 1989).

Our work presented here and in related papers supports the concept that wide plate boundary zones can form not only within continental lithosphere, as is already widely recognized, but also within oceanic lithosphere: between the Indian and Australian plates, and between the North and South American plates. Moreover, the remaining systematic misfits to azimuth data along the eastern Southeast Indian Ridge and Macquarie Ridge, and along the western oceanic (South Atlantic) part of the Antarctic–South American plate boundary, also suggest small but significant diffuse deformation of oceanic lithosphere, which may be confined to small, awkwardly shaped salients of major plates.

DIRECTIONS OF FUTURE RESEARCH

The lack of a Philippine plate leaves a large area of oceanic lithosphere unrepresented in NUVEL-1; we are currently

working to remedy this deficiency. Similarly, we have been frustrated by the difficulties of developing a successful model for motion between Nubia and Somalia. Simply adding the spreading rates from the Red Sea is not enough for our inversion procedure to give a result consistent with observations in the East Africa rift valleys. We are currently working on models that use the less precise slip vectors from the rifts to aid in estimating a Nubia–Somalia Euler vector that is consistent with all pertinent observations. The motion of smaller plates, especially the Rivera plate, should be studied using the many data now available to investigate the accuracy of the plate tectonic model when applied to small plates.

Some improvements of NUVEL-1 over prior models have come less from adding new data than from reducing systematic errors (especially in spreading rates) and revising the plate geometry in the Indian Ocean. Future estimates of plate motion will presumably improve upon NUVEL-1 through further elimination of systematic errors. The half of our spreading rates determined from non-digital data may be less precise than those from digital data because of small systematic errors from drafting, reduction, and enlargement, and from the computer programs used in producing the published figures. We were surprised by the large number of published profiles that have erroneous distance scales.

We expect the biggest improvements to any future global plate motion model will come from data qualitatively different from that typically available now. In many places additional slip vectors will only modestly improve plate motion models because the many slip vectors now available render random errors negligible relative to systematic errors. Similarly, significant improvements in spreading rates will come mainly from closely spaced profiles. Detailed surveys are needed in several critical areas, especially along the poorly surveyed Central Indian Ridge, which is offset in many places by transform faults. Because all profiles now available across the Chile Rise cross fracture zones, closely spaced tracks parallel to predicted directions of plate motion are needed to determine reliable spreading rates.

Although conventional bathymetric surveys of transform faults in the poorly charted southern oceans would be useful, most significant improvements will come from side-scan and high resolution seafloor mapping tools. Such surveys of transform faults would be helpful nearly anywhere, but are especially needed along the Southeast Indian Ridge (along the Australia–Antarctica Discordance and eastwards) to test if the eastern Australian plate (or its Antarctic counterpart) is deforming measurably or if the azimuthal misfits are due to biases in the data. Surveys are also needed along the Chile fracture zone (where slip vectors and transform trends disagree) and along the many important, but poorly surveyed, transform faults along the SW Pacific–Antarctic Rise.

Independent estimates of motion across convergent and diffuse plate boundaries can be obtained from space geodesy, which can directly measure the rate and direction of motion across boundaries currently estimated only through plate circuit closure, slip vector azimuths, or both. Geodetic data can link the motions of Pacific Basin plates to those of other plates more accurately than is possible with conventional geophysical data. For pairs of plates with relative motions well determined by NUVEL-1, geodetic measurements can test the steadiness of plate motions: whether motions averaged over years differ from motions averaged over millions of years. Space geodesy can also test many otherwise untestable predictions such as the motion between North and South America, and between India and Australia. For example, the NUVEL-1 India–Australia Euler vector predicts measurable shortening of 12 ± 3 mm yr^{-1} along a baseline connecting Calcutta and Sydney. The slow motion of the Caribbean plate relative to North America and South America also should be measurable. The suggested motion of lithospheric slivers overriding trenches can be tested through geodesy, through geologic mapping aimed at evaluating whether the slivers are bounded by active faults, and by studies of microearthquakes.

REFERENCES

Abe, K., 1972. Mechanisms and tectonic implications of the 1966 and 1970 Peru earthquakes, *Phys. Earth planet Inter.*, **5**, 367–379.

Adamek, S., Frohlich, C. & Pennington, W., 1988. Seismicity of the Caribbean–Nazca boundary: Constraints on microplate tectonics of the Panama region, *J. geophys. Res.*, **93**, 2053–2075.

Allan, T. D., 1970. Magnetic and gravity fields over the Red Sea, *Phil. Trans. R. Soc. London A*, **267**, 153–180.

Anderson, R. N. & Sclater, J. G., 1972. Topography and evolution of the East Pacific Rise between 5°S and 20°S, *Earth planet. Sci. Lett.*, **14**, 433–441.

Anderson, R. N., Forsyth, D. W., Molnar, P. & Mammerickx, J., 1974. Fault plane solutions of earthquakes on the Nazca plate boundaries and the Easter plate, *Earth planet. Sci. Lett.*, **24**, 188–202.

Anderson-Fontana, S., Engeln, J. F., Lundgren, P., Larson, R. L. & Stein, S., 1987. Tectonics of the Nazca–Antarctica plate boundary, *Earth planet. Sci. Lett.*, **86**, 46–56.

Argus, D. F. & Gordon, R. G., 1989. The present-day motion and boundary between the North American and South American plates, *J. geophys. Res.*, submitted.

Argus, D. F., Gordon, R. G., DeMets, C. & Stein, S., 1989. Closure of the Africa–Eurasia–North America plate circuit and tectonics of the Gloria fault, *J. geophys. Res.*, **94**, 5585–5602.

Alwater, T., 1970. Implications of plate tectonics for the Cenozoic evolution of western North America, *Bull. geol. Soc. Am.*, **81**, 3513–3536.

Aydin, A. & Page, B. M., 1984. Diverse Pliocene–Quaternary tectonics in a transform environment, San Francisco Bay region, California, *Bull. geol. Soc. Am.*, **95**, 1303–1317.

Banghar, A. R. & Sykes, L. R., 1969. Focal mechanisms of earthquakes in the Indian Ocean and adjacent regions, *J. geophys. Res.*, **74**, 632–649.

Baranowski, J., Armbruster, J., Seeber, L. & Molnar, P., 1984. Focal depths and fault plane solutions of earthquakes and active tectonics of the Himalaya, *J. geophys. Res.*, **89**, 6918–6928.

Barker, P. F. & Lawver, L. A., 1988. South American–Antarctic plate motion over the past 50 Myr, and the evolution of the South American–Antarctic ridge, *Geophys. J.*, **94**, 377–386.

Belderson, R. H., Jones, E. J. W., Gorini, M. A. & Kenyon, N. H., 1984. A long range side-scan sonar (GLORIA) survey of the Romanche active transform in the equatorial Atlantic, *Mar. Geol.*, **56**, 65–78.

Berberian, M., 1981. Active faulting and tectonics of Iran, in *Zagros, Hindu Kush, Himalaya, Geodynamic Evolution, Geodynamics Series* 3, pp. 33–69, eds Gupta, H. K. & Delany, F. M., AGU, Washington, DC and GSA, Boulder, CO.

Bergh, H. W. & Norton, I. O., 1976. Prince Edward fracture zone and the evolution of the Mozambique Basin, *J. geophys. Res.*, **81**, 5221–5239.

Bergman, E. A., 1986. Intraplate earthquakes and the state of stress in oceanic lithosphere, *Tectonophysics*, **132**, 1–35.

Bergman, E. A. & Solomon, S. C., 1985. Earthquake source mechanisms from body waveform inversion and intraplate tectonics in the northern Indian Ocean, *Phys. Earth planet. Inter.*, **40**, 1–23.

Bergman, E. A. & Solomon, S. C., 1988. Transform fault earthquake in the North Atlantic: source mechanisms and depth of faulting, *J. geophys. Res.*, **93**, 9027–9057.

Bibby, H. M., 1981. Geodetically determined strain across the southern end of the Tonga–Kermadec–Hikurangi subduction zone, *Geophys. J. R. astr. Soc.*, **66**, 513–533.

Bicknell, J. D., Macdonald, K. C., Miller, S. P., Lonsdale, P. F. & Becker, K., 1986. Tectonics of the Nereus Deep, Red Sea: A deep-tow investigation of site of initial rifting, *Mar. geophys. Res.*, **8**, 131–148.

Blakeley, R. & Cox, A., 1972. Identification of short polarity events by transforming marine magnetic profiles to the pole, *J. geophys. Res.*, **77**, 4339–4349.

Brozena, J. M., 1986. Temporal and spatial variability of seafloor spreading processes in the northern South Atlantic, *J. geophys. Res.*, **91**, 497–510.

Burbach, G. V., Frolich, C., Pennington, W. D. & Matumoto, T., 1984. Seismicity and tectonics of the subducted Cocos plate, *J. geophys. Res.*, **89**, 7719–7735.

Carey, S. W., 1958. The tectonic approach to continental drift, in *Continental Drift; a Symposium*, pp. 177–358, ed. Carey, S. W., University of Tasmania, Hobart.

Chael, E. P. & Stewart, G. S., 1982. Recent large earthquakes along the Middle America Trench and their implications for the subduction process, *J. geophys. Res.*, **87**, 329–338.

Chandra, U., 1974. Seismicity, earthquake mechanisms, and tectonics along the western coast of North America, from 42 °N to 61 °N, *Bull. seism. Soc. Am.*, **64**, 1529–1549.

Chapman, M. E. & Solomon, S. C., 1976. North American–Eurasian plate boundary in Northeast Asia, *J. geophys. Res.*, **81**, 921–930.

Chase, C. G., 1972. The *n*-plate problem of plate tectonics, *Geophys. J. R. astr. Soc.*, **29**, 117–122.

Chase, C. G., 1978. Plate kinematics: The Americas, East Africa, and the rest of the world, *Earth planet. Sci. Lett.*, **37**, 355–368.

Choy, G. L. & Dewey, J. W., 1988. Rupture process of an extended earthquake sequence: Teleseismic analysis of the Chilean earthquake of March 3, 1985, *J. geophys. Res.*, **93**, 1103–1118.

Clark, T. A., Gordon, D., Himwich, W. E., Ma, C., Mallama, A. & Ryan, J. W., 1987. Determination of relative site motions in the western United States using Mark II very long baseline radio interferometry, *J. geophys. Res.*, **92**, 12 741–12 750.

Cochran, J. R., 1981. The Gulf of Aden: Structure and evolution of a young ocean basin and continental margin, *J. geophys. Res.*, **86**, 263–287.

Collette, B. J. & Slootweg, A. P., 1978. Reply to Atwater and Macdonald, 'Are spreading centers perpendicular to their transform faults?', *Nature*, **274**, 187–190.

Collette, B. J., Slootweg, A. P. & Twigt, W., 1979. Mid-Atlantic Ridge crest topography between 12° and 15 °N, *Earth planet Sci. Lett.*, **42**, 103–108.

Courtillot, V., Galdeano, A. & Le Mouël, J. L., 1980. Propagation of an accreting plate boundary: A discussion of new aeromagnetic data in the Gulf of Tadjurah and southern Afar, *Earth planet. Sci. Lett.*, **47**, 144–160.

CYAMEX Scientific Team & Pastouret, L., 1981. Submersible structural study of the Tamayo transform fault: East Pacific Rise, 23 °N (Project Rita), *Mar. geophys. Res.*, **4**, 381–401.

Dauphin, P. & Ness, G., 1989. Bathymetry of the Gulf and Peninsular province of the Californias, *AAPG Memoir*, **47**, in press.

Dean, B. W. & Drake, D. L., 1978. Focal mechanism solutions and tectonics of the Middle America arc, *J. Geol.*, **86**, 111–128.

DeMets, C., Gordon, R. G. & Argus, D. F., 1988. Intraplate deformation and closure of the Australia–Antarctica–Africa plate circuit, *J. geophys. Res.*, **93**, 11 877–11 897.

DeMets, C., Gordon, R. G., Stein, S. & Argus, D. F., 1987. A revised estimate of Pacific–North America motion and implications for western North America plate boundary zone tectonics, *Geophys. Res. Lett.*, **14**, 911–914.

Dewey, J. F. & Sengor, A. M. C., 1979. Aegean and surrounding regions: complex multiplate and continuum tectonics in a convergent zone, *Bull. geol. Soc. Am.*, **90**, 84–92.

Dickson, G. L., Pitman, W. C., III & Heirtzler, J. R., 1968. Magnetic anomalies in the South Atlantic and ocean floor spreading, *J. geophys. Res.*, **73**, 2087–2100.

Dorel, J., 1981. Seismicity and seismic gap in the Lesser Antilles Arc and earthquake hazards in Guadeloupe, *Geophys. J. R. astr. Soc.*, **67**, 679–695.

Dziewonski, A. M. & Woodhouse, j. H., 1983. An experiment in systematic study of global seismicity: Centroid-moment tensor solutions for 201 moderate and large earthquakes of 1981, *J. geophys. Res.*, **88**, 3247–3271.

Dziewonski, A. M., Chou, T.-A. & Woodhouse, J. H., 1981. Determination of earthquake source parameters from waveform data for studies of global and regional seismicity, *J. geophys. Res.*, **86**, 2825–2852.

Dziewonski, A. M., Friedman, A., Giardini, D. & Woodhouse, J. H., 1983a. Global seismicity of 1982: centroid-moment tensor solutions for 308 earthquakes, *Phys. Earth planet. Inter.*, **33**, 76–90.

Dziewonski, A. M., Friedman, A. & Woodhouse, J. H., 1983b. Centroid-moment tensor solutions for January–March 1983, *Phys. Earth planet. Inter.*, **33**, 71–75.

Dziewonski, A. M., Franzen, J. E. & Woodhouse, J. H., 1983c. Centroid-moment tensor solutions for April–June 1983, *Phys. Earth planet. Inter.*, **33**, 243–249.

Dziewonski, A. M., Franzen, J. E. & Woodhouse, J. H., 1984a. Centroid-moment tensor solutions for July–September 1983, *Phys. Earth planet. Inter.*, **34**, 1–8.

Dziewonski, A. M., Franzen, J. E. & Woodhouse, J. H., 1984b. Centroid-moment tensor solutions for October–December 1983, *Phys. Earth planet. Inter.*, **34**, 129–136.

Dziewonski, A. M., Franzen, J. E. & Woodhouse, J. H., 1984c. Centroid-moment tensor solutions for January–March 1984, *Phys. Earth planet. Inter.*, **34**, 209–219.

Dziewonski, A. M., Franzen, J. E. & Woodhouse, J. H., 1985a.

Centroid-moment tensor solutions for April–June 1984, *Phys. Earth planet. Inter.*, **37**, 87–96.

Dziewonski, A. M., Franzen, J. E. & Woodhouse, J. H., 1985b. Centroid-moment tensor solutions for July–September 1984, *Phys. Earth planet. Inter.*, **38**, 203–213.

Dziewonski, A. M., Franzen, J. E. & Woodhouse, J. H., 1985c. Centroid-moment tensor solutions for October–December 1984, *Phys. Earth planet. Inter.*, **39**, 147–156.

Dziewonski, A. M., Franzen, J. E. & Woodhouse, J. H., 1985d. Centroid-moment tensor solutions for January–March 1985, *Phys. Earth planet. Inter.*, **40**, 249–258.

Dziewonski, A. M., Franzen, J. E. & Woodhouse, J. H., 1986a. Centroid-moment tensor solutions for April–June 1985, *Phys. Earth planet. Inter.*, **41**, 215–224.

Dziewonski, A. M., Franzen, J. E. & Woodhouse, J. H., 1986b. Centroid-moment tensor solutions for July–September 1985, *Phys. Earth planet. Inter*, **42**, 205–214.

Dziewonski, A. M., Franzen, J. E. & Woodhouse, J. H., 1986c. Centroid-moment tensor solutions for October–December 1985, *Phys. Earth planet. Inter.*, **43**, 185–195.

Dziewonski, A. M., Ekstrom, G., Franzen, J. E. & Woodhouse, J. H., 1987a. Centroid-moment tensor solutions for January–March 1986, *Phys. Earth planet. Inter.*, **45**, 1–10.

Dziewonski, A. M., Ekstrom, G., Franzen, J. E. & Woodhouse, J. H., 1987b. Centroid-moment tensor solutions for April–June 1986, *Phys. Earth planet. Inter.*, **45**, 229–239.

Dziewonski, A. M., Ekstrom, G., Franzen, J. E. & Woodhouse, J. H., 1987c. Centroid-moment tensor solutions for July–September 1986, *Phys. Earth planet Inter.*, **46**, 305–315.

Dziewonski, A. M., Ekstrom, G., Woodhouse, J. H. & Zwart, G., 1987d. Centroid-moment tensor solutions for October–December 1986, *Phys. Earth planet. Inter.*, **48**, 5–17.

Dziewonski, A. M., Ekstrom, G., Franzen, J. E. & Woodhouse, J. H., 1987e. Global seismicity of 1977: centroid-moment tensor solutions for 471 earthquakes, *Phys. Earth planet. Inter.*, **45**, 11–36.

Dziewonski, A. M., Ekstrom, G., Franzen, J. E. & Woodhouse, J. H., 1987f. Global seismicity of 1978: centroid-moment tensor solutions for 512 earthquakes, *Phys. Earth planet. Inter.*, **46**, 316–342.

Dziewonski, A. M., Ekstrom, G., Franzen, J. E. & Woodhouse, J. H., 1987g. Global seismicity of 1979: centroid-moment tensor solutions for 524 earthquakes, *Phys. Earth planet. Inter.*, **48**, 18–47.

Dziewonski, A. M., Ekstrom, G., Franzen, J. E. & Woodhouse, J. H., 1988a. Global seismicity of 1980: centroid-moment tensor solutions for 515 earthquakes, *Phys. Earth planet. Inter.*, **50**, 127–154.

Dziewonski, A. M., Ekstrom, G., Franzen, J. E. & Woodhouse, J. H., 1988b. Global seismicity of 1981: centroid-moment tensor solutions for 542 earthquakes, *Phys. Earth planet. Inter.*, **50**, 155–182.

Dziewonski, A. M., Ekstrom, G., Woodhouse, J. H. & Zwart, G., 1988c. Centroid-moment tensor solutions for January–March 1987, *Phys. Earth planet. Inter.*, **50**, 116–126.

Dziewonski, A. M., Ekstrom, G., Woodhouse, J. H. & Zwart, G., 1988d. Centroid-moment tensor solutions for April–June 1987, *Phys. Earth planet. Inter.*, **50**, 215–225.

Dziewonski, A. M., Ekstrom, G., Woodhouse, J. H. & Zwart, G., 1988e. Centroid-moment tensor solutions for July–September 1987, *Phys. Earth planet. Inter.*, **53**, 1–11.

Eissler, H. K. & McNally, K. C., 1984. Seismicity and tectonics of the Rivera plate and implications for the 1932 Jalisco, Mexico, earthquake, *J. geophys. Res.*, **89**, 4520–4530.

Ekstrom, G. & Engdahl, E. R., 1989. Earthquake source parameters and stress distribution in the Adak Island region of the central Aleutian Islands, Alaska, *J. geophys. Res.*, **94**, 15 499–15 519.

Emery, K. O. & Uchupi, E., 1984. *The Geology of the Atlantic Ocean*, Springer-Verlag, New York.

Engdahl, E. R., Sleep, N. H. & Lin, M. T., 1977. Plate effects in North Pacific subduction zones, *Tectonophysics*, **37**, 95–116.

Engel, C. G. & Fisher, R. L., 1975. Granitic to ultramafic rock complexes of the Indian Ocean ridge system, western Indian Ocean, *Bull. geol. Soc. Am.*, **86**, 1553–1578.

Engeln, J. F., Wiens, D. A. & Stein, S., 1986. Mechanisms and depths of Atlantic transform earthquakes, *J. geophys. Res.*, **91**, 548–577.

Falconer, R. K. H., 1973. Indian–Pacific rotation pole determined from earthquake epicenters, *Nature*, **243**, 97–99.

Feden, R. H., Vogt, P. R. & Fleming, H. S., 1979. Magnetic and bathymetric evidence for the 'Yermak Hot Spot' northwest of Svalbard in the Arctic Basin, *Earth planet. Sci. Lett.*, **44**, 18–38.

Fisher, R. L. & Sclater, J. G., 1983. Tectonic evolution of the Southwest Indian Ocean since the mid-Cretaceous: Plate motions and stability of the pole of Antarctica/Africa for at least 80 Myr, *Geophys. J. R. astr. Soc.*, **73**, 553–576.

Fisher, R. L., Sclater, J. G. & McKenzie, D. P., 1971. Evolution of the central Indian Ridge, western Indian Ocean, *Bull. geol. Soc. Am.*, **82**, 553–562.

Fitch, T. J., 1972. Plate convergence, transcurrent faults, and internal deformation adjacent to Southeast Asia and the western Pacific, *J. geophys. Res.*, **77**, 4432–4460.

Forsyth, D. W., 1972. Mechanisms of earthquakes and plate motions in the East Pacific, *Earth planet. Sci. Lett.*, **17**, 189–193.

Forsyth, D. W., 1975. Fault plane solutions and tectonics of the South Atlantic and Scotia Sea, *J. geophys. Res.*, **80**, 1429–1443.

Fox, P. J. & Gallo, D. G., 1984. A tectonic model for ridge–transform–ridge plate boundaries: Implications for the structure of oceanic lithosphere, *Tectonophysics*, **104**, 205–242.

Fox, P. J. & Gallo, D. G., 1986. The geology of North Atlantic transform plate boundaries and their aseismic extensions, in *The Geology of North America, Volume M, The Western North Atlantic Region*, pp. 157–172, eds Vogt, P. R., & Tucholke, B. E., GSA, Boulder, CO.

Fukao, Y., 1973. Thrust faulting at a lithospheric plate boundary: The Portugal earthquake of 1969, *Earth planet. Sci. Lett.*, **18**, 205–216.

Gallo, D. G., Fox, P. J. & Macdonald, K. C., 1986. A Seabeam investigation of the Clipperton transform fault: The morphotectonic expression of a fast slipping transform boundary, *J. geophys. Res.*, **91**, 3455–3467.

Gallo, D. G., Fornari, D. J., Madsen, J. A., Perfit, M. R. & Shor, A., 1987. SeaMarc II survey of the Siqueiros transform, *EOS Trans. Am. geophys. Un.*, **68**, 1505.

Geist, E. L., Childs, J. R. & Scholl, D. W., 1987. Evolution and petroleum geology of Amlia and Amukta intra-arc summit basins, Aleutian Ridge, *Mar. petrol. Geol.*, **4**, 334–352.

Geist, E. L., Childs, J. R. & Scholl, D. W., 1988. The origin of summit basins of the Aleutian Ridge: Implications for block rotation of an arc massif, *Tectonics*, **7**, 327–341.

Girdler, R. W., Brown, C., Noy, D. J. M. & Styles, P., 1980. A geophysical survey of the westernmost Gulf of Aden, *Phil. Trans. R. Soc. Lond., A*, **298**, 1–43.

Goff, J. A., Bergman, E. A. & Solomon, S. C., 1987. Earthquake source mechanisms and transform fault tectonics in the Gulf of California, *J. geophys. Res.*, **92**, 10 485–10 510.

Gordon, R. G. & DeMets, C., 1989. Present-day motion along the Owen fracture zone and Dalrymple trough in the Arabian Sea, *J. geophys. Res.*, **94**, 5560–5570.

Gordon, R. G., Stein, S., DeMets, C. & Argus, D. F., 1987. Statistical tests for closure of plate motion circuits, *Geophys. Res. Lett.*, **14**, 587–590.

Gordon, R. G., DeMets, C. & Argus, D. F., 1989. Kinematic constraints on distributed lithospheric deformation in the equatorial Indian Ocean from present-day motion between the Australian and Indian plates, *Tectonics,* in press.

Goreau, P. D. E., 1983. The tectonic evolution of the north-central Caribbean plate margin, *PhD thesis,* Woods Hole Oceanographic Institution, Woods Hole, MA.

Grimison, N. L. & Chen, W.-P., 1986. The Azores–Gibraltar plate boundary: focal mechanisms, depths of earthquakes, and their tectonic implications, *J. geophys. Res.,* **91,** 2029–2047.

Hamilton, W. & Myers, W. B., 1966. Cenozoic tectonics of the western United States, *Rev. Geophys.,* **4,** 509–549.

Harbert, W. P., 1987. New paleomagnetic data from the Aleutian islands; Implications for terrane migration and deposition of the Zodiac fan, *Tectonics,* **6,** 585–602.

Harland, W. B., Cox, A. V., Llewellyn, P. G., Pickton, C. A. G., Smith, A. G. & Walters, R., 1982. *A Geologic Time Scale,* Cambridge University Press, New York.

Haxby, W. F., 1987. Gravity field of the world's oceans, *Map,* NOAA, Boulder, CO.

Herron, E. M., Cande, S. C. & Hall, B. R., 1981. An active spreading center collides with a subduction zone: A geophysical survey of the Chile margin triple junction, *Geol. Soc. Am. Mem.,* **154,** 683–702.

Hey, R., Johnson, G. L. & Lowrie, A., 1977. Recent plate motions in the Galapagos area, *Bull. geol. Soc. Am.,* **88,** 1385–1403.

Hodgson, J. H. & Milne, W. G., 1951. Directions of faulting in certain earthquakes of the North Pacific, *Bull. seism. Soc. Am.,* **41,** 221–242.

Holcombe, T. L., Vogt, P. R., Matthews, J. E. & Murchison, R. R., 1973. Evidence for seafloor spreading in the Cayman Trough, *Earth planet. Sci. Lett.,* **20,** 357–371.

House, L. S. & Jacob, K. H., 1983. Earthquakes, plate subduction, and stress reversals in the eastern Aleutian Arc, *J. geophys. Res.,* **88,** 9347–9373.

Humphreys, E. & Weldon, R., 1989. Kinematic constraints on the rifting of Baja California, *AAPG Memoir,* **47,** in press.

Jackson, J. & McKenzie, D., 1984. Active tectonics of the Alpine Himalayan Belt between western Turkey and Pakistan, *Geophys. J.,* **77,** 185–264.

Jackson, J. & McKenzie, D., 1988. The relationship between plate motions and seismic moment tensors, and the rates of active deformation in the Mediterranean and Middle East, *Geophys. J.,* **93,** 45–73.

Jarrard, R. D., 1986a. Terrane motion by strike–slip faulting of forearc slivers, *Geology,* **14,** 780–783.

Jarrard, R. D., 1986b. Relations among subduction parameters, *Rev. Geophys.,* **24,** 217–284.

Jordan, T. H., 1975. The present-day motions of the Caribbean plate, *J. geophys. Res.,* **80,** 4433–4439.

Kanamori, H. & Stewart, G. S., 1978. Seismological aspects of the Guatemala earthquake of February 4, 1976, *J. geophys. Res.,* **83,** 3427–3434.

Kastens, K. A., Macdonald, K. C. & Becker, K., 1979. The Tamayo transform fault in the mouth of the Gulf of California, *Mar. geophys. Res.,* **4,** 129–151.

Klitgord, K. D. & Mammerickx, J., 1982. Northern East Pacific Rise: Magnetic anomaly and bathymetric framework, *J. geophys. Res.,* **87,** 6725–6750.

Klitgord, K. D., Mudie, J. D., Larson, P. A. & Grow, J. A., 1973. Fast seafloor spreading on the Chile Ridge, *Earth planet. Sci. Lett.,* **20,** 93–99.

Kovacs, L. C., Bernero, C., Johnson, G. L., Pilger, R. H. Jr, Taylor, P. T. & Vogt, P. R., 1982. *Residual magnetic anomaly chart of the Arctic Ocean region,* Naval Research Laboratory, and Naval Ocean Research and Development Activity, Washington, DC.

Kroger, P. M., Lyzenga, G. A., Wallace, K. S. & Davidson, J. M., 1987. Tectonic motion in the western United States inferred from very long baseline interferometry measurements, 1980–1986, *J. geophys. Res.,* **92,** 14 151–14 163.

Kureth, C. L. & Rea, D. K., 1982. Large-scale oblique features in an active transform fault, the Wilkes fracture zone near 9 °S on the East Pacific Rise, *Mar. geophys. Res.,* **5,** 119–137.

Kurita, K. & Ando, M., 1974. Large earthquakes in Kamchatka and the motion of the Pacific plate (abstract) (in Japanese), *Japan seism. Soc.,* **1,** 14.

LaBrecque, J. L. & Zitellini, N., 1985. Continuous sea-floor spreading in Red Sea: An alternative interpretation of magnetic anomaly patterns, *Bull. Am. Assoc. Petrol. Geol.,* **69,** 513–524.

Lahr, J. C. & Plafker, G., 1980. Holocene Pacific–North American plate interaction in southern Alaska: Implications for the Yakataga seismic gap, *Geology,* **8,** 483–486.

Laughton, A. S., Whitmarsh, R. B. & Jones, M. T., 1970. The evolution of the Gulf of Aden, *Phil. Trans. R. Soc. Lond., A,* **267,** 227–266.

Laughton, A. S., Whitmarsh, R. B., Rusby, J. S. M. Somers, M. L., Revie, J., McCartney, B. S. & Nafe, J. E., 1972. A continuous E–W fault of the Azores–Gibraltar Ridge, *Nature,* **327,** 217–220.

Lawver, L. A. & Dick, H. J. B., 1983. The American–Antarctic Ridge, *J. geophys. Res.,* **88,** 8193–8202.

LeDouaran, S., Needham, H. D. & Francheteau, J., 1982. Pattern of opening rates along the axis of the Mid-Atlantic Ridge, *Nature,* **300,** 254–257.

Lisowski, M., Savage, J. C., Prescott, W. H. & Dragert, H., 1987. Strain accumulation along the Cascadia subduction zone in western Washington (abstract), *EOS, Trans. Am. geophys. Un.,* **68,** 1240.

Lonsdale, P. & Klitgord, K. D., 1978. Structure and tectonic history of the eastern Panama Basin, *Bull. geol. Soc. Am.,* **89,** 981–999.

Loomis, T. P. & Morgan, W. J., 1973. Sea-floor spreading rate changes in the south Atlantic, *Mar. Geophys. Res.,* **2,** 3–9.

Macdonald, K. C., 1977. Near bottom magnetic anomalies, asymmetric spreading, oblique spreading, and tectonics of the Mid-Atlantic Ridge near Lat 37 °N, *Bull. geol. Soc. Am.,* **88,** 541–555.

Macdonald, K. C., 1986. The crest of the Mid-Atlantic ridge: Models for crustal generation processes and tectonics, in *The Geology of North America, Volume M, The Western North Atlantic Region,* eds Vogt, P. R. & Tucholke, B. E., GSA, Boulder, CO.

Macdonald, K. C., Kastens, K., Spiess, F. N. & Miller, S., 1979. Deep-tow studies of the Tamayo transform fault, *Mar. Geophys. Res.,* **4,** 37–70.

Macdonald, K. C., Castillo, D., Miller, S., Fox, P. J., Kastens, K. & Bonatti, E., 1986. Deep-tow studies of the Vema fracture zone, 1, tectonics of a major slow slipping transform fault and its intersection with the Mid-Atlantic ridge, *J. geophys. Res.,* **91,** 3334–3354.

Madsen, J. A., Macdonald, K. C. & Fox, P. J., 1986. Morphotectonic fabric of the Orozco fracture zone: Results from a Sea Beam investigation, *J. geophys. Res.,* **91,** 3439–3454.

Malahoff, A., Feden, R. H. & Fleming, H. S., 1982. Magnetic anomalies and tectonic fabric of marginal basins north of New Zealand, *J. geophys. Res.,* **87,** 4109–4125.

Malgrange, M., Deschamps, A. & Madariaga, R., 1981. Thrust and extensional faulting under the Chilean coast 1965, 1971 Aconcagua earthquakes, *Geophys. J. R. astr. Soc.,* **66,** 313–331.

Mammerickx, J., 1984. The morphology of propagating spreading centers: New and old, *J. geophys. Res.,* **89,** 1817–1828.

Mammerickx, J., 1985. East Pacific Rise between 10° and 20 °N,

Ocean Margin Drilling Program and Regional Atlas Series, Atlas 8, Marine Science International, Woods Hole, MA.

Mammerickx, J., Naar, J. F. & Tyce, R. L., 1988. The Mathematician paleoplate, *J. geophys. Res.,* **93,** 3025–3040.

Mammerickx, J., Anderson, R. N., Menard, H. W. & Smith, S. M., 1975. Morphology and tectonic evolution of the East-Central Pacific, *Bull. geol. Soc. Am.,* **86,** 111–118.

Mann, P. & Burke, K., 1984. Neotectonics of the Caribbean, *Rev. Geophys. Space Phys.,* **22,** 309–362.

Manton, W. I., 1987. Tectonic interpretation of the morphology of Honduras, *Tectonics,* **6,** 633–651.

Matthews, D. H., 1966. The Owen fracture zone and the northern end of the Carlsberg ridge, *Phil. Trans. R. Soc. Lond., A,* **259,** 172–186.

McGregor, B. A., Harrison, C. G. A., Lavelle, J. W. & Rona, P. A., 1977. Magnetic anomaly patterns on Mid-Atlantic Ridge crest at 26 °N, *J. geophys. Res.,* **82,** 231–238.

McKenzie, D. P., 1972. Active tectonics of the Mediterranean region, *Geophys. J. R. astr. Soc.,* **30,** 109–185.

McKenzie, D. P. & Sclater, J. G., 1971. The evolution of the Indian Ocean since the late Cretaceous, *Geophys. J. R. astr. Soc.,* **24,** 437–528.

Miller, S. P., Macdonald, K. C. & Lonsdale, P. F., 1985. Near bottom magnetic profiles across the Red Sea, *Mar. geophys. Res.,* **7,** 401–418.

Minster, J. B. & Jordan, T. H., 1978. Present-day plate motions, *J. geophys. Res.,* **83,** 5331–5354.

Minster, J. B. & Jordan, T. H., 1984. Vector constraints on Quaternary deformation of the western United States east and west of the San Andreas Fault, in *Tectonics and Sedimentation along the California Margin,* Fieldtrip Guidebook 38, pp. 1–16, eds Crouch, J. K. & Bachman, S. B., SEPM, Pacific Section, Los Angeles, CA.

Minster, J. B. & Jordan, T. H., 1987. Vector constraints on western U. S. deformation from space geodesy, neotectonics and plate motions, *J. geophys. Res.,* **92,** 4798–4804.

Minster, J. B., Jordan, T. H., Molnar, P. & Haines, E., 1974. Numerical modeling of instantaneous plate tectonics, *Geophys. J. R. astr. Soc.,* **36,** 541–576.

Molnar, P. & Sykes, L. R., 1969. Tectonics of the Caribbean and middle America regions from focal mechanisms and seismicity, *Bull. geol. Soc. Am.,* **80,** 1639–1684.

Molnar, P., Atwater, T., Mammerickx, J. & Smith, S. M., 1975. Magnetic anomalies, bathymetry and the tectonic evolution of the South Pacific since the Late Cretaceous, *Geophys. J. R. astr. Soc.,* **40,** 383–420.

Mount, V. S. & Suppe, J., 1987. State of stress near the San Andreas fault: Implications for wrench tectonics, *Geology,* **15,** 1143–1146.

Norton, I. O., 1976. The present relative motion between Africa and Antarctica, *Earth planet. Sci. Lett.,* **33,** 219–230.

Oppenheimer, D. H., Reasenberg, P. A. & Simpson, R. W., 1988. Fault plane solutions for the 1984 Morgan Hill, California, earthquake sequence: Evidence for the state of stress on the Calaveras fault, *J. geophys. Res.,* **93,** 9007–9026.

Page, B. M. & Engebretson, D. C., 1984. Correlation between the geologic record and computed plate motions for central California, *Tectonics,* **3,** 133–155.

Pennington, W. D., 1981. Subduction of the eastern Panama Basin and seismotectonics of northwestern South America, *J. geophys. Res.,* **86,** 10 753–10 770.

Perez, O. J. & Jacob, K. H., 1980. Tectonic model and seismic potential of the eastern Gulf of Alaska and Yakataga seismic gap, *J. geophys. Res.,* **85,** 7132–7150.

Perry, R. K., Fleming, H. S., Cherkis, N. Z., Feden, R. H. & Vogt, P. R., 1978. *Bathymetry of the Norwegian–Greenland and Western Barents Seas,* Naval Research Laboratory, Acoustics Division, Washington, DC.

Pitman, W. C., Herron, E. M. & Heirtzler, J. R., 1968. Magnetic anomalies in the Pacific and sea-floor spreading, *J. geophys. Res.,* **73,** 2069–2085.

Pockalny, R. A., Detrick, R. S. & Fox, P. J., 1988. The morphology and tectonics of the Kane transform from Seabeam bathymetry data, *J. geophys. Res.,* **94,** 3179–3194.

Prescott, W. H., Lisowski, M. & Savage, J. C., 1981. Geodetic measurement of crustal deformation of the San Andreas, Hayward, and Calaveras faults near San Francisco, California, *J. geophys. Res.,* **86,** 10 853–10 869.

Quittmeyer, R. C. & Kafka, A. L., 1984. Constraints on plate motions in southern Pakistan and the northern Arabian Sea from the focal mechanisms of small earthquakes, *J. geophys. Res.,* **89,** 2444–2458.

Rabinowitz, P. D. & Schouten, H. (eds), 1985. *Mid-Atlantic ridge between 22° and 38°N, Atlas* 11, *Ocean Margin Drilling Program, Regional Atlas Series,* Marine Science International, Woods Hole, MA.

Raff, A. D., 1968. Sea-floor spreading—another rift, *J. geophys. Res.,* **73,** 3699–3705.

Rea, D. K., 1976a. Changes in the axial configuration of the East Pacific Rise near 6 °S during the last 2 m.y., *J. geophys. Res.,* **81,** 1495–1504.

Rea, D. K., 1976b. Analysis of a fast-spreading rise crest: The East Pacific Rise, 9° to 12° South, *Mar. geophys. Res.,* **2,** 291–313.

Rea, D. K., 1977. Local axial migration and spreading rate variations, East Pacific Rise, 31 °S, *Earth planet. Sci. Lett.,* **34,** 78–84.

Rea, D. K., 1978. Asymmetric sea-floor spreading and a nontransform axis offset: The East Pacific Rise 20 °S survey area, *Bull. geol. Soc. Am.,* **89,** 836–844.

Riddihough, R. P., 1977. A model for recent plate interactions off Canada's west coast, *Can J. Earth Sci.,* **14,** 384–396.

Riddihough, R., 1984. Recent movements of the Juan de Fuca plate system, *J. geophys. Res.,* **89,** 6980–6994.

Roeser, H. A., 1975. A detailed magnetic survey of the southern Red Sea, *Geologisches Jahrbuch,* **13,** 131–153.

Roest, W. R., Searle, R. C. & Collette, B. J., 1984. Fanning of fracture zones and a three-dimensional model of the Mid-Atlantic ridge, *Nature,* **308,** 527–531.

Romanowicz, B. & Ekstrom, G., 1989. Macquarie earthquake of May 23, 1989: The largest strike–slip event in more than 10 years, *EOS, Trans. Am. geophys. Un.,* **70,** 700.

Rona, P. A. & Gray, D. F., 1980. Structural behavior of fracture zones symmetric and asymmetric about a spreading axis: Mid-Atlantic Ridge (latitude 23 °N to 27 °N), *Bull. geol. Soc. Am.* **91,** 485–494.

Rosencrantz, E., Ross, M. & Sclater, J., 1988. Age and spreading history of the Cayman Trough as determined from depth, heat flow, and magnetic anomalies, *J. geophys. Res.,* **93,** 2141–2157.

Ruegg, J. C., Kasser, M., Tarantola, A., Lepine, J. C. & Chouikrat, B., 1982. Deformations associated with the El Asnam earthquake of 10 October 1980: Geodetic determination of vertical and horizontal movements, *Bull. seism. Soc. Am.,* **72,** 2227–2244.

Ruff, L. & Cazenave, A., 1985. Seasat geoid anomalies and the Macquarie ridge complex, *Phys. Earth planet Inter.,* **38,** 59–69.

Sandwell, D. T., 1984. Along track deflection of the vertical from Seasat; GEBCO overlays, *NOAA Tech. Memo NOS NGS*-40, Rockville, MD.

Savage, J. C., Lisowski, M. & Prescott, W. H., 1981. Geodetic strain measurements in Washington, *J. geophys. Res.,* **86,** 4929–4940.

Savostin, L. A. & Karasik, A. M., 1981. Recent plate tectonics of the Arctic Basin and of northeastern Asia, *Tectonophysics,* **74,** 111–145.

Schlich, R., 1982. The Indian Ocean: Aseismic ridges, spreading centers, and oceanic basins, in *The Ocean Basins and Margins,*

6, *The Indian Ocean,* pp. 51–147, eds Naim, A. E. N. & Stehli, F. G., Plenum, New York.

Schlich, R. & Patriat, P., 1971. Mise en évidence d'anomalies magnétiques axiales sur la branche ouest de la dorsale médio-indienne, *C. R. Acad. Sci.,* **272,** 700–703.

Schouten, H. & McCamy, K., 1972. Filtering marine magnetic anomalies, *J. geophys. Res.,* **77,** 7089–7099.

Sclater, J. G. & Klitgord, K. D., 1973. A detailed heat flow, topographic, and magnetic survey across the Galapagos spreading center at 86 °W, *J. geophys. Res.,* **78,** 6951–6975.

Sclater, J. G., Anderson, R. N. & Bell, M. L., 1971. Elevation of ridges and evolution of the central east Pacific, *J. geophys. Res.,* **76,** 7888–7915.

Sclater, J. G., Bowin, C., Hey, R., Hoskins, H., Peirce, J., Phillips, J. & Tapscott, C., 1976a. The Bouvet triple junction, *J. geophys. Res.,* **81,** 1857–1869.

Sclater, J. G., Luyendyk, B. P. & Meinke, L., 1976b. Magnetic lineations in the southern part of the Central Indian Basin, *Bull. geol. Soc. Am.,* **87,** 371–378.

Sclater, J. G., Dick, H., Norton, I. O. & Woodroffe, D., 1978. Tectonic structure and petrology of the Antarctic plate boundary near the Bouvet triple junction, *Earth planet. Sci. Lett.,* **37,** 393–400.

Sclater, J. G., Fisher, R. L., Patriat, P., Tapscott, C. & Parsons, B., 1981. Eocene to recent development of the South-west Indian Ridge, a consequence of the evolution of the Indian Ocean triple junction, *Geophys. J. R. astr. Soc.,* **64,** 587–604.

Scott, D. R. & Kanamori, H., 1985. On the consistency of moment tensor source mechanisms with first-motion data, *Phys. Earth planet. Inter.,* **37,** 97–107.

Searle, R., 1981. The active part of Charlie-Gibbs fracture zone: A study using sonar and other geophysical techniques, *J. geophys. Res.,* **86,** 243–262.

Searle, R. C., 1983. Multiple, closely spaced transform faults in fast-slipping fracture zones, *Geology,* **11,** 607–610.

Searle, R. C., 1986. GLORIA investigations of oceanic fracture zones: Comparative study of the transform fault zone, *J. geol. Soc. Lond.* **143,** 743–756.

Searle, R. C. & Laughton, A. S., 1977. Sonar studies of the Mid-Atlantic Ridge and Kurchatov fracture zone, *J. geophys. Res.,* **82,** 5313–5328.

Seno, T., 1985. 'Northern Honshu microplate' hypothesis and tectonics in the surrounding region, *J. geod. Soc. Japan,* **31,** 106–123.

Seno, T., Moriyama, T., Stein, S., Woods, D. F., DeMets, C., Argus, D. & Gordon, R., 1987. Redetermination of the Philippine sea plate motion (abstract), *EOS Trans. Am. geophys. Un.,* **68,** 1474.

Sieh, K. E. & Jahns, R., 1984. Holocene activity of the San Andreas fault at Wallace Creek, California, *Bull. geol. Soc. Am.,* **95,** 883–896.

Silver, E. A., 1971. Tectonics of the Mendocino triple junction, *Bull. geol. Soc. Am.,* **82,** 2965–2978.

Speed, R. C., 1985. Cenozoic collision of the Lesser Antilles arc and continental South America and the origin of the El Pilar fault, *Tectonics,* **4,** 41–69.

Spence, W., 1977. The Aleutian arc; Tectonic blocks, episodic subduction, strain diffusion, and magma generation, *J. geophys. Res.,* **82,** 213–230.

Stauder, W., 1973. Mechanism and spatial distribution of Chilean earthquakes with relation to subduction of the oceanic plate, *J. geophys. Res.,* **78,** 5033–5061.

Stauder, W., 1975. Subduction of the Nazca plate under Peru as evidenced by focal mechanisms and by seismicity, *J. geophys. Res.,* **80,** 1053–1064.

Stauder, W. & Bollinger, G. A., 1966. The focal mechanism of the Alaska earthquake and its aftershocks, *J. geophys. Res.,* **71,** 5283–5926.

Stein, S., 1978. An earthquake swarm on the Chagos-Laccadive Ridge and its tectonic implications, *Geophys. J. R. astr. Soc.,* **55,** 577–588.

Stein, S. & Gordon, R. G., 1984. Statistical tests of additional plate boundaries from plate motion inversions, *Earth planet. Sci. Lett.,* **69,** 401–412.

Stein, R. S. & King, G. C. P., 1984. Seismic potential revealed by surface folding: 1983 Coalinga, California, earthquake, *Science,* **224,** 869–872.

Stein, S. & Okal, E. A., 1978. Seismicity and tectonics of the Ninetyeast Ridge area: Evidence for internal deformation of the Indian plate, *J. geophys. Res.,* **83,** 2233–2245.

Stein, C. A., Cloetingh, S. & Wortel, R., 1989. Seasat-derived gravity constraints on stress and deformation in the Northeastern Indian Ocean, *Geophys. Res. Lett.,* **16,** 823–826.

Stein, S., Wiens, D. A., Engeln, J. F. & Fujita, K., 1986a. Comment on 'Subduction of aseismic ridges beneath the Caribbean plate: Implications for the tectonics and seismic potential of the northeastern Caribbean' by W. R. McCann and L. R. Sykes, *J. geophys. Res.,* **91,** 784–786.

Stein, S., Engeln, J. F., Wiens, D. A., Fujita, K. & Speed, R. C., 1982. Subduction seismicity and tectonics in the Lesser Antilles arc, *J. geophys. Res.,* **87,** 8642–8664.

Stein, S., Engeln, J. F., DeMets, C., Gordon, R. G., Woods, D., Lundgren, P., Argus, D., Stein, C. & Wiens, D. A., 1986b. The Nazca–South America convergence rate and the recurrence of the great 1960 Chilean earthquake, *Geophys. Res. Lett.,* **13,** 713–716.

Stein, S., DeMets, C., Gordon, R. G., Brodholt, J., Engeln, J. F., Wiens, D. A., Argus, D., Lundgren, P., Stein, C. & Woods, D., 1988. A test of alternative Caribbean plate relative motion models, *J. geophys. Res.,* **93,** 3041–3050.

Stewart, L. M., 1983. Strain release along oceanic transform faults, *PhD thesis,* Yale University.

Suarez, G., Molnar, P. & Burchfiel, B. C., 1983. Seismicity, fault plane solutions, depth of faulting, and active tectonics of the Andes of Peru, Ecuador, and southern Colombia, *J. geophys. Res.,* **88,** 10 403–10 428.

Sykes, L. R., 1967. Mechanism of earthquakes and nature of faulting on the mid-oceanic ridges, *J. geophys. Res.,* **72,** 2131–2153.

Sykes, L. R., 1970. Focal mechanism solutions for earthquakes along the world rift system, *Bull. seism. Soc. Am.,* **60,** 1749–1752.

Sykes, L. R., McCann, W. R. & Kafka, A. L., 1982. Motion of Caribbean plate during last 7 million years and implications for earlier Cenozoic movements, *J. geophys. Res.,* **87,** 10 656–10 676.

Sylvester, A. G., 1988. Strike–slip faults, *Bull. geol. Soc. Am.,* **100,** 1666–1703.

Taber, J. J. & Smith, S. W., 1985. Seismicity and focal mechanisms associated with the subduction of the Juan de Fuca plate beneath the Olympic Peninsula, Washington, *Bull. seism. Soc. Am.* **75,** 237–249.

Talwani, M., Windisch, C. C. & Langseth, M. G., 1971. Reykjanes ridge crest: A detailed geophysical study, *J. geophys. Res.,* **76,** 473–517.

Tamsett, D. & Girdler, R. W., 1982. Gulf of Aden axial magnetic anomaly and the Curie temperature isotherm, *Nature,* **298,** 149–151.

Tamsett, D. & Searle, R. C., 1988. Structure and development of the mid-ocean ridge plate boundary in the Gulf of Aden: Evidence from GLORIA side scan sonar, *J. geophys. Res.,* **94,** 3157–3178.

Tapscott, C., Patriat, P., Fisher, R. L., Sclater, J. G., Hoskins, H. & Parsons, B., 1980. The Indian Ocean triple junction, *J. geophys. Res.,* **85,** 4723–4739.

Tchalenko, J. S. & Braud, J., 1974. Seismicity and structure of the Zagros (Iran): The Main Recent Fault between 33° and 35 °N, *Phil. Trans. R. Soc. Lond., A,* **277,** 1–25.

Tobin, D. G. & Sykes, L. R., 1968. Seismicity and tectonics of the northeast Pacific Ocean, *J. geophys. Res.,* **73,** 3821–3845.

Toksoz, M. N., Minear, J. W. & Julian, B. R., 1971. Temperature field and geophysical effects of a downgoing slab, *J. geophys. Res.,* **76,** 1113–1138.

Torrini, R. Jr & Speed, R. C., 1989. Tectonic wedging in the forearc basin—Accretionary prism transition, Lesser Antilles forearc, *J. geophys. Res.,* **94,** 10 549–10 584.

van Andel, T. H., Rea, D. K., Von Herzen, R. P. & Hoskins, H., 1973. Ascension fracture zone, Ascension island, and the Mid-Atlantic Ridge, *Bull. geol. Soc. Am.,* **84,** 1527–1546.

Vogt, P. R., Johnson, G. L. & Kristjansson, L., 1980. Morphology and magnetics anomalies north of Iceland, *J. Geol.,* **47,** 67–80.

Vogt, P. R., Cherkis, N. Z. & Morgan, G. A., 1983. Project Investigator—I: Evolution of the Australia Antarctic Discordance deduced from a detailed aeromagnetic study, in *Antarctic Earth Science,* pp. 608–613. eds Oliver, R. L., James, P. R. & Jago, J. B., Australian Academy of Sciences, Canberra.

Vogt, P. R., Taylor, P. T., Kovacs, L. C. & Johnson, G. L., 1979. Detailed aeromagnetic investigation of the Arctic Basin, *J. geophys. Res.,* **84,** 1071–1089.

Vogt, P. R., Kovacs, L. C., Bernero, C. & Srivastava, S. P., 1982. Asymmetric geophysical signatures in the Greenland–Norwegian and southern Labrador Seas and the Eurasia Basin, *Tectonophysics,* **89,** 95–160.

Walcott, R. I., 1984. The kinematics of the plate boundary zone through New Zealand: A comparison of short- and long-term deformations, *Geophys. J. R. astr. Soc.,* **79,** 613–633.

Wald, D. J. & Wallace, T. C., 1986. A seismically active segment of the Southwest Indian Ridge, *Geophys. Res. Lett.,* **13,** 1003–1006.

Weissel, J. K. & Hayes, D. E., 1972. Magnetic anomalies in the southeast Indian Ocean, in *Antarctic Oceanology II: The Australian–New Zealand Sector, Antarctic Research Series,* 19, pp. 165–196, ed. Hayes, D. E., AGU, Washington, DC.

Weissel, J. K., Hayes, D. E. & Herron, E. M., 1977. Plate tectonics synthesis: The displacements between Australia, New Zealand, and Antarctica since the Late Cretaceous, *Mar. Geol.,* **25,** 231–277.

Weissel, J. K., Anderson, R. N. & Geller, C. A., 1980. Deformation of the Indo-Australian plate, *Nature,* **287,** 284–291.

Welch, S. M., Macdonald, K. C., Miller, S. P. & Fox, P. J., 1986. Magnetic analysis of slow spreading in the south Atlantic (abstract), *EOS, Trans. Am. Geophys. Un.,* **67,** 1227.

Weldon, R. & Humphreys, E., 1986. A kinematic model of southern California, *Tectonics,* **5,** 33–48.

White, R. S., 1984. Active and passive plate boundaries around the Gulf of Oman, northwest Indian Ocean, *Deep-Sea Research, Part A: Oceanographic Research Papers* 31 (6-8A), pp. 731–745.

Wiens, D. A., 1986. Historical seismicity near Chagos: A complex deformation zone in the equatorial Indian Ocean, *Earth planet. Sci. Lett.,* **76,** 350–360.

Wiens, D. A. & Stein, S., 1984. Intraplate seismicity and stresses in young oceanic lithosphere, *J. geophys. Res.,* **89,** 11 442–11 464.

Wiens, D. A. *et al.,* 1985. A diffuse plate boundary model for Indian Ocean tectonics, *Geophys. Res. Lett.,* **12,** 429–432.

Wilson, D. S., 1988. Tectonic history of the Juan de Fuca Ridge over the last 40 million years, *J. geophys. Res.,* **93,** 11 863–11 876.

Wise, D. U., 1963. An outrageous hypothesis for the tectonics pattern of the North American Cordillera, *Bull. geol. Soc. Am.,* **74,** 357–362.

Yielding, G., 1985. Control of rupture by fault geometry during the 1980 El Asnam (Algeria) earthquake, *Geophys. J. R. astr. Soc.,* **81,** 641–670.

Zoback, M. D. *et al.,* 1987. New evidence on the state of stress of the San Andreas Fault System, *Science,* **238,** 1105–1111.

Zonenshain, L. P. & Karasik, L. A., 1981. Movement of lithospheric plates relative to subduction zones: formation of marginal seas and active continental margins, *Tectonophysics,* **74,** 57–87.